

Assessment of an analysis for predicting the mixing of two laminar flows
by Frederick Louis Yapuncich

A thesis submitted in partial fulfillment of the requirements for the degree of Master of Science in Mechanical Engineering
Montana State University
© Copyright by Frederick Louis Yapuncich (1990)

Abstract:
An independent assessment has been made of a theory recently proposed for the analysis of two laminar, steady, two-dimensional streams mixing beyond the trailing edge of a thin partition. By superimposing the wake-flow solutions of Demetriades and the free-shear-layer solution of Chapman, this theory known as the "Partition Flow Theory" (PFT) provides closed-form equations for the variables of a great variety of flows. In the present work numerical solutions were obtained with the PFT for a wide class of wake flows, base flows, and partition flows. Adding to tests of the PFT performed previously against numerical solutions and wake test data, in the present work the theory was tested against two sets of partition flow experiments. The first of these dealt with the merging of two supersonic flows, one at Mach 2.9 and the other at Mach 2.29. The second experiment had provided for a Mach 3 stream and a Mach 8 stream. The comparison of the PFT with these data showed that the PFT generally predicted lower values for the velocity in the mixing layer than exhibited by the data. In the case of the hypersonic data the minimum velocities predicted by the PFT and those of the data matched which strengthens the postulate that the minimum velocities of the free shear layer and the wake flow should coincide at the dividing stream line of the wake component. Suggested improvements to the PFT consist of (a) use of a polynomial or hyperbolic tangent for an initial profile due to the inability of the exponential to provide a close fit to the actual trailing edge boundary layer profile, and (b) considerations of Prandtl number other than unity. The latter is difficult because the PFT utilizes the Busseman-Crocco temperature relationship which is based on the assumption that the temperature is a function of the velocity only. This assumption causes the thermal and velocity boundary thicknesses to be equal.

ASSESSMENT OF AN ANALYSIS FOR PREDICTING THE MIXING OF TWO LAMINAR FLOWS

by

Frederick Louis Yapuncich

A thesis submitted in partial fulfillment
of the requirements for the degree

of

Master of Science

in

Mechanical Engineering

MONTANA STATE UNIVERSITY
Bozeman, Montana

May 1990

11378
Y199

APPROVAL

of a thesis submitted by

Frederick Louis Yapuncich

This thesis has been read by each member of the thesis committee and has been found to be satisfactory regarding content, English usage, format, citations, bibliographic style, and consistency, and is ready for submission to the College of Graduate Studies.

5/3/90
Date

Chairperson, Graduate Committee

Approved for the Major Department

May 5, 1990
Date

W. E. Larsen
Head, Major Department

Approved for the College of Graduate Studies

May 3, 1990
Date

Henry L. Parsons
Graduate Dean

STATEMENT OF PERMISSION TO USE

In presenting this thesis in partial fulfillment of the requirements for a master's degree at Montana State University, I agree that the Library shall make it available to borrowers under rules of the Library. Brief quotations from this thesis are allowable without special permission, provided that accurate acknowledgment of source is made.

Permission for extensive quotation from or reproduction of this thesis may be granted by my major professor, or in his absence, by the Dean of Libraries when, in the opinion of either, the proposed use of the material is for scholarly purposes. Any copying or use of the material in this thesis for financial gain shall not be allowed without my written permission.

Signature 

Date 3 May 1990

ACKNOWLEDGMENTS

The author is indebted to the following for their contributions to this investigation:

His advisor, Dr. Anthony Demetriades, for his guidance and insight throughout the investigation.

Tim Brower, for furnishing his test data on supersonic shear layers.

Dr. Alan George and Dr. Thomas Reihman for their support as committee members.

The Mechanical Engineering Department of Montana State University and the Rocketdyne Division of Rockwell International Corporation for financial assistance.

Rene' Tritz for typing and checking the final revision.

Special thanks go to his wife Pam Pruitt and his two children Kate and John for their support and encouragement during this graduate program.

TABLE OF CONTENTS

Page

LIST OF TABLES vii

LIST OF FIGURES viii

NOMENCLATURE xiii

ABSTRACT xvi

1. INTRODUCTION 1

2. PARTITION FLOW THEORY (PFT) 4

Overview 4
Wake Flow 6
Free Shear Layer 9
Temperature Field 11
Superposition of Flows 12

3. APPLICATIONS OF THE PFT 14

Overview 14
Wake Flow Solutions 15
Base Flow Solutions 16
Partition Flow Solutions 16

4. TESTS OF THE PFT 36

Overview 36
Comparison with Wake Flow Results 36
Comparison with Numerical Results 36
Comparison with Partition Flow Results 37
Supersonic Laminar Mixing 37
Experimental Setup 37
Trailing Edge Boundary Layer 40

TABLE OF CONTENTS—Continued

Page

4. TESTS OF THE PFT (continued)

Comparison of Original Supersonic Velocity Profiles and the PFT 41
Resolution of Disparity between Supersonic Data and the PFT 45
Comparison of Revised Supersonic Velocity Profiles and the PFT 47
Hypersonic Laminar Mixing 50
Experimental Setup 50
Trailing Edge Boundary Layer 54
Comparison of Hypersonic Laminar Velocity Profiles with the PFT 59
Hypersonic Turbulent/Laminar Mixing 64
Conclusions on the Comparison with Test Data 68

5. EXTENSIONS OF THE PFT 70

Overview 70
Oseen Approximations 70
Initial Velocity Profile 71
Variable Prandtl Number 73

6. CONCLUSIONS 76

REFERENCES CITED 79

APPENDICES 83

Appendix A – Integration of Gold's Velocity Equation 84
Appendix B – The PFT Algorithm "Shear 14" 89

LIST OF TABLES

Table Page

1. Flow Fields Predicted by the PFT 17

2. Hypersonic Experimental Parameters 53

LIST OF FIGURES

Figure — Page

1. Schematic of Partition Flow 5

2. Determination of S for a Laminar Boundary Profile (Blasius Profile) 8

3. Explanation of Postulate of Superposition 13

4. Flow in the symmetric low-speed wake of a cooled plate (Case 1) 18

5. Flow in the symmetric low-speed wake of an adiabatic plate (Case 2) 19

6. Flow in the symmetric low-speed wake of a heated plate (Case 3) 20

7. Flow in the symmetric supersonic wake of a cooled plate (Case 4) 21

8. Flow in the symmetric supersonic wake of an adiabatic plate (Case 5) 22

9. Flow in the symmetric supersonic wake of a heated plate (Case 6) 23

10. Flow in the symmetric hypersonic wake of a cooled plate (Case 7) 24

11. Flow in the hypersonic wake of an adiabatic plate (Case 8) 25

12. Low-speed base flow; cooled partition and stagnant region (Case 9) 26

LIST OF FIGURES—Continued

Figure Page

13. Low-speed base flow; adiabatic partition and stagnant region (Case 10) 27

14. Low-speed base flow; heated partition and stagnant region (Case 11) 28

15. Supersonic base flow; cooled partition and stagnant region (Case 12) 29

16. Supersonic base flow; adiabatic partition and stagnant region (Case 13) 30

17. Hypersonic base flow; cooled partition and stagnant region (Case 14) 31

18. Hypersonic base flow; adiabatic partition and stagnant region (Case 15) 32

19. Hypersonic film-cooling example; cooled low-speed flow and equal boundary layer thickness (Case 16) 33

20. Typical hypersonic flow cooling example: moderately cooled slow stream (Case 17) 34

21. Hypersonic film-cooling example: insufficiently cooled slow stream (Case 18) 35

22. Schematic of MSU Tunnel Modifications 38

23. Verification of Data/Code Reinstallation 40

24. Initial Determination of S for Supersonic Data 41

25. Comparison of PFT with Experimental Supersonic Minimum Velocities 42

LIST OF FIGURES—Continued

Figure — Page

26. Comparison of PFT with Supersonic Data $x^* = .25$ inches 43

27. Comparison of PFT with Supersonic Data $x^* = .5$ inches 43

28. Comparison of PFT with Supersonic Data $x^* = .75$ inches 44

29. Comparison of PFT with Supersonic Data $x^* = 1$ inch 44

30. Iteration to Match Minimum Velocities via θ_1 46

31. Determination of S for Revised Supersonic Data 47

32. Comparison of PFT with Revised Supersonic Data $x^* = .25$ inches 48

33. Comparison of PFT with Revised Supersonic Data $x^* = .5$ inches 48

34. Comparison of PFT with Revised Supersonic Data $x^* = .75$ inches 49

35. Comparison of PFT with Revised Supersonic Data $x^* = 1$ inch 49

36. Schematic of Hypersonic Model 51

37. Velocity Profile used in Determining θ_1 55

38. Density Profile used in Determining θ_1 55

LIST OF FIGURES—Continued

Figure — Page

39. Spark-Schlieren Photographs of the Partition Flow for Air, Mach 8 fast stream, Mach 3 slow stream 56

40. Determination of S for Hypersonic Initial Profile 58

41. Comparison of PFT and Initial Profile 58

42. Comparison of PFT and Laminar Hypersonic Minimum Velocities 59

43. Comparison of PFT with Laminar Hypersonic Data $x^* = .1$ inches 60

44. Comparison of PFT with Laminar Hypersonic Data $x^* = .4$ inches 61

45. Comparison of PFT and Laminar Hypersonic Data $x^* = 1.5$ inches 62

46. Comparison of PFT and Laminar Hypersonic Data $x^* = 3$ inches 62

47. Comparison of PFT and Laminar Hypersonic Data $x^* = 4.5$ inches 63

48. Comparison of PFT and Laminar Hypersonic Data $x^* = 7.5$ inches 63

49. Comparison of PFT and Laminar Hypersonic Data $x^* = 9$ inches 64

50. Comparison of PFT and Turbulent Hypersonic Data $x^* = .4$ inches 65

51. Comparison of PFT and Turbulent Hypersonic Data $x^* = 2$ inches 66

LIST OF FIGURES—Continued

Figure Page

52. Comparison of PFT and Turbulent Hypersonic Data $x^* = 4$ inches 66

53. Comparison of PFT and Turbulent Hypersonic Data $x^* = 6$ inches 67

54. Comparison of PFT and Turbulent Hypersonic Data $x^* = 9$ inches 67

55. Polynomial Fit of Blasius Profile 72

56. Hyperbolic Tangent Fit of Blasius Profile 72

57. Busseman-Crocco Temperature Profile 74

58. Similarity Temperature Profile 74

59. The PFT Algorithm "Shear 14" 90

NOMENCLATURE

B,C	Constants in Gold's temperature profile, equation (29)
C_n	polynomial constants for free shear fit, equation (23)
C'_n	polynomial constants for free shear fit, equation (24)
ERFC	compliment of error functions $(1 - erf)$, equations (19), (29)
FSL	Free Shear Layer
G	function in the wake component velocity solution, equation (3)
$\overline{h}$	non-dimensional temperature, equation (2)
$\overline{h}_0$	initial value of h at the trailing edge, equation (2)
$\tilde{\overline{h}}_0$	temperature defect, equation (43)
MSU	Montana State University
M	Mach number
p	static pressure
p_0	stagnation pressure
P'	Asymmetry Parameter, equation (14)
PFT	Partition Flow Theory
Pr	Prandtl number
r	recovery factor, equation (45)
Re'	unit Reynolds number
Re_L	Reynolds number for Gold's solution, equation (6)
S	Stretching parameter, equation (7)
SHEAR 14	PFT algorithm (Appendix B)
T	static temperature

NOMENCLATURE—Continued

T_0	total temperature
T_W	wall temperature
u	local dimensional velocity, equation (1)
u_m	minimum velocity in velocity profile
$\overline{u}$	longitudinal non-dimensional wake velocity, equation (1)
$\overline{u}_0$	initial non-dimensional velocity at trailing edge, equation (9)
x^*	dimensional longitudinal distance from the trailing edge
$\overline{x}$	non-dimensional longitudinal variable, equation (40)
$\overline{\overline{x}}$	non-dimensional longitudinal variable, equation (5)
x'	non-dimensional longitudinal variable, equation (19)
y	non-dimensional lateral variable, equation (10)
y'	non-dimensional lateral variable, equation (12)
y''	non-dimensional lateral variable, equations (11), (19)
y'_m	lateral position of the dividing stream line minimum in the wake component velocity profile, equation (13)
Y^*	dimensional lateral position
$\tilde{Y}^*$	compressible-transformed lateral variable
$\overline{\overline{y}}$	non-dimensional lateral variable, equation (5)
ξ	dummy variable, equations (1), (2), (3)
ρ	density
$(\ )_e$	constant wake-edge condition
$(\ )_{\mathrm{FSL}}$	quantity derived from the FSL component only
$(\ )_{\mathrm{WAKE}}$	quantity derived from the WAKE component only
$(\ )_1$	given constant pertaining to stream 1

NOMENCLATURE—Continued

$(\ )_2$	given constant pertaining to stream 2
$(\ )_\infty$	given constant pertaining to free stream conditions
$\overline{\eta}, \overline{\overline{\eta}}$	lateral variable in FSL velocity profile, equations (20), (27)
η	similarity variable ($= y^* \text{sqrt}(U_1/(2x^*))$
θ	momentum thickness
γ	specific heat ratio
α_1	variable in velocity solution, equation (19)
α_2	variable in velocity solution, equation (19)
α_3	variable in temperature solution, equation (29)
α_4	variable in temperature solution, equation (29)

ABSTRACT

An independent assessment has been made of a theory recently proposed for the analysis of two laminar, steady, two-dimensional streams mixing beyond the trailing edge of a thin partition. By superimposing the wake-flow solutions of Demetriades and the free-shear-layer solution of Chapman, this theory known as the "Partition Flow Theory" (PFT) provides closed-form equations for the variables of a great variety of flows. In the present work numerical solutions were obtained with the PFT for a wide class of wake flows, base flows, and partition flows. Adding to tests of the PFT performed previously against numerical solutions and wake test data, in the present work the theory was tested against two sets of partition flow experiments. The first of these dealt with the merging of two supersonic flows, one at Mach 2.9 and the other at Mach 2.29. The second experiment had provided for a Mach 3 stream and a Mach 8 stream. The comparison of the PFT with these data showed that the PFT generally predicted lower values for the velocity in the mixing layer than exhibited by the data. In the case of the hypersonic data the minimum velocities predicted by the PFT and those of the data matched which strengthens the postulate that the minimum velocities of the free shear layer and the wake flow should coincide at the dividing stream line of the wake component. Suggested improvements to the PFT consist of (a) use of a polynomial or hyperbolic tangent for an initial profile due to the inability of the exponential to provide a close fit to the actual trailing edge boundary layer profile, and (b) considerations of Prandtl number other than unity. The latter is difficult because the PFT utilizes the Busseman-Crocco temperature relationship which is based on the assumption that the temperature is a function of the velocity only. This assumption causes the thermal and velocity boundary thicknesses to be equal.

CHAPTER 1

INTRODUCTION

The purpose of this thesis was to determine to what extent existing analyses of parallel, two-dimensional, laminar mixing beyond the trailing edge of a partition can successfully predict the experimental observations.

The two typical flows beyond a partition are the wake and the free shear layer. Wakes are flows behind a partition where viscous effects are involved due to a finite boundary layer at the trailing edge while both streams usually have the same freestream velocities. Free shear layers occur when the two streams upstream of the partition have different freestream velocities and are usually analyzed by assuming that the trailing edge of the partition has zero boundary layer thickness. In other words, only an inviscid effect due to the difference in velocities attributes to this type of flow.

In this work the partition is restricted to a thin one in order to avoid the recirculating region that exists directly behind a bluff body. This region complicates the problem by adding an interior region which is different from both streams on either side of it. Also, the bluff body adds the problem of reattachment which further complicates the flow.

Chapman [1] found an exact solution for the free shear layer without boundary layers. Denison and Baum [2] utilized Chapman's work in deriving a numerical solution for the free shear layer problem including initial boundary thickness but limited to one side of the partition having zero velocity. Kubuta and Dewey [3]

solved the free shear layer problem using momentum-integral methods again for zero velocity on one side. However, when this momentum-integral method was compared with Denison and Baum's numerical solution the agreement found was rather poor [4]. All these solutions have two major drawbacks with respect to this work. First they all deal with the near wake only and secondly do not cover the entire flow field.

The far wake has also been investigated extensively. Tollmien [5] derived the classic asymptotic solution for an incompressible wake. Goldstein [6] improved on Tollmien's work by utilizing the Oseen approximations (small velocity defects). Kubota [7] developed a closed form solution for the compressible far wake problem by the use of the Oseen approximations (to linearize the momentum and energy equations) with arbitrary streamwise pressure gradients assuming delta function initial profiles. Gold [8] extended Kubota's work to allow for arbitrary initial profiles. The drawbacks of these far wake solutions were the same as for the near wake solutions; specifically, no free shear layer and an incomplete treatment was given of the entire flow field.

The treatment of the entire wake was accomplished by Zeiberg and Kaplan [9]. They utilized a "modified Oseen" approximation to be able to combine the near and far wakes. Steiger and Bloom [10] developed a closed-form solution to the entire incompressible constant-pressure wake by applying the one-strip integral method. Demetriades [11] solved for the entire wake flow field by utilizing Gold's work but without a shear layer.

More recently Demetriades presented a new theory known as the Partition Flow Theory (PFT) [12] which combines his earlier wake solutions and Chapman's free shear layer solution by superpositioning the wake onto the free shear layer. Though Gold's wake solution is based on the Oseen approximations (restricted to

far wake only) the comparison of the PFT with Goldstein's near wake solution showed excellent agreement [12]. Therefore it was decided that the PFT best matched the criteria set forth at the beginning of this chapter.

In this work, after a detailed review of the PFT for completeness, the PFT was used to compute a large number of classic flows. Earlier, the PFT had been compared against experimental data on wakes. In this work it was compared with experimental data on partition flows.

The two sets of partition flows that were compared with the PFT results consisted of supersonic mixing [13] and hypersonic mixing data [14]. The hypersonic data consisted of two sets of profiles. The first set consisted of seven laminar profiles. The second set of five hypersonic profiles were turbulent fast stream and laminar slow stream data. Though the PFT is restricted to laminar flows, a comparison was made on the basis that it would be interesting to observe how the theory shows the differences between turbulent and laminar flows. Also since the slow side was initially laminar the theory would also give an indication of the degree of mixing between a turbulent/laminar flow as opposed to a laminar/laminar flow.

Several improvements in the PFT are suggested in this work concerning the modeling of the initial profile and the restriction of a Prandtl number of unity.

CHAPTER 2

PARTITION FLOW THEORY (PFT)

Overview

This chapter gives an abbreviated overview of the PFT as developed by Demetriades. For a complete explanation of the PFT see [12].

The advantages of a closed form analytic solution to the mixing of two laminar streams are twofold. First, extensive difficulties exist in obtaining numerical codes to solve the mixing problem. Second, an in-depth knowledge of computational fluid dynamics is needed to utilize these numerical codes and interpret the output. The PFT does not require the user to have more than a basic knowledge of fluid flow and gas dynamics.

The Partition Flow Theory (PFT) [12] was developed to solve the problem of the mixing of two steady, laminar, two-dimensional, flows with dissimilar velocities behind a thin plate. Figure 1 shows the basic problem and the nomenclature used to describe it. The PFT combines known analytical solutions for the wake flow and the free shear layer into one closed form analytical equation. The uniqueness of the PFT is the superposition of the wake flow onto the free shear layer component.

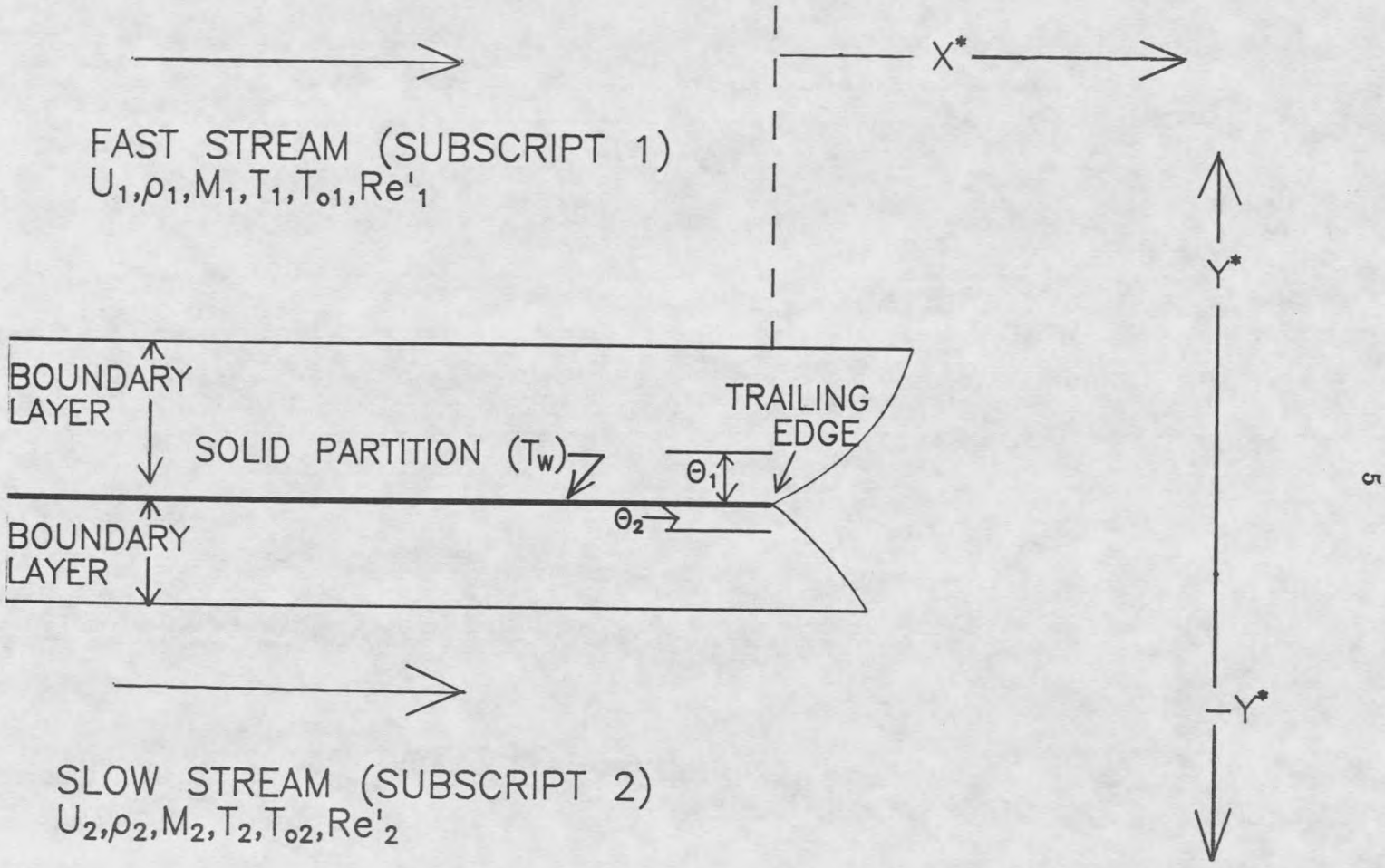


Figure 1. Schematic of Partition Flow.

Wake Flow

The equations describing the wake flow are those proposed by Demetriades [12] who based his approach on that of Gold [8]. Gold's work [8] extended Kubota's work [7] on laminar wakes with streamwise pressure gradient to allow for arbitrary initial profiles. In the PFT the streamwise pressure gradient (dp/dx) is assumed zero which simplifies Gold's solutions considerably. The velocity solution is

$$\overline{u} = 1 - \frac{u}{u_e} = \frac{1}{2\sqrt{\overline{\overline{x}}}} \int_{-\infty}^{\infty} \overline{u}_0(\xi) G\left(\xi; \overline{\overline{x}}, \overline{\overline{y}}\right) d\xi \quad . \tag{1}$$

The temperature solution is

$$\overline{h} = \frac{T}{T_e} - 1 = \frac{1}{2\sqrt{\overline{\overline{x}}}} \int_{-\infty}^{\infty} \overline{h}_0(\xi) G\left(\xi; \overline{\overline{x}}, \overline{\overline{y}}\right) d\xi \tag{2}$$

where

$$G = \frac{1}{\sqrt{\pi}} \exp\left[-\left(\overline{\overline{y}} - \xi\right)^2 / 4\overline{\overline{x}}\right] \quad , \tag{3}$$

$$\begin{aligned} \overline{u}_0 &= \text{initial velocity profile} \\ \overline{h}_0 &= \text{initial temperature profile} \quad , \end{aligned} \tag{4}$$

$$\overline{\overline{y}} = \frac{\tilde{Y}^*}{L} \mathrm{Re}_L \quad , \quad \overline{\overline{x}} = \frac{x^*}{L} \quad , \quad \tilde{Y}^* = \int_0^{Y^*} \rho/\rho_e dY^* \quad , \tag{5}$$

$$\mathrm{Re}_L = \frac{u_e L}{\nu_e} \quad , \quad L = \text{Length} \quad , \quad u = \text{local velocity} \quad , \quad T = \text{local temperature} \quad , \tag{6}$$

$$x^* \ , \ Y^* = \text{dimensional coordinates} \quad , \quad \rho = \text{density} \tag{7}$$

and

(8) ν = kinematic viscosity , $(\ )_e$ = edge conditions .

Demetriades [15] chose an exponential for the initial profile. This was an arbitrary decision based on ease of the mathematics. The problem with an exponential profile is that it shows a much thinner profile than the Blasius [16] profile. Therefore a stretching factor S was added to the exponent

(9) $$\overline{u}_0 = e^{-y/S}$$

where

(10) $y = Y^*/\theta_1$, θ_1 = fast stream momentum thickness .

The S parameter acts as a control knob to allow for all types of initial profiles. Figure 2 shows how the S parameter can be chosen to fit the Blasius [16] profile. As shown in Figure 2, θ_1 was used as a characteristic length. This length (θ_1) was utilized in the rest of this work to non-dimensionalize Y^*. θ_1 was determined by the actual trailing edge profile being modeled by the PFT. The S is then incorporated into the succeeding profiles by altering the y coordinate to

(11) $$y'' = \frac{y' + (S-1)y'_m}{S}$$

where

(12) $$y' = \left(\frac{P'}{P'+1}\right)\frac{\tilde{Y}^*}{\theta_1} \quad , \quad P' = \text{asymmetry factor}$$

(13) $y'_m = y'$ position where the wake velocity is a minimum .

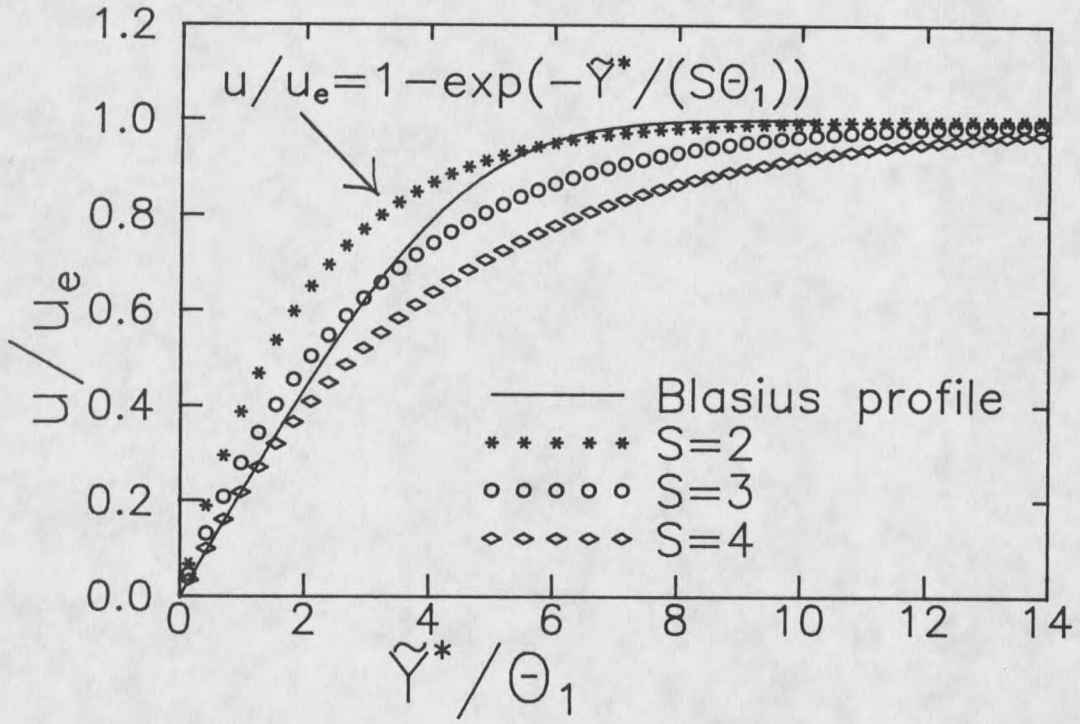


Figure 2. Determination of S for a Laminar Boundary Profile (Blasius Profile).

Physically, the y'' coordinate is the mechanism through which the parameter S stretches or constricts the profiles downstream of the trailing edge of the thin partition.

A second important parameter in the PFT is the asymmetry factor. This parameter allows the wake profile to take into account uneven boundary layer growth ($\theta_1 \neq \theta_2$) and to allow for dissimilar flows ($\rho_1 \neq \rho_2$):

(14) $$P' = \frac{\rho_1 \theta_1}{\rho_2 \theta_2}$$

(15) $$(\ )_1 = \text{fast stream} \ , \ (\ )_2 = \text{slow stream} \ .$$

With the following initial velocity profiles,

$$\overline{u}_0 = e^{(-y/S)} \quad , \quad y > 0 \quad , \tag{16}$$

$$\overline{u}_0 = e^{(P'y/S)} \quad , \quad y < 0 \quad , \tag{17}$$

$$y = \frac{\tilde{Y}^*}{\theta_1} \quad , \quad \tilde{Y}^* = \int_0^{Y^*} \frac{\rho}{\rho_e}\, dY^* \quad , \tag{18}$$

$$Y^* = \text{dimensional lateral coordinates} \quad ,$$

Gold's velocity solution (1) becomes (see Appendix A for details)

$$\overline{u} = \frac{1}{2} \exp\left(\frac{-y''^2}{4x'}\right) \left(\exp(\alpha_1^2) Erfc(\alpha_1) + \exp(\alpha_2^2) Erfc(\alpha_2)\right) \tag{19}$$

where

$$x' = \frac{P'^2}{(P'+2)} \frac{x^*}{\theta_1 \mathrm{Re}_{\theta_1}} \quad , \quad y'' = \frac{y' + (S-1)y'_m}{S} \quad ,$$

$$\alpha_1 = (P+1)\left(\sqrt{x'}\right) + \frac{y''}{2\sqrt{x'}}$$

$$\alpha_2 = \frac{(P+1)}{P}\left(\sqrt{x'}\right) - \frac{y''}{2\sqrt{x'}} \quad .$$

Equation (19) is valid for all laminar wake flows including uneven boundary layers.

Free Shear Layer

Chapman's model [1] for laminar mixing based on zero boundary-layer thickness was used for modeling the free shear layer between the two flows. The PFT utilizes Chapman's relationship of

$$\left(\frac{u}{u_1}\right)_{\mathrm{FSL}} = \overline{\eta} = \frac{y'}{\sqrt{x'}} \quad . \tag{20}$$

But to be applicable to the PFT three alterations were needed. First, in Chapman's model the velocity on the slow side is zero while in PFT u_2 can vary from 0 to u_1. Therefore the following form must be used:

$$(21) \quad \left(\frac{u}{u_1}\right)_{\text{FSL}} = \left(1 - \frac{u_2}{u_1}\right) f\left(\frac{y'}{\sqrt{x'}}\right) + \frac{u_2}{u_1} \quad , \quad \text{FSL} = \text{Free Shear Layer} \quad .$$

Secondly, Chapman's final form was numerical and the PFT required an analytical form. A polynomial fit over the following domains was used:

$$(22) \quad \overline{\eta} < -10 : \frac{u}{u_1} = \frac{u_2}{u_1}$$

$$(23) \quad -10 < \overline{\eta} < 0 : f = \sum_0^6 C_n \left(\overline{\eta}\right)^n$$

$$(24) \quad 0 < \overline{\eta} < 8 : f = \sum_0^6 C'_n \left(\overline{\eta}\right)^n$$

$$(25) \quad \overline{\eta} > 8 : f = 1$$

$$(26) \quad C_n \ , \ C'_n = \text{numerical constants ([12])} \quad .$$

Thirdly, in the Chapman model the two flows separated at $u/u_1 = .587$ while in the wake flow the flows separated at the minimum velocities. To superimpose the wake onto the free shear layer the Chapman variable must be altered to

$$(27) \quad \overline{\overline{\eta}} = \frac{y' - y'_m}{\sqrt{x'}} \quad .$$

This concept is a critical part of Demetriades' postulate of superposition which will be discussed shortly.

Temperature Field

To determine the changes in temperature through the entire flow field the Busemann-Crocco temperature relationship was utilized [17]:

$$(28) \qquad \frac{T - T_W}{T_\infty} = \left(1 - \frac{T_W}{T_\infty}\right) \frac{u}{u_\infty} + \frac{\gamma - 1}{2} M_\infty^2 \left(\frac{u}{u_\infty}\right)\left(1 - \frac{u}{u_\infty}\right) \quad .$$

For the wake component the initial velocity profiles (16) and (17) were substituted into the Busemann-Crocco relationship (28). In turn (28) was substituted for $\overline{h}_0$ in Gold's solution (2) and the following temperature profile was found:

$$(29) \qquad \overline{h} = B\overline{u} + \frac{C}{2} \exp\left(\frac{-y''^2}{4x'}\right)\left(\exp(\alpha_3^2) Erfc(\alpha_3) + \exp(\alpha_4^2) Erfc(\alpha_4)\right)$$

where

$$B \equiv \frac{\gamma - 1}{2} M_e^2 - 1 + \frac{T_W}{T_e}$$

$$C \equiv -\left(\frac{\gamma - 1}{2}\right) M_e^2$$

$$\alpha_3 = 2(P + 1)\left(\sqrt{x'}\right) + \frac{y''}{2\sqrt{x'}}$$

$$\alpha_4 = 2\,\frac{(P + 1)}{P}\,\left(\sqrt{x'}\right) - \frac{y''}{2\sqrt{x'}} \quad .$$

The free shear layer uses Crocco's relation directly by substituting Chapman's velocity relation (21) into (28) and obtaining

$$(30) \qquad \left(\frac{T}{T_1}\right)_{FSL} = 1 + \frac{\gamma + 1}{2} M_1^2 \left[1 - \left(\frac{u}{u_1}\right)_{FSL}^2\right]$$

$$+ \left[\frac{1 - (T_2/T_1)}{1 - (u_2/u_1)} + \frac{\gamma - 1}{2} M_1^2 \left(1 + \frac{u_2}{u_1}\right)\right] * \left[\left(\frac{u}{u_1}\right)_{FSL} - 1\right] \quad .$$

Superposition of Flows

The real uniqueness of the PFT is the superpositioning of the wake flow onto the free shear layer. The basic postulate is

$$\frac{u}{u_1} = \left(\frac{u}{u_{FSL}}\right)\left(\frac{u_{FSL}}{u_1}\right) \quad . \tag{31}$$

This concept can be explained by assuming

$$\frac{u}{u_1} = \left(\frac{u}{u_e}\right)_{wake}\left(\frac{u}{u_1}\right)_{FSL} \tag{32}$$

and then utilizing Figure 3 the following derivation can be shown:

$$u = u_{FSL} - \Delta u \tag{33}$$

$$\Delta u = u_e - u = u_e\left[1 - \left(\frac{u}{u_e}\right)_{wake}\right] \tag{34}$$

$$u = u_{FSL} - u_e\left[1 - \left(\frac{u}{u_e}\right)_{wake}\right] \quad . \tag{35}$$

As part of the postulate replace the constant wake-edge condition with that of the free shear layer:

$$u_e = u_{FSL} \tag{36}$$

$$u = u_{FSL} - u_{FSL}\left[1 - \left(\frac{u}{u_e}\right)_{wake}\right] = u_{FSL}\left(\frac{u}{u_e}\right)_{wake} \tag{37}$$

therefore

$$\frac{u}{u_1} = \frac{u_{FSL}}{u_1}\left(\frac{u}{u_e}\right)_{wake} = \left(\frac{u}{u_e}\right)_{wake}\left(\frac{u}{u_1}\right)_{FSL} \quad . \tag{38}$$

The same concept determined the temperature profile :

$$\frac{T}{T_1} = \left(\frac{T}{T_e}\right)_{wake}\left(\frac{T}{T_1}\right)_{FSL} \quad . \tag{39}$$

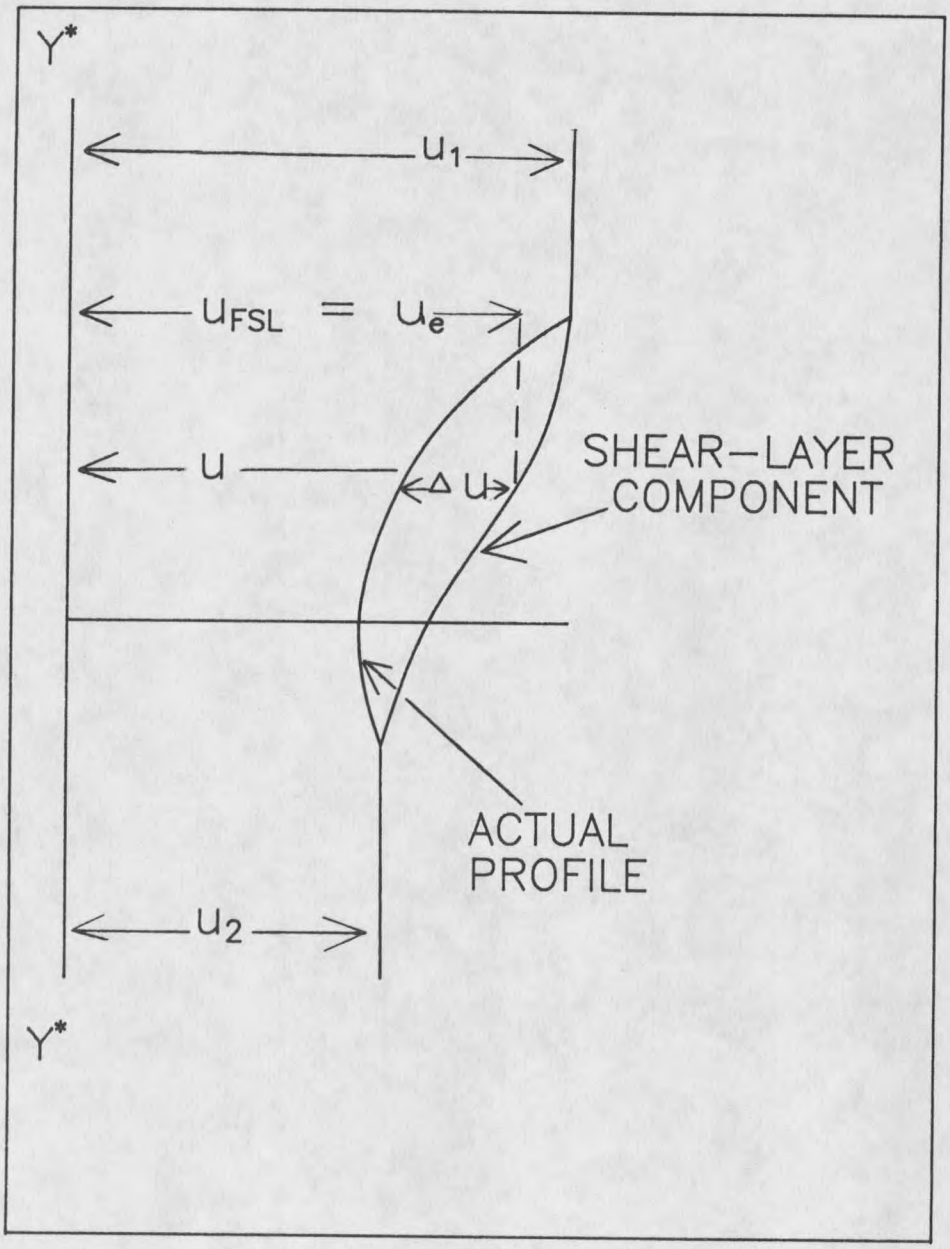


Figure 3. Explanation of Postulate of Superposition.

CHAPTER 3

APPLICATIONS OF THE PFT

Overview

The equations of the PFT (e.g. equations (19), (21), (29), (30)) have been developed [12] into an algorithm (see Appendix B) that was utilized to solve for wake, base, and partition flows. In this work the wake and base flows were solved by the PFT under subsonic, supersonic, and hypersonic conditions. The partition flow was solved for under supersonic and hypersonic conditions. As outlined in Table 1 each case was subjected to various temperature ratios. The general idea was to observe how the PFT solved such classic wake configurations as an adiabatic plate, a hot plate, and a cold plate.

Each of the following plots is composed of a family of velocity or temperature profiles. The medium used in all cases was air with a specific heat ratio of 1.4. A Blasius profile was assumed at the trailing edge and therefore an S of 3 was used as an input in all the cases. The shift between each profile enabled the plotting of nine profiles on one plot, thereby giving a sense of how the entire flow field was developing. For example in Figure 4 each profile has been shifted to the right by a factor of .2 from the previous profile. The number directly above each profile is its position in the flow downstream of the trailing edge ($x^* = 0$) of a thin plate. This nondimensional variable $\overline{x}$ is defined as

$$\overline{x} = \frac{x^*}{\theta_i^2 \mathrm{Re}_i'} \quad . \tag{40}$$

Due to the intricate temperature profiles in Figures 9, 10, 11 and 14 the $\overline{x}$ position has been designated in the legend rather than above each respective profile.

One observation that applies to all the profiles is the lack of any discontinuities in the flow field. In each of the following sections a number of the cases will be discussed.

Wake Flow Solutions

Figures 4 through 11 are solutions to the wake problem by the PFT. By allowing $u_1/u_2 = 1$ the inviscid free shear layer was removed, while setting $\theta_1/\theta_2 = 1$ caused the PFT to solve for a symmetrical wake.

The temperature profiles of Figures 4 through 6 predict the direction of heat transfer correctly under a low speed condition. As the temperature profiles approach the zero streamline ($Y^*/\theta_1 = 0$) near the trailing edge of the plate the direction of the slope (dT/dy) is determined solely by the ratio of wall temperature to freestream temperature. Figure 6 demostrates vividly how a hot plate affects the temperature profile beyond the trailing edge.

Figures 7 through 9 examine the PFT's ability to handle supersonic flow. The temperature in Figure 7 increased dramatically near the zero streamline ($Y^*/\theta_1 = 0$) due to the transfer of kinetic energy to thermal energy then abruptly decreased due to the cold plate condition. Not until a considerable distance downstream with respect to the first few profiles did this temperature "hump" dissipate. The temperature profile of Figure 8 shows the transfer of energy under adiabitic conditions.

Shifting from subsonic to supersonic conditions the velocity profiles begin to thicken due to the increase of the boundary layer thickness. This can be attributed

to the increase in viscosity of air as the temperature increases. The hypersonic cases amplify the findings of the supersonic profiles.

Base Flow Solutions

The base flows are flows where u_2 is considered zero. Many of the comments from the wake solutions apply to these cases. The uniqueness of these temperature and velocity profiles was the determination of the size of the "dead air" region.

Figures 12 through 14 consider base flows under low-speed conditions. Again the temperature of the thin plate determined whether the slope of the temperature profile was positive, negative, or unchanging.

Figures 15 through 17 show base flows under supersonic conditions. The transfer of kinetic to thermal energy has been correctly predicted by the PFT in these plots.

Figure 18 is base flow under hypersonic conditions with an adiabatic plate. In this plot the PFT has predicted a greater increase in temperature than the supersonic case in Figure 16. This is due to the increased transfer of kinetic to thermal energy in the trailing edge boundary layer when transferring from supersonic to hypersonic conditions.

Partition Flow Solutions

Figures 19 through 21 predict flows for $u_1 \neq u_2$ which introduced the inviscid free shear layer. Concurrently, a finite boundary layer thickness was present introducing the viscous component (i.e. the wake). The shift of the minimum velocities away from the zero streamline ($Y^*/\theta_1 = 0$) can be observed to be towards

the slow side and slowly increasing in magnitude as the velocity profiles progress downstream.

Case No.	Type	S	γ	M_1	T_W/T_{01}	T_{02}/T_{01}	u_2/u_1	θ_1/θ_2
1	Wake	3	1.4	0	0.2	1	1	1
2					1			
3					5			
4				3	0.2			
5					1			
6					5			
7				10	0.2			
8					1			
9	Base Flow			0	0.2	0.2	0	1000
10					1	1		
11					5	5		
12				3	0.2	0.2		
13					1	1		
14				10	0.2	0.2		
15					1	1		
16	Partition Flow			8	0.6	.25	.5	1
17					.714	.428	.544	1.34
18					.943	.886	.783	.797

Table 1. Flow Fields Predicted by the PFT.

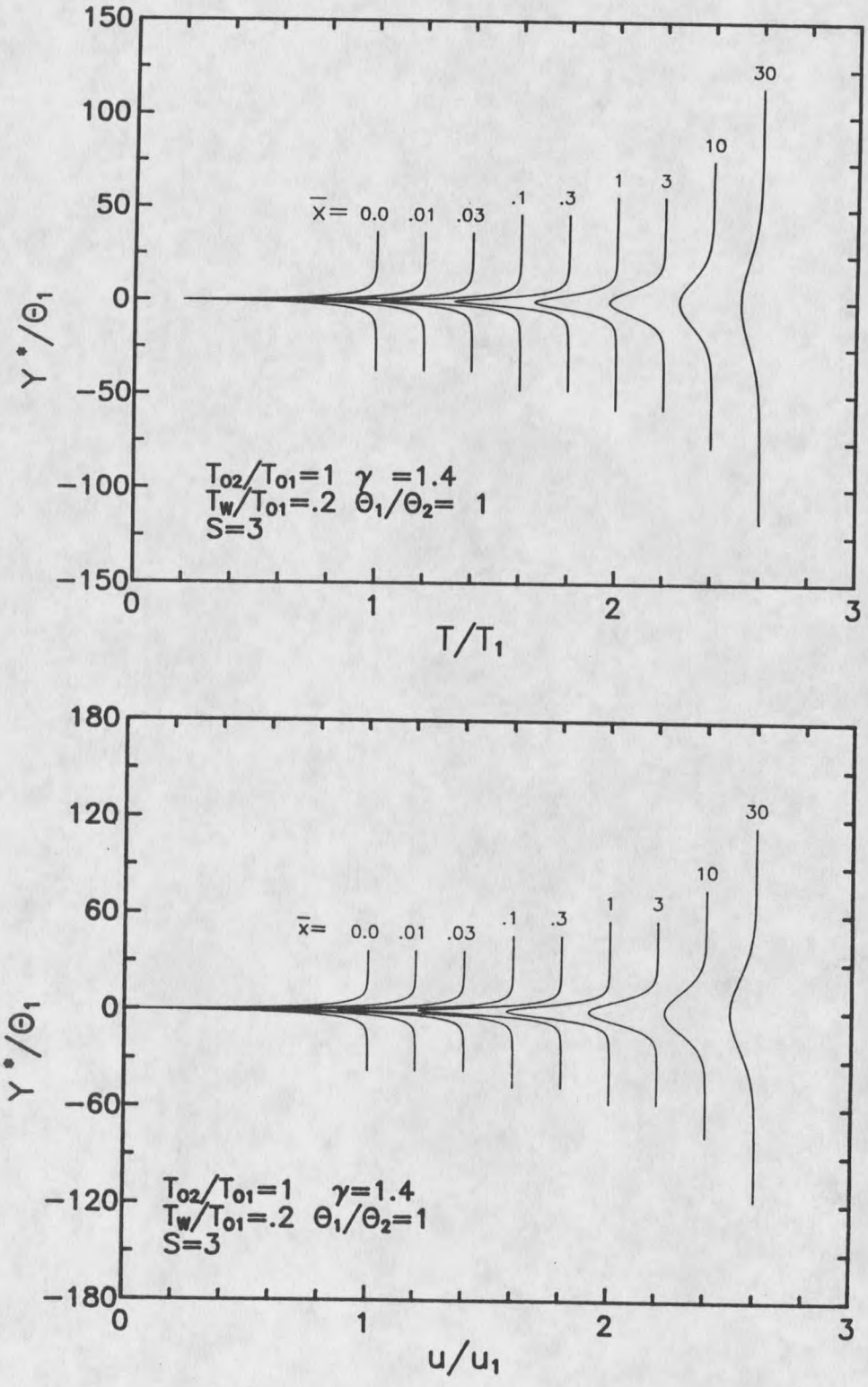


Figure 4. Flow in the symmetric low-speed wake of a cooled plate (Case 1).

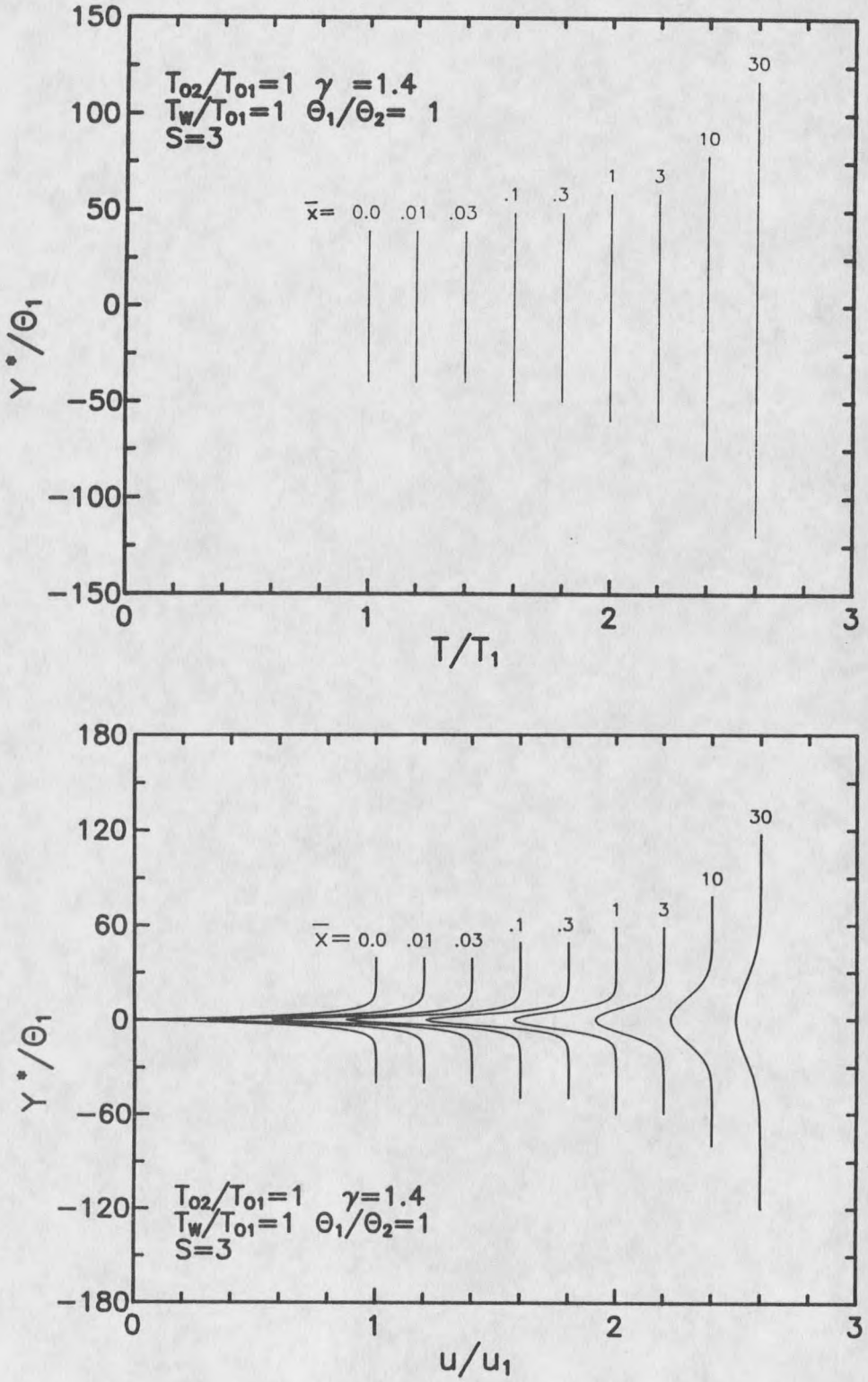


Figure 5. Flow in the symmetric low-speed wake of an adiabatic plate (Case 2).

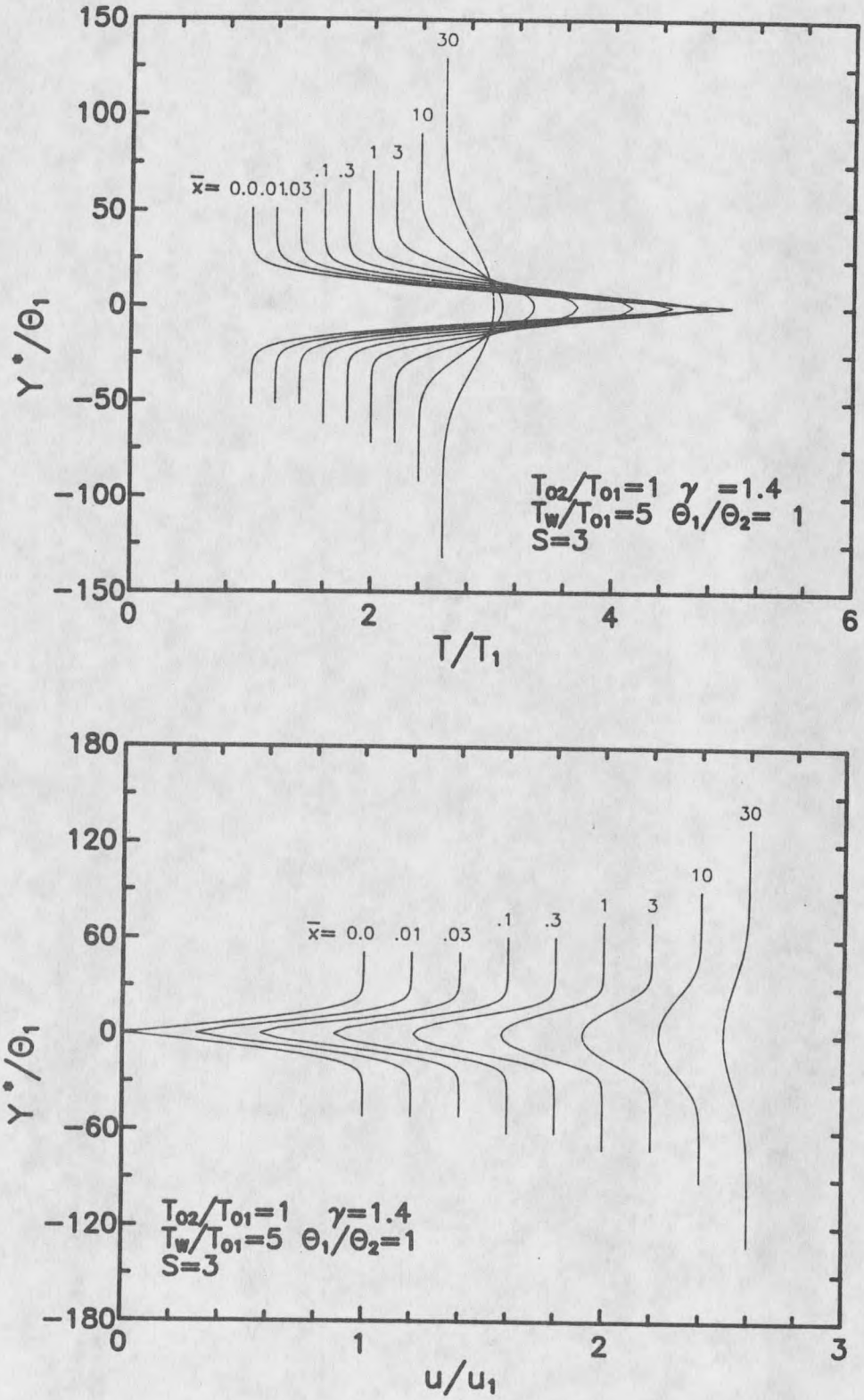


Figure 6. Flow in the symmetric low-speed wake of a heated plate (Case 3).

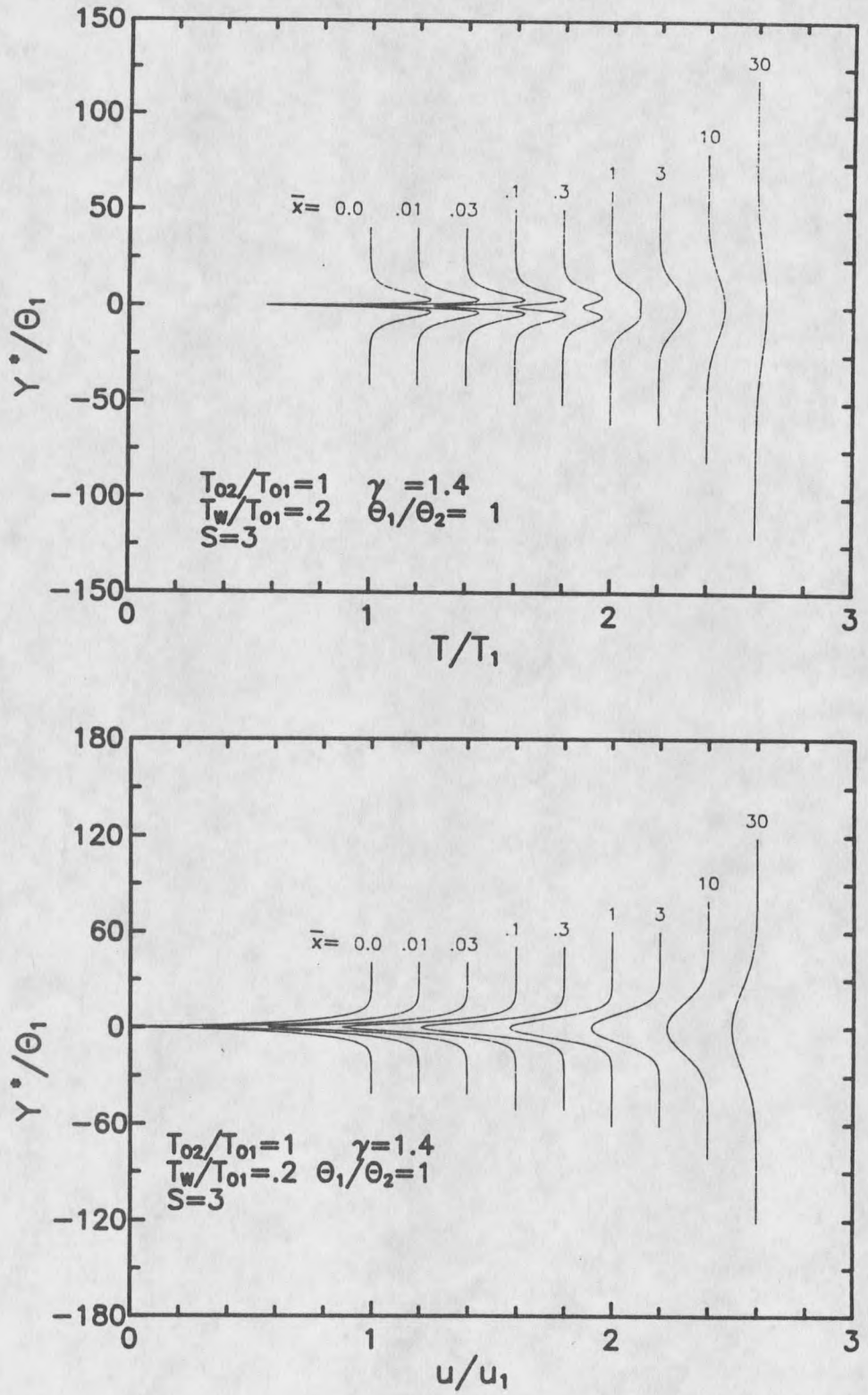


Figure 7. Flow in the symmetric supersonic wake of a cooled plate (Case 4).

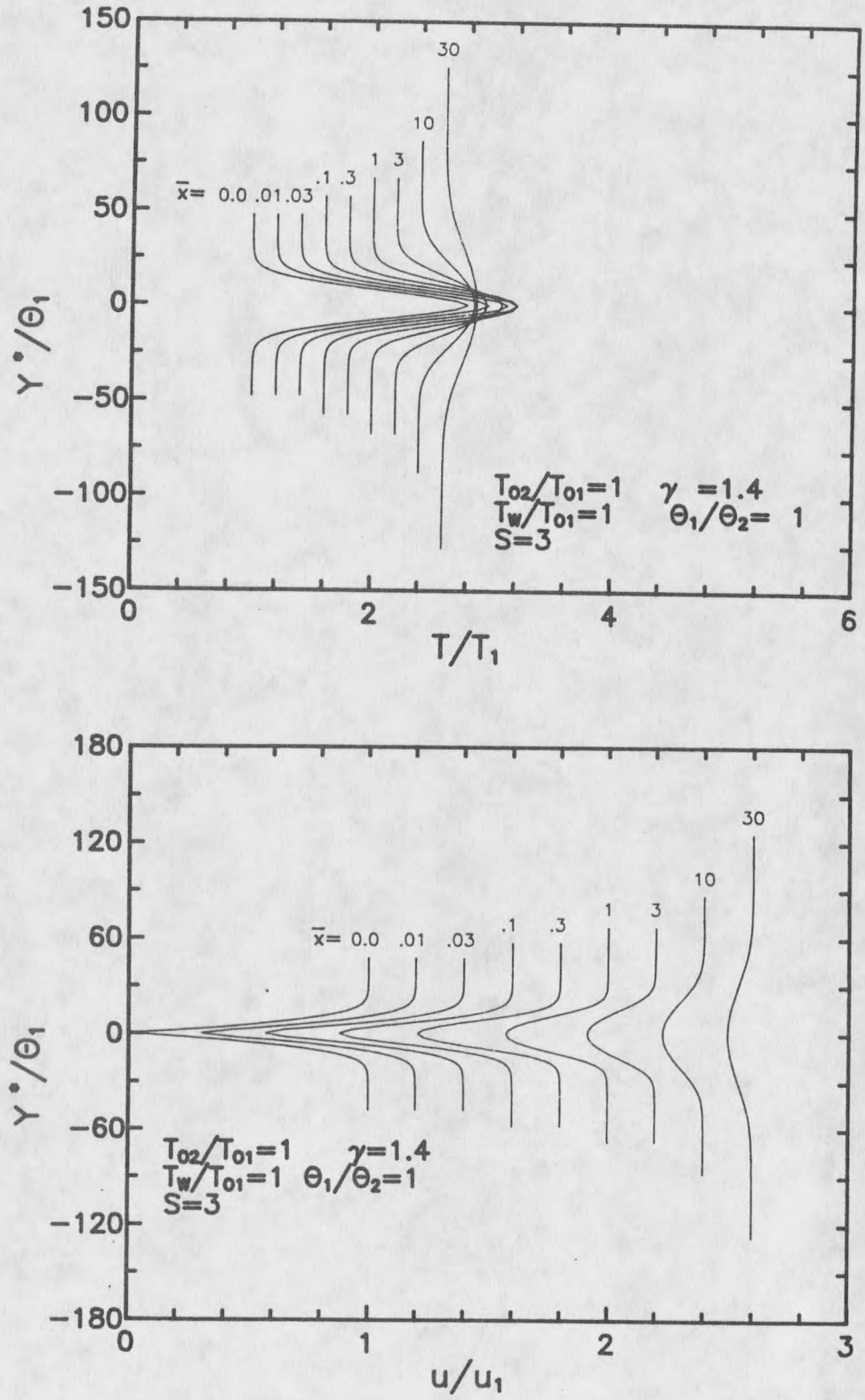


Figure 8. Flow in the symmetric supersonic wake of an adiabatic plate (Case 5).

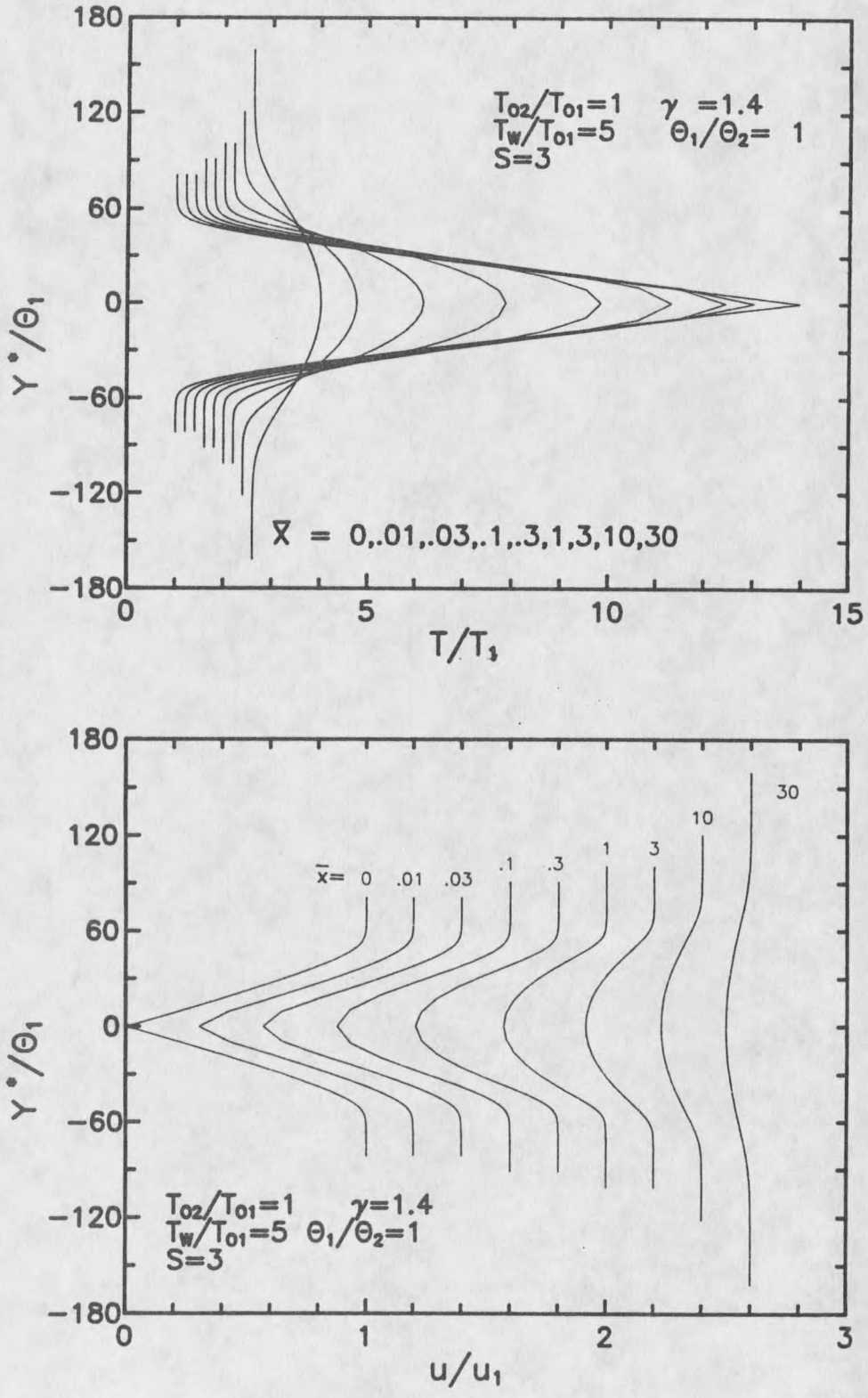


Figure 9. Flow in the symmetric supersonic wake of a heated plate (Case 6).

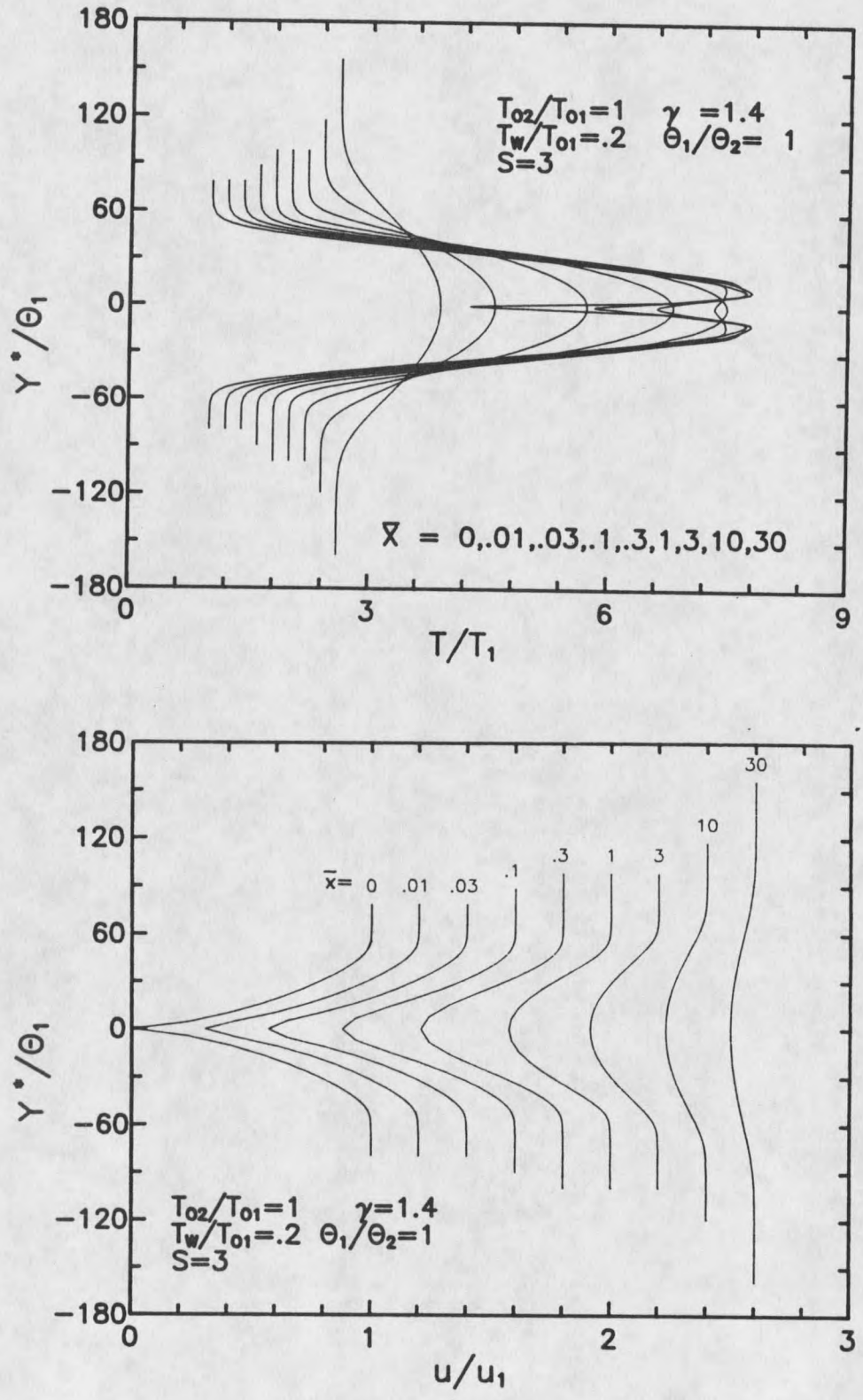


Figure 10. Flow in the symmetric hypersonic wake of a cooled plate (Case 7).

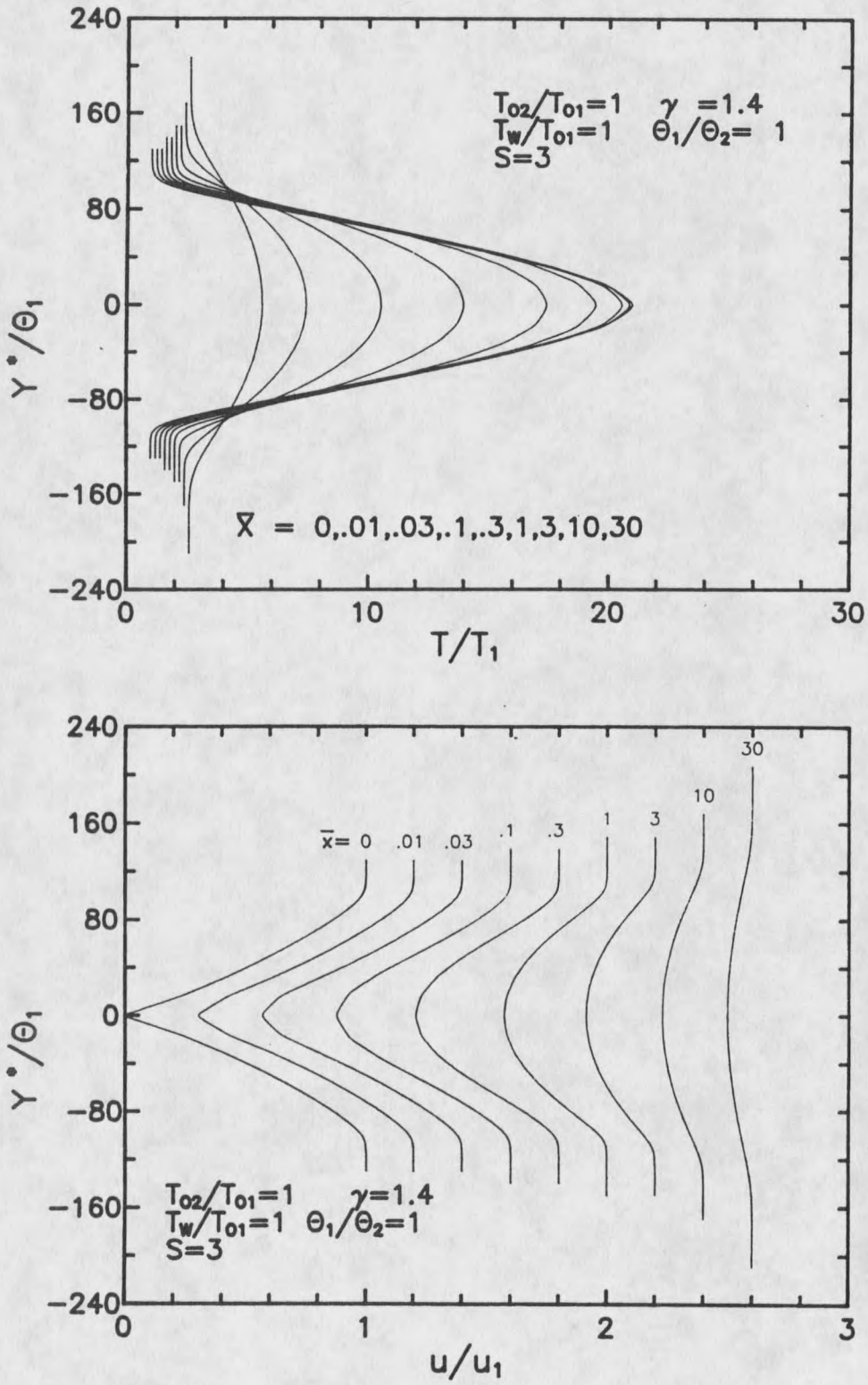


Figure 11. Flow in the hypersonic wake of an adiabatic plate (Case 8).

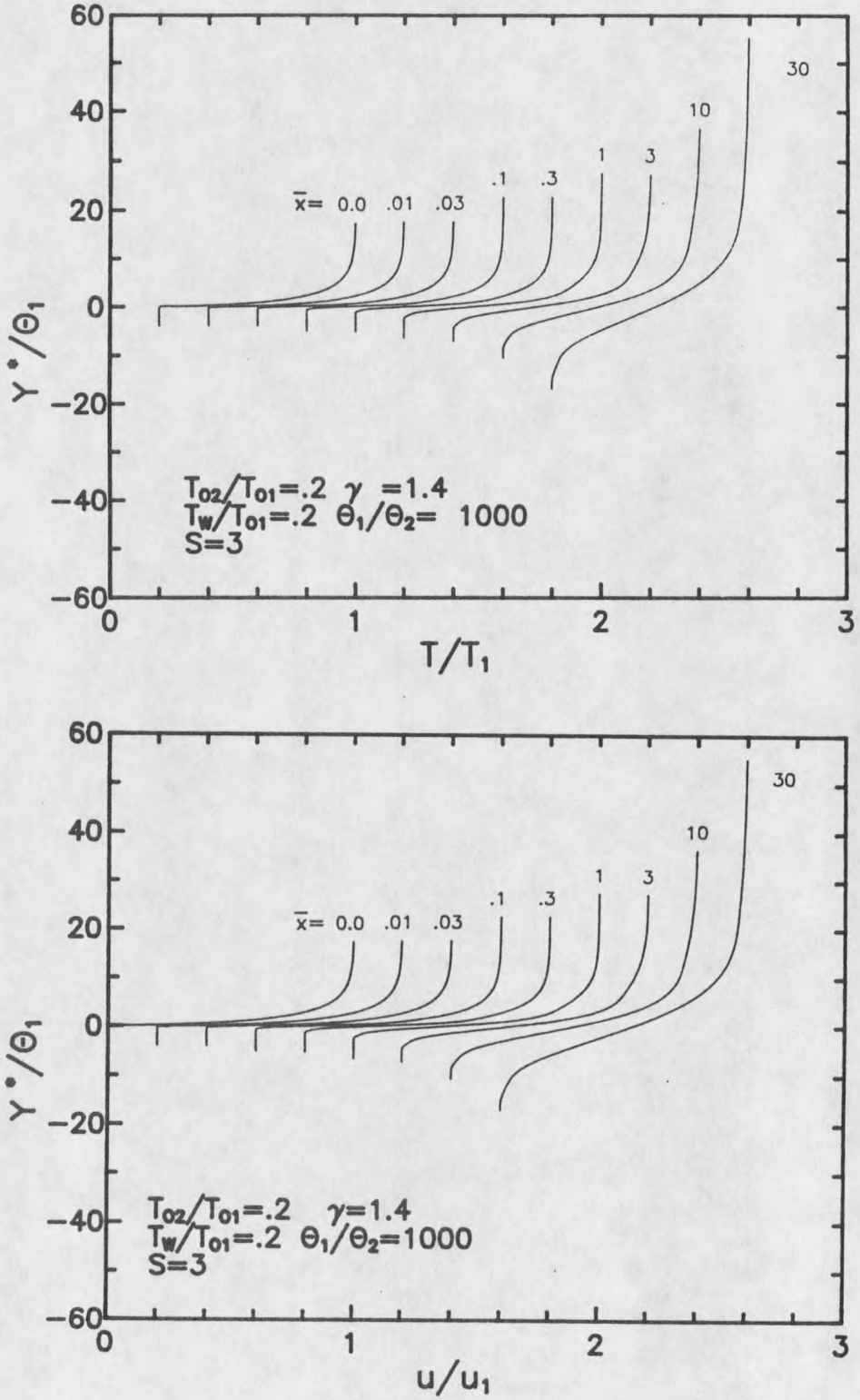


Figure 12. Low-speed base flow; cooled partition and stagnant region (Case 9).

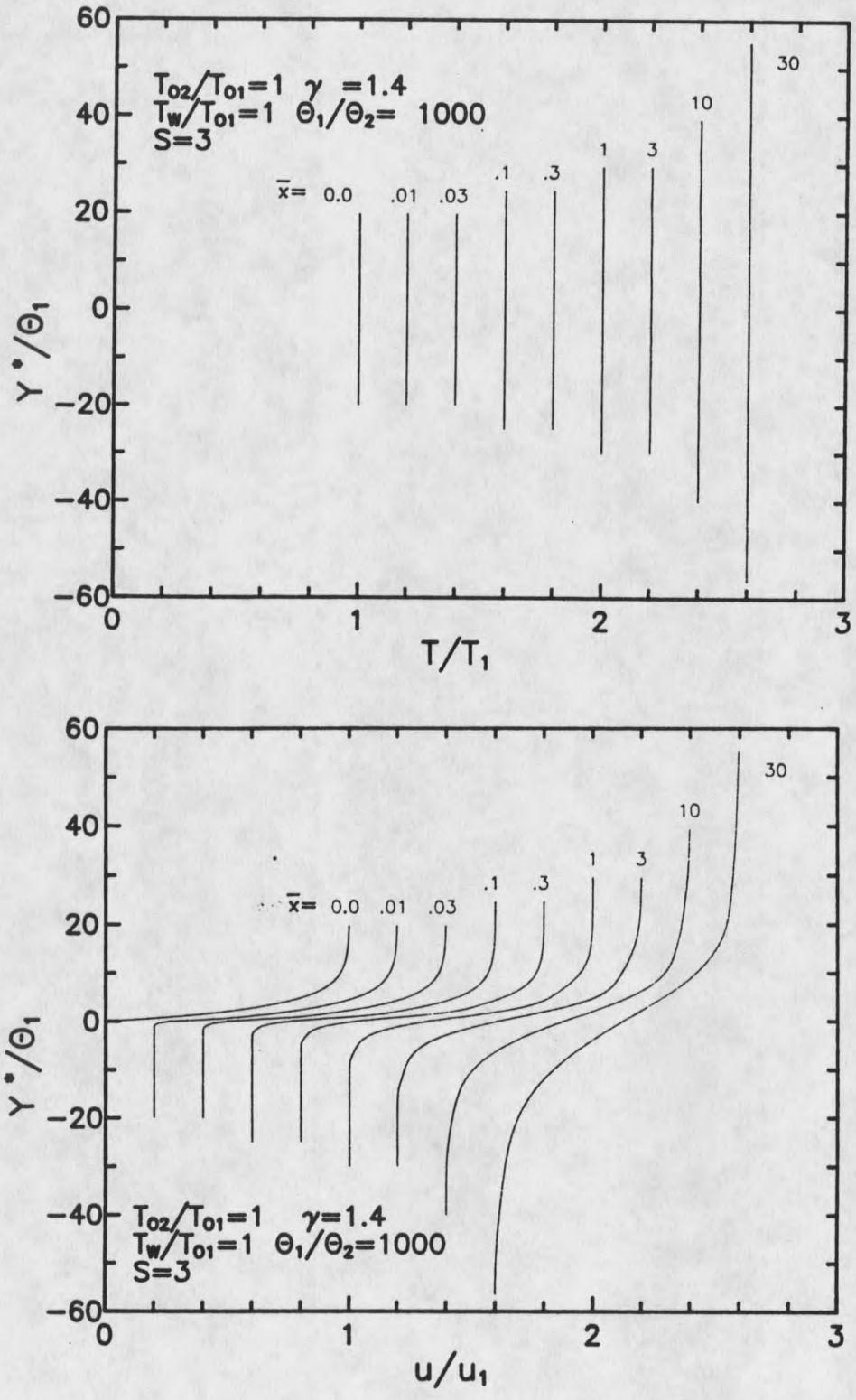


Figure 13. Low-speed base flow; adiabatic partition and stagnant region (Case 10).

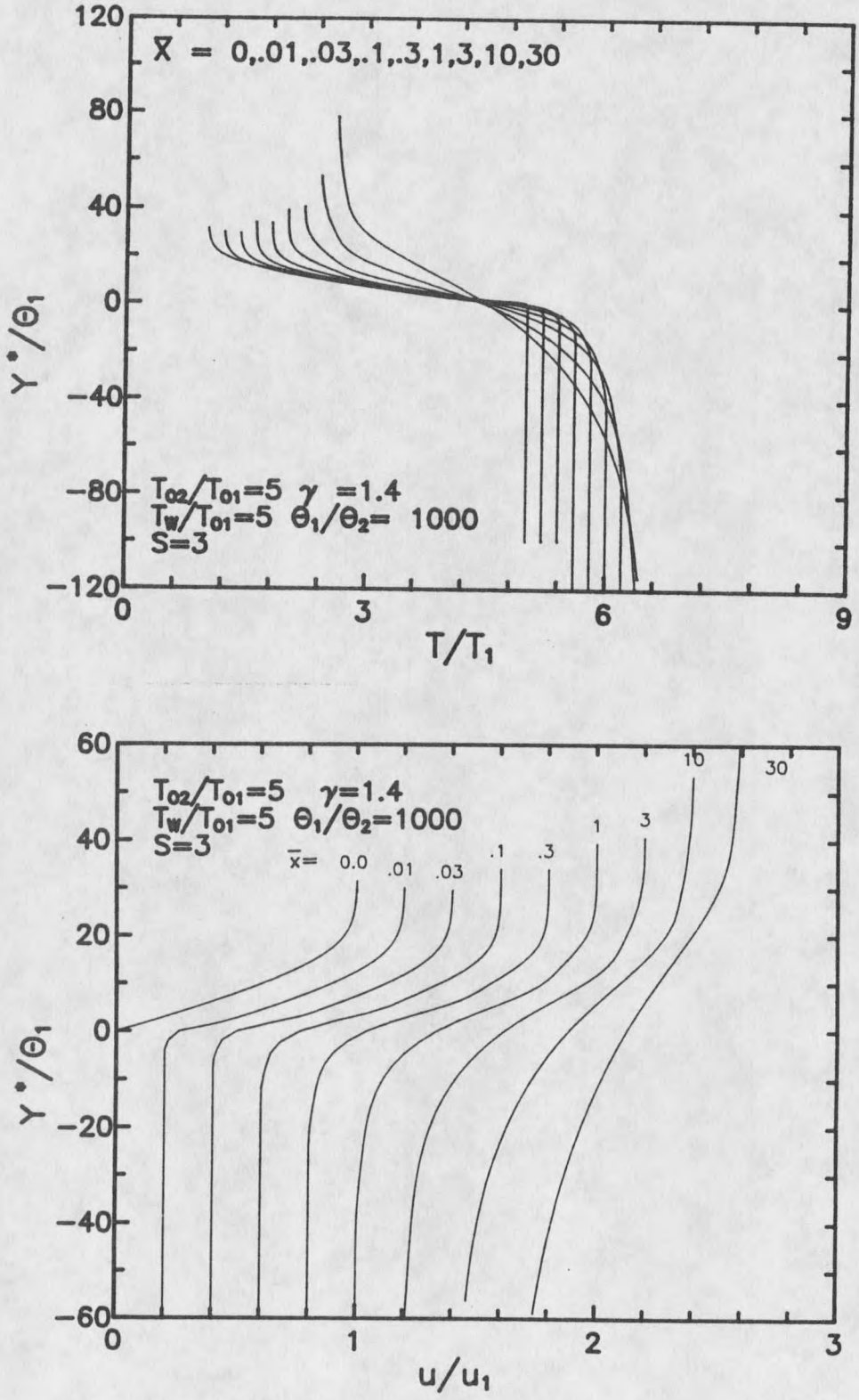


Figure 14. Low-speed base flow; heated partition and stagnant region (Case 11).

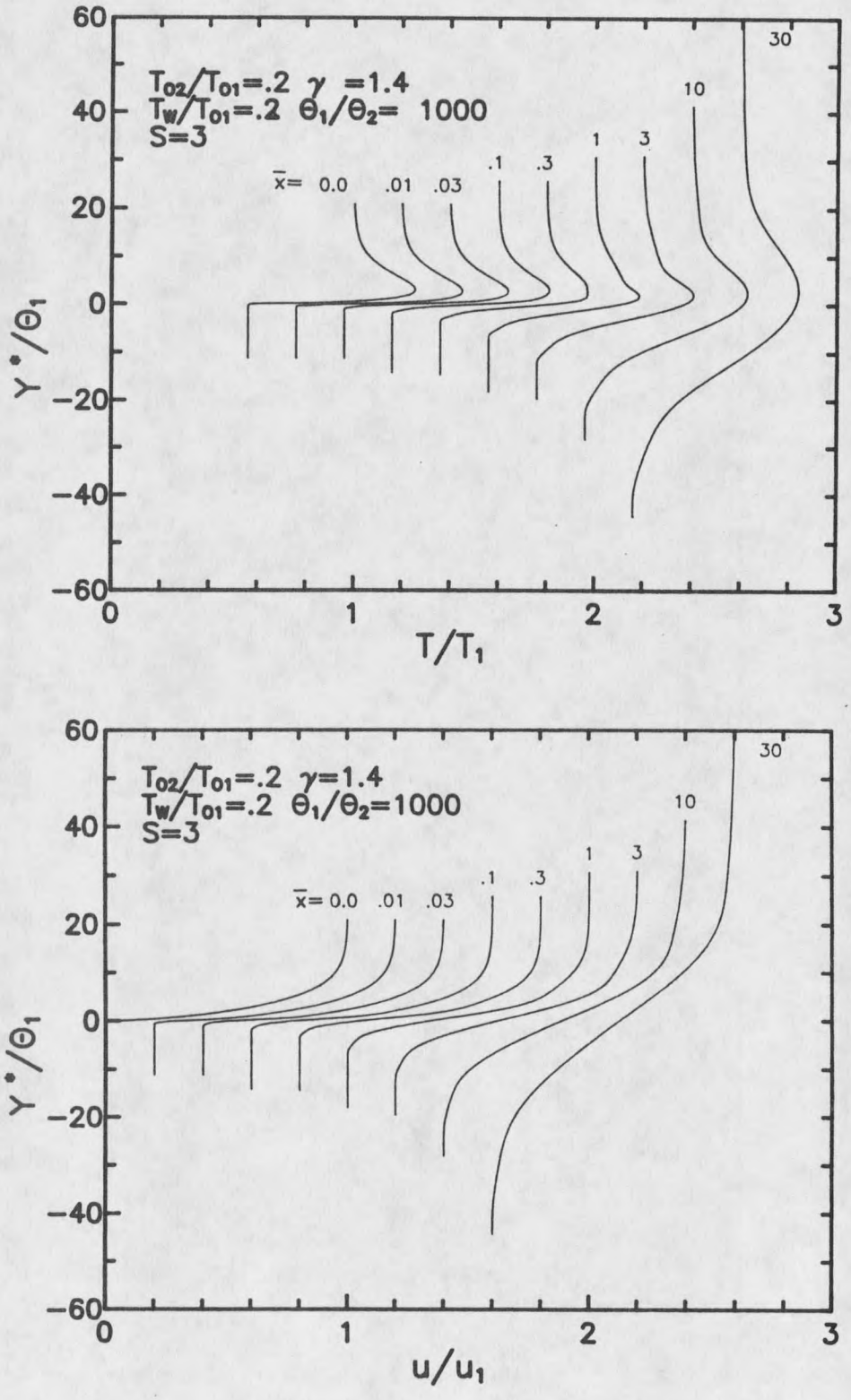


Figure 15. Supersonic base flow; cooled partition and stagnant region (Case 12).

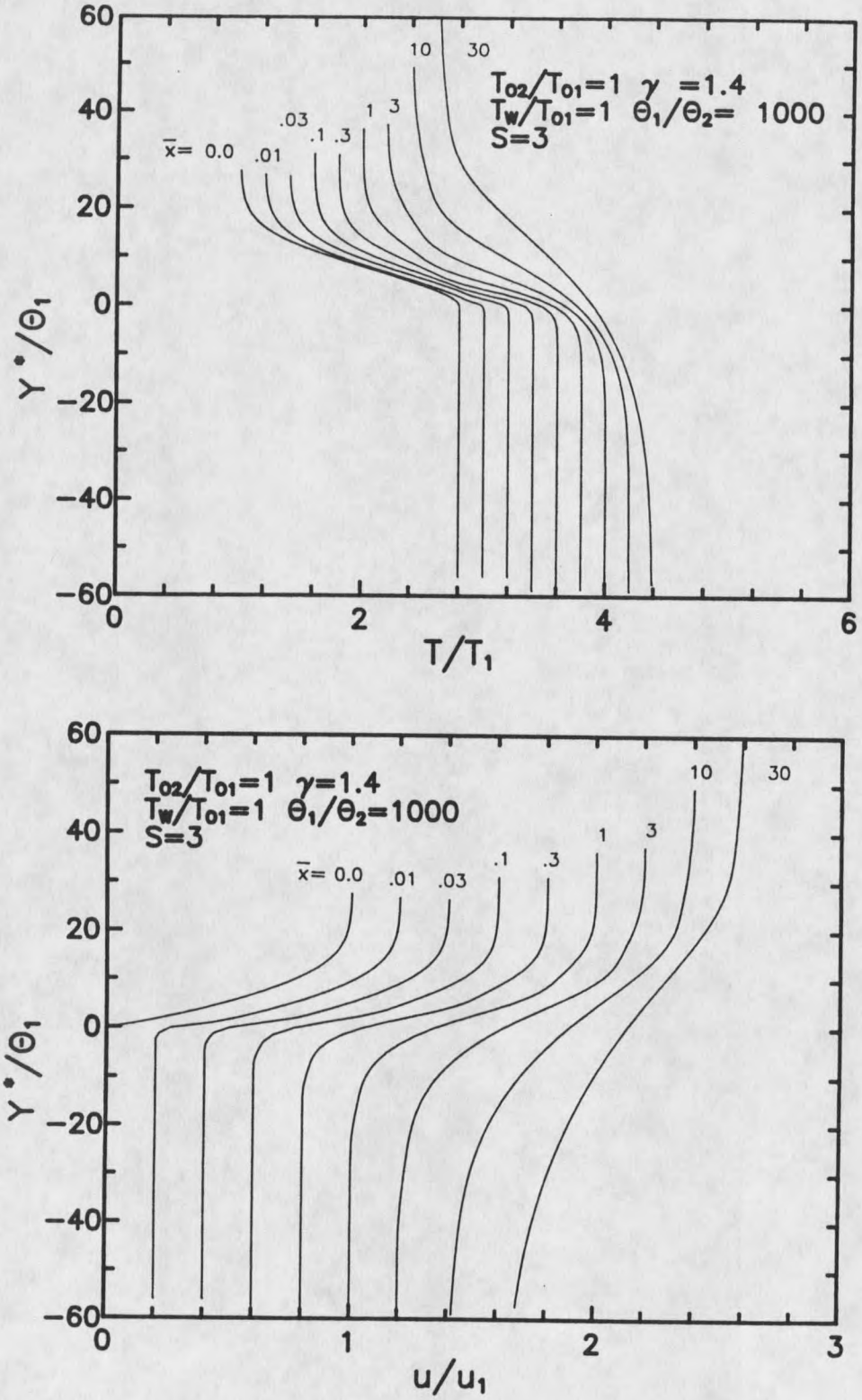
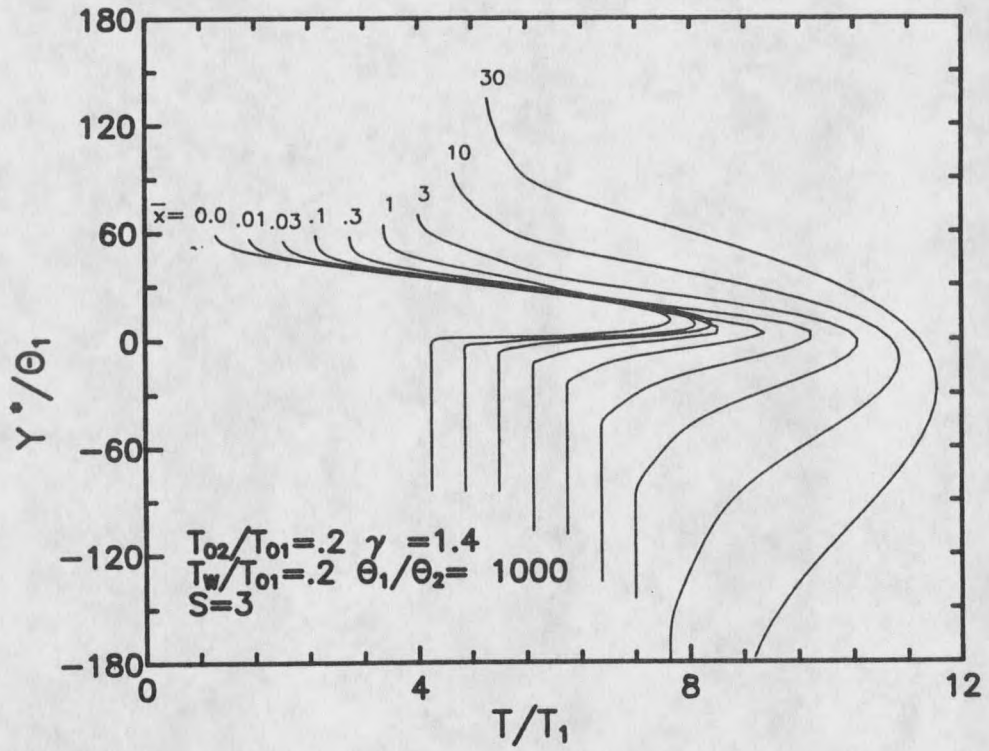


Figure 16. Supersonic base flow; adiabatic partition and stagnant region (Case 13).



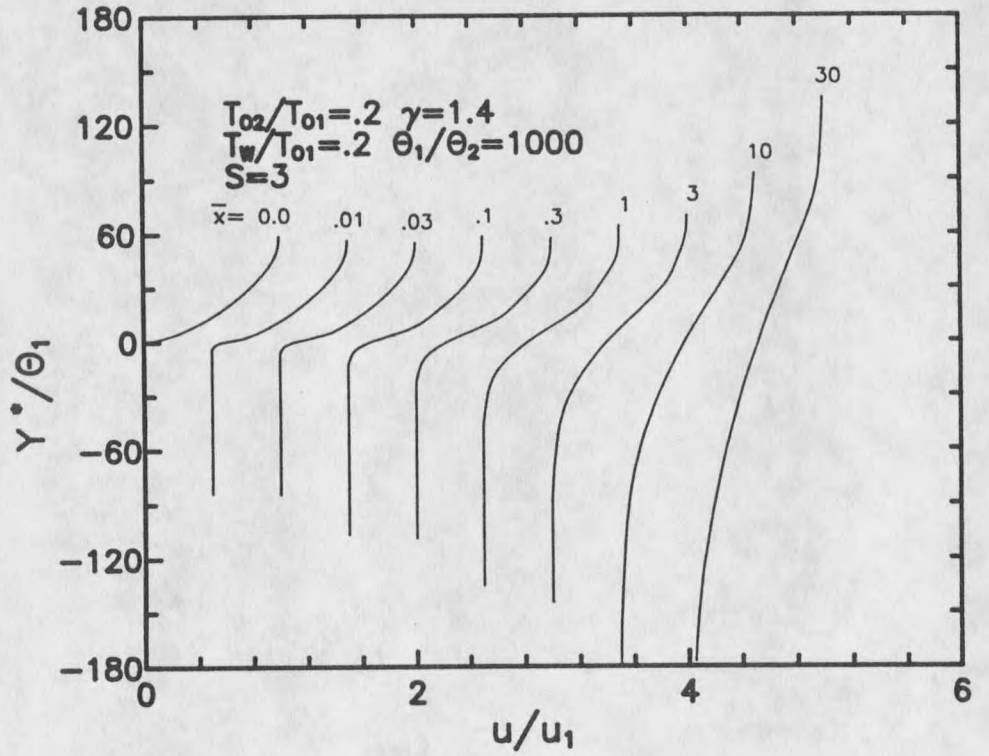


Figure 17. Hypersonic base flow; cooled partition and stagnant region (Case 14).

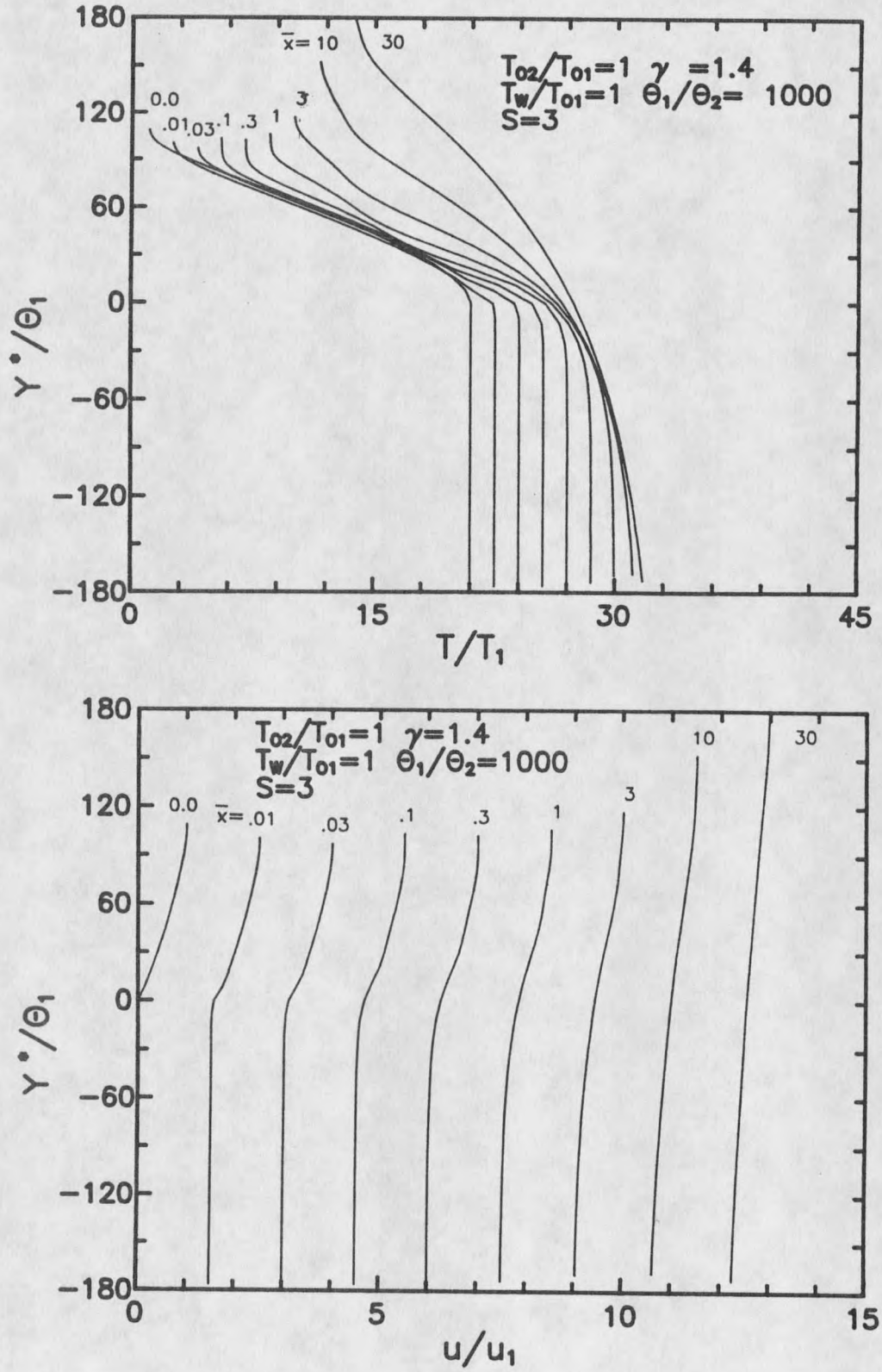


Figure 18. Hypersonic base flow; adiabatic partition and stagnant region (Case 15).

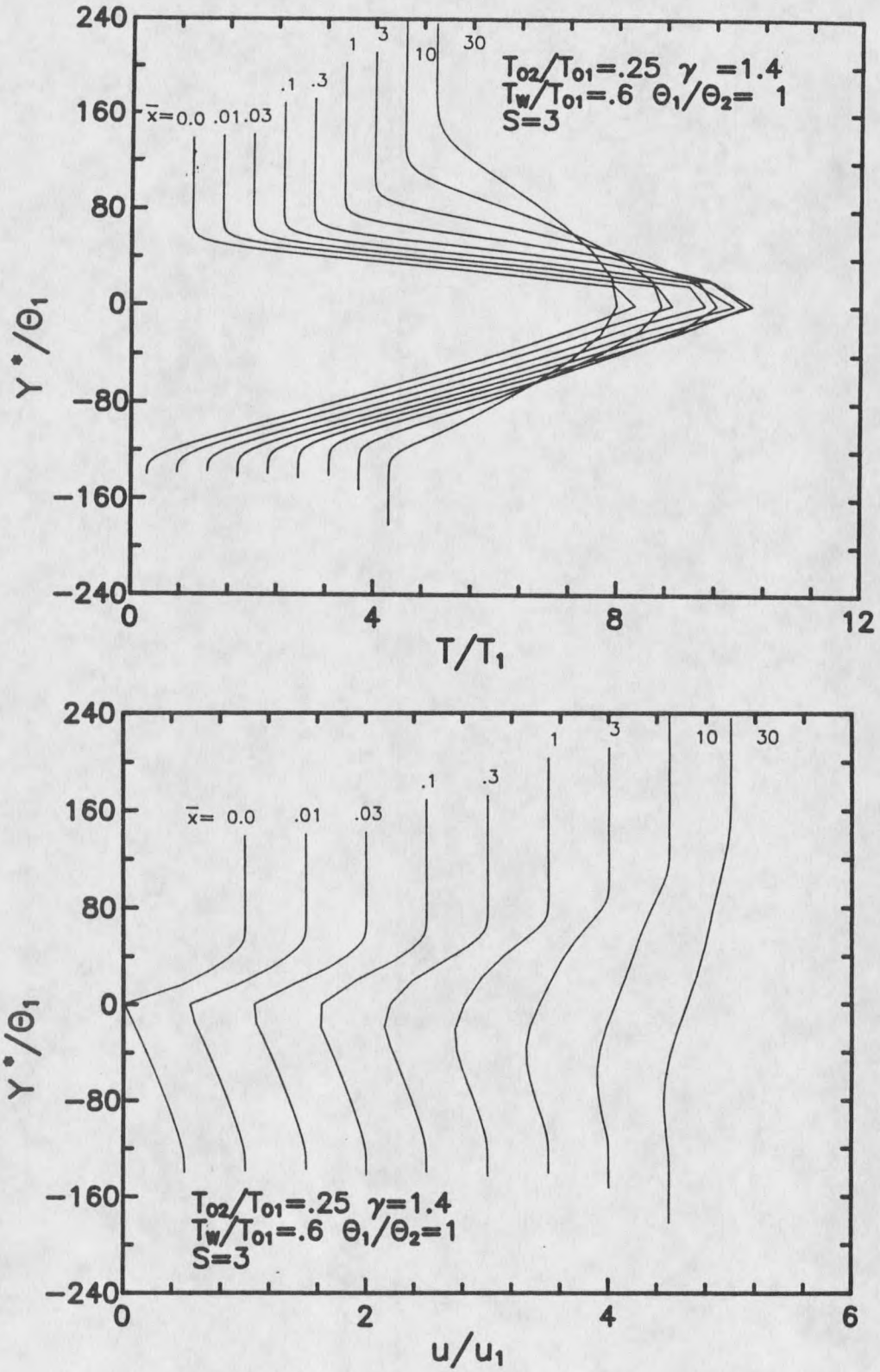


Figure 19. Hypersonic film-cooling example; cooled low-speed flow and equal boundary layer thicknesses (Case 16).

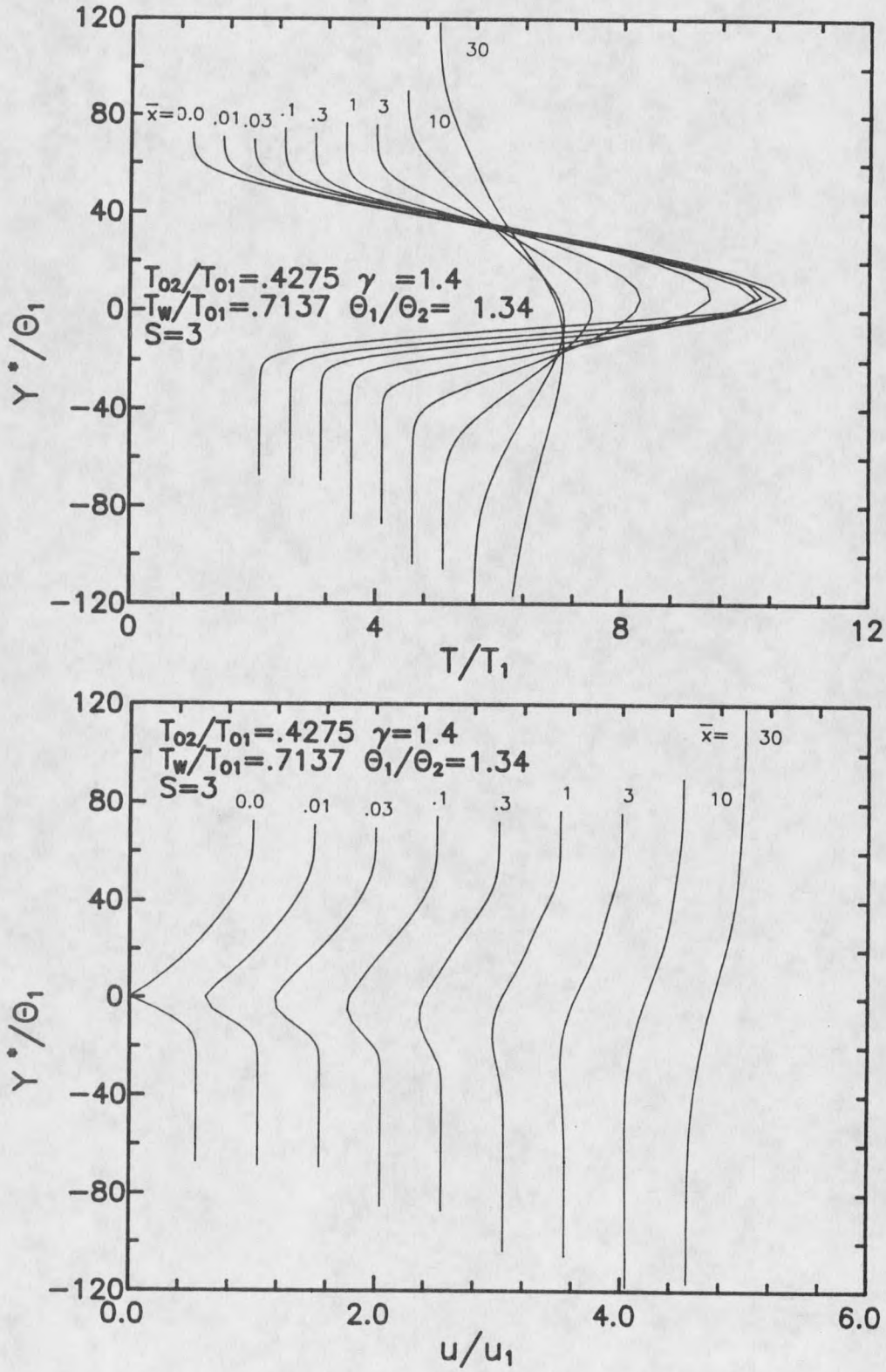


Figure 20. Typical hypersonic flow cooling example: moderately cooled slow stream (Case 17).

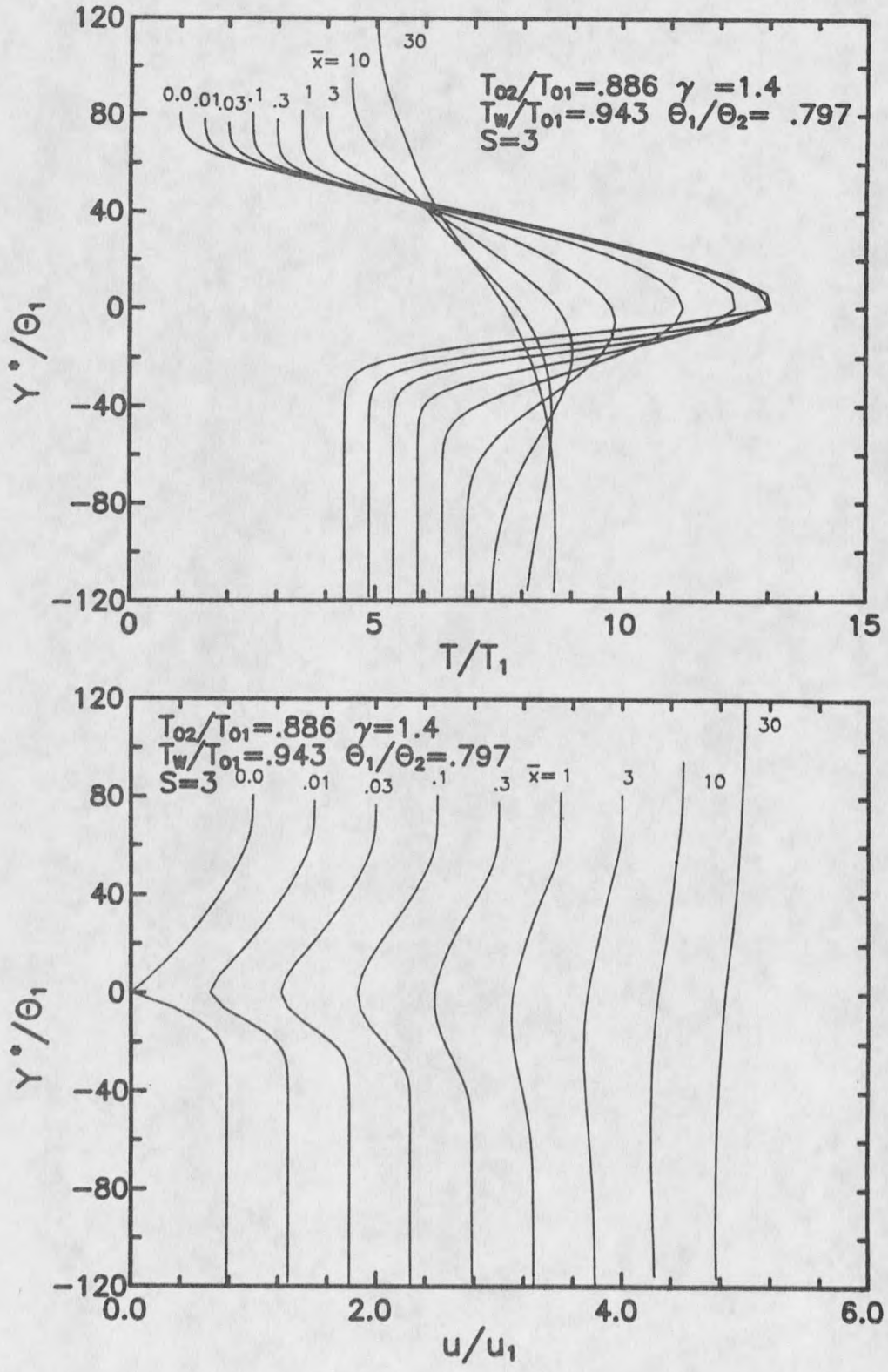


Figure 21. Hypersonic film-cooling example: insufficiently cooled slow stream (Case 18).

CHAPTER 4

TESTS OF THE PFT

Overview

It is vital for any theory to be rigorously tested by all means available to verify its ability to perform as desired. This work will compare the PFT with numerical work and experimental wake flow and partition flow data. The numerical and wake results will be presented briefly due to the detailed references already available on these results. The partition flow results were extensively investigated.

Comparison with Wake Flow Results

Two experimental sets of data were compared with an earlier version of the PFT. This earlier version of the PFT contained only the wake component, not the free shear layer. Sato and Kuriki [18] showed good agreement with the PFT but only two points were available. Demetriades' [19] experimental data also showed good agreement. However in both cases only the zero streamline velocity was compared. The details of these experiments can be found in their references, and their comparison with the PFT is shown in [12].

Comparison with Numerical Results

The PFT was compared with two different numerical results. In both cases as in the wake experimental results only the zero streamline velocity was compared.

In the first case the PFT was compared against the incompressible wake computations of Goldstein [6] with excellent results. Secondly, the PFT and Denison and Baum's [2] base flow computations were compared. Again agreement was very good. The details of these numerical comparisons can be found in [12].

Comparison with Partition Flow Results

Supersonic Laminar Mixing

Experimental Setup. The experiment which is provided by [13] consisted of two streams of air separated by a splitter plate as shown in Figure 22. Mach numbers for the fast side stream ranged from 2.76 to 2.9 while the slow side Mach number ranged from 1.87 to 2.29.

Mean flow measurements at the trailing edge were taken by a pitot probe to determine the boundary layer profile. A second pitot probe was utilized to take mean flow measurements of the free shear layer. A Schlieren Optical System along with a hot-film anemometer determined transition to turbulence. Static pressure and total temperature were also recorded at each point in the profiles. Eight velocity profiles downstream of the splitter plate were recorded. Transition to turbulence was determined to occur at approximately 1.8 inches downstream of the trailing edge. Therefore only four of the eight profiles were laminar and considered usable in a comparison with the PFT.

The actual data and computer codes used to determine the velocity profiles were not found in usable format. The electronic signals (counts) for the total and static pressures and the total temperature had to be converted from archaic format specific to an Intertek Superbrain microcomputer to generic BASIC format usable on any late model microcomputer.

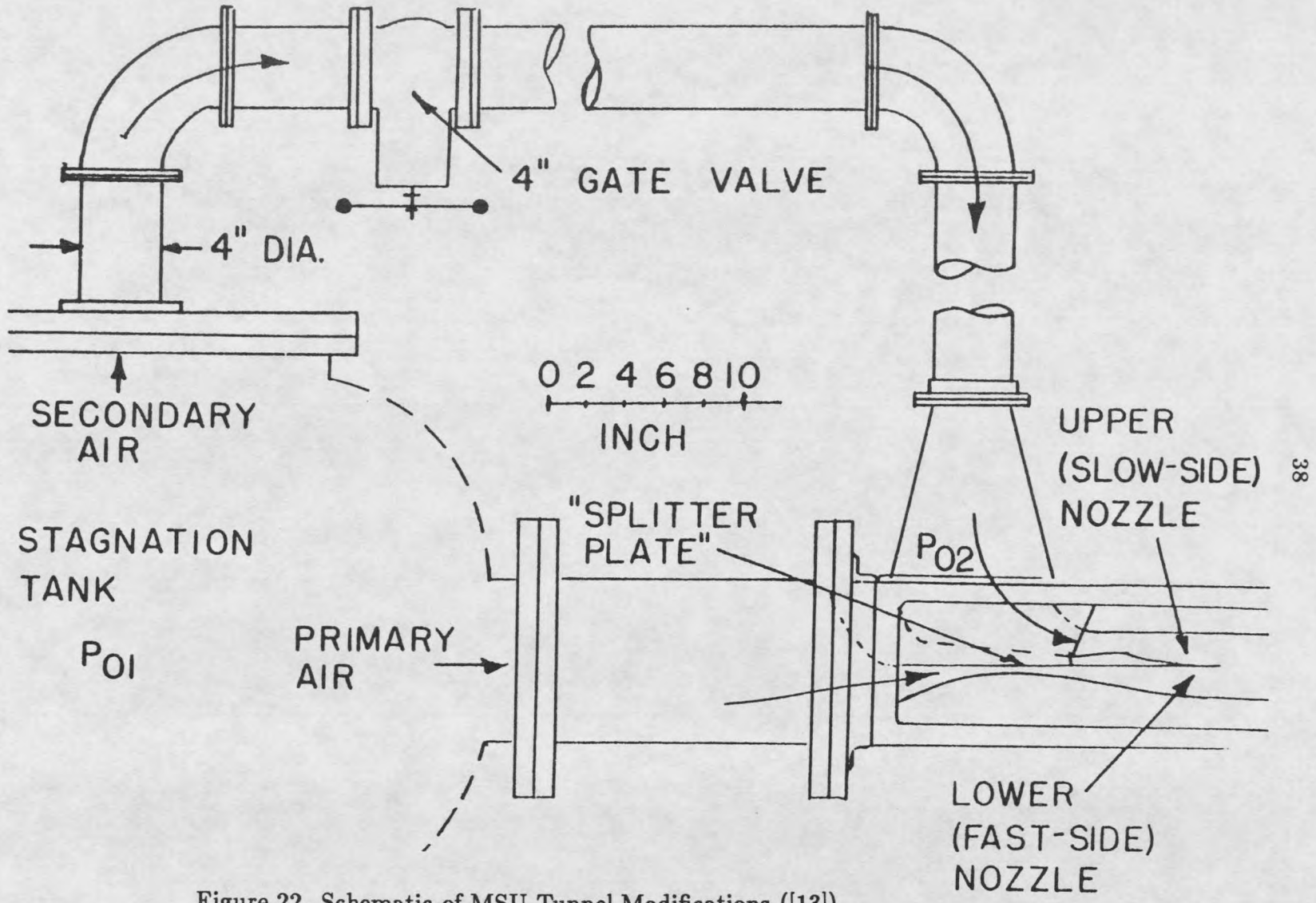


Figure 22. Schematic of MSU Tunnel Modifications ([13]).

Computer codes [20] utilizing the counts to determine the boundary layer and the velocity profiles also needed to be converted. Additionally the syntax used by the codes had to be manually updated from an outdated form of BASIC to current QUICKBASIC standards.

To verify that this process had been accomplished correctly the trailing edge boundary layers of the fast and slow side were determined and plotted as shown in Figure 23. This figure is an exact duplication of Figure 27 in Brower's work [20] thereby verifying the updating process. This procedure was carried out on several of the velocity profiles to ensure the velocity profile code was also correctly converted.

The comparison of these supersonic mixing data with the PFT was carried out in the following manner:

1. A direct comparison was made of the original supersonic data with the current PFT. The stretching parameter S was determined from the measured trailing edge boundary layer.
2. Any differences between the experimental data and the PFT were explained.
3. The momentum thickness (θ_1) of the supersonic data was recalculated in order to match the minimum velocities of the PFT and the data.
4. The supersonic profiles were recalculated with the revised θ_1. A new S based on the new trailing edge velocity profile was determined.
5. The updated supersonic velocity profiles were compared against the PFT for a second time.

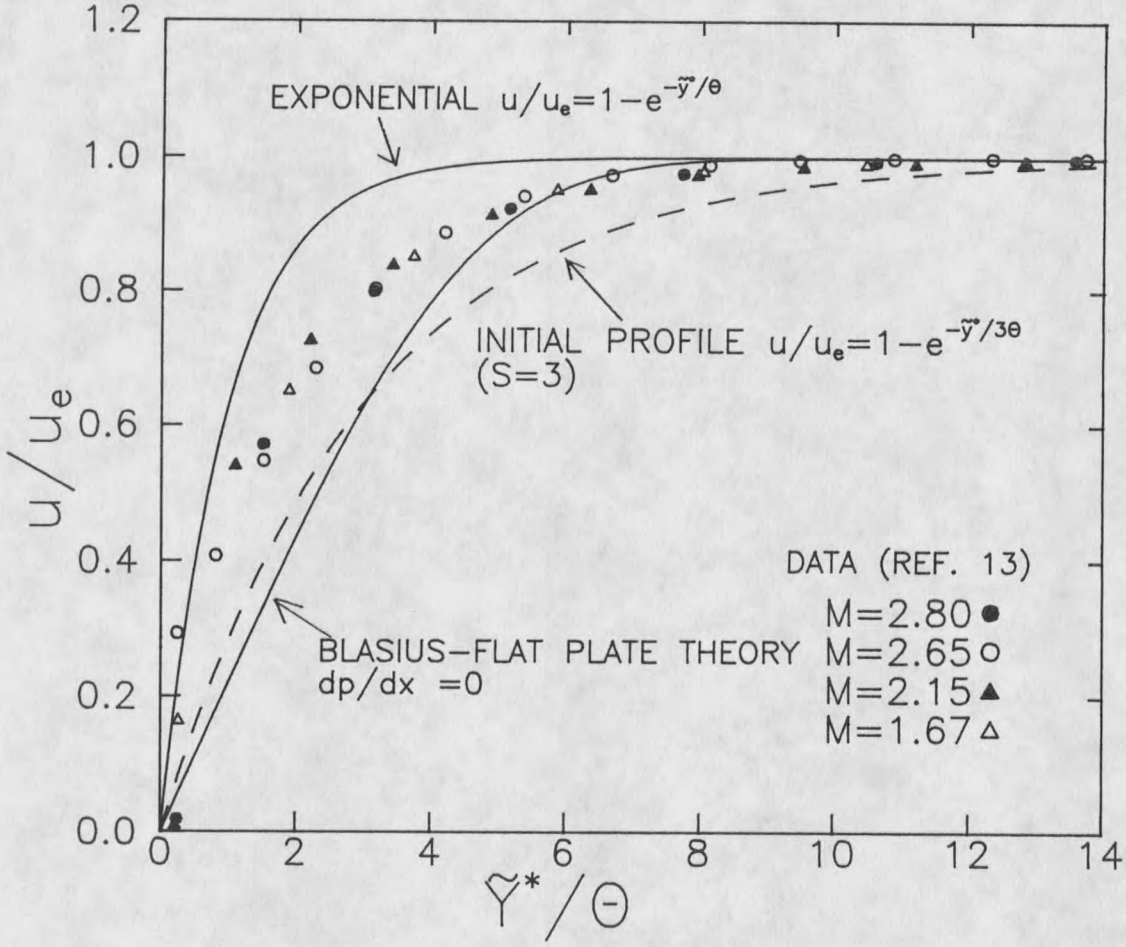


Figure 23. Verification of Data/Code Reinstallation.

Trailing Edge Boundary Layer. The initial conditions for the data and the PFT must be the same if a comparison is to be made. Therefore it was necessary to determine the stretching factor S that causes the exponential to fit the trailing edge velocity profile. Figure 24 shows the curvefit of the boundary layer. An S of 1.8 is an acceptable fit.

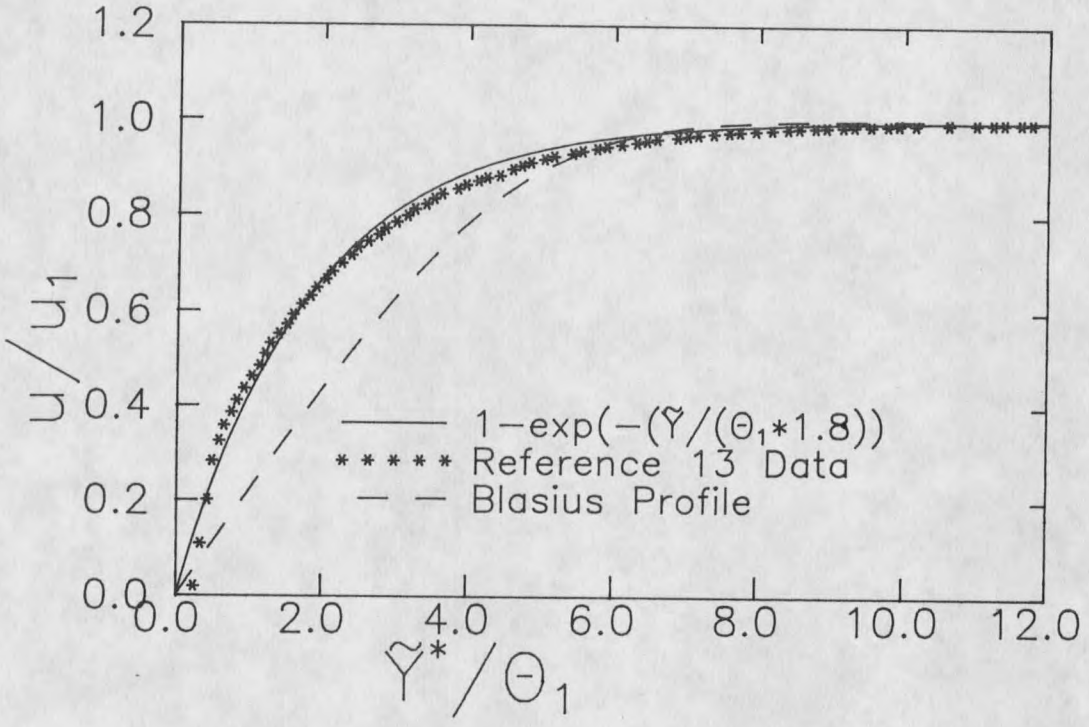


Figure 24. Initial Determination of S for Supersonic Data.

Comparison of Original Supersonic Velocity Profiles and the PFT. The following parameters from the supersonic data runs were used in the PFT to solve for the velocity profiles:

$M_1 = 2.9$ $\qquad$ $T_{02}/T_{01} = .98$

$\theta_1/\theta_2 = .809$ $\qquad$ $T_W/T_{01} = 1$

$\gamma = 1.4$ $\qquad$ $u_2/u_1 = .893$

$S = 1.8$

The Mach number and the velocity ratio stated above varied slightly from run to run.

The resulting minimum velocities from the PFT were compared with the minimum velocities of the data at various downstream positions. Figure 25 shows the disparity between the theoretical results and those of the experimental data.

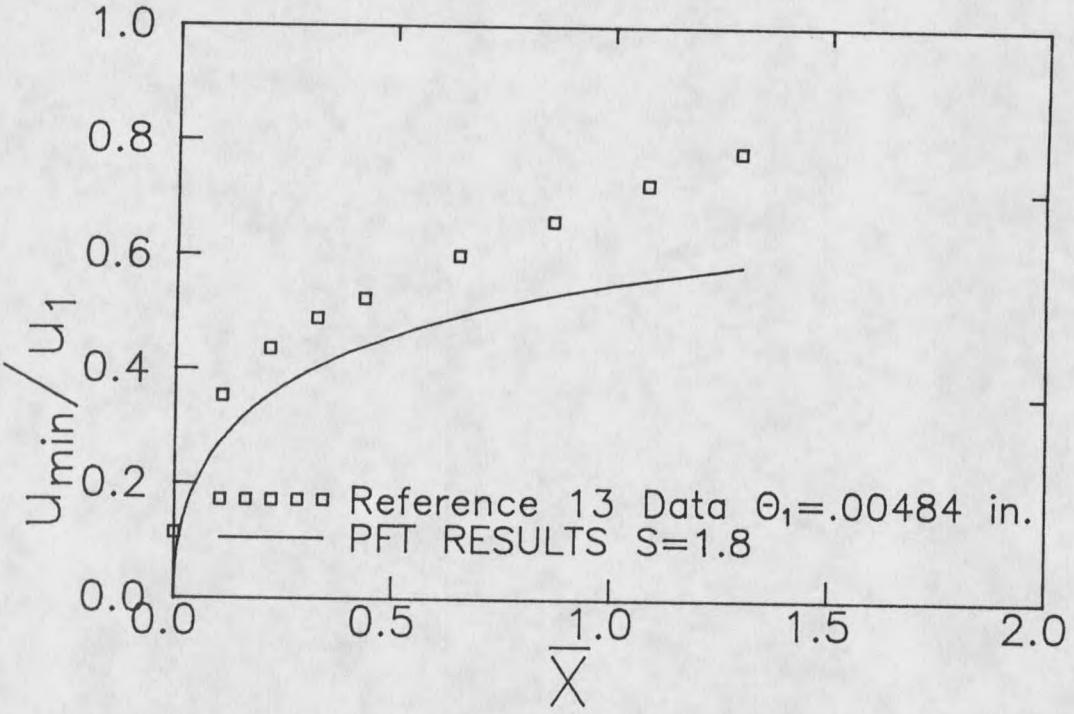


Figure 25. Comparison of PFT with Experimental Supersonic Minimum Velocities.

Next the complete profiles were computed and plotted in Figures 26 through 29. As the profiles develop downstream the PFT shows a thicker profile than the experimental profiles and as expected the minimum velocities do not match.

One of the possibilities for the disparity in thickness is the assumption in the PFT of a Prandtl number of 1. As the Prandtl number decreases the velocity profile thins. Since air has a Pr of .73 the recovery factor [21] could cause the profiles downstream of the trailing edge to thin and show better agreement with the experimental profiles.

Another possibility is an error in one of the parameters in the experimental data. This possibility will be investigated in the next section.

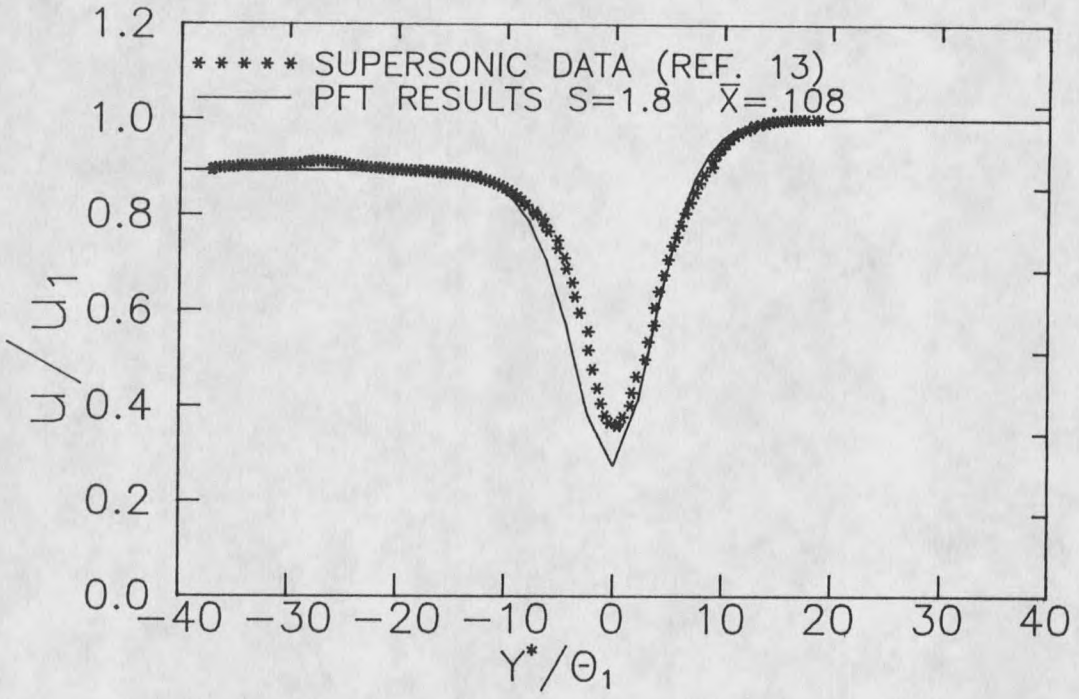


Figure 26. Comparison of PFT with Supersonic Data
$x^* = .25$ inches.

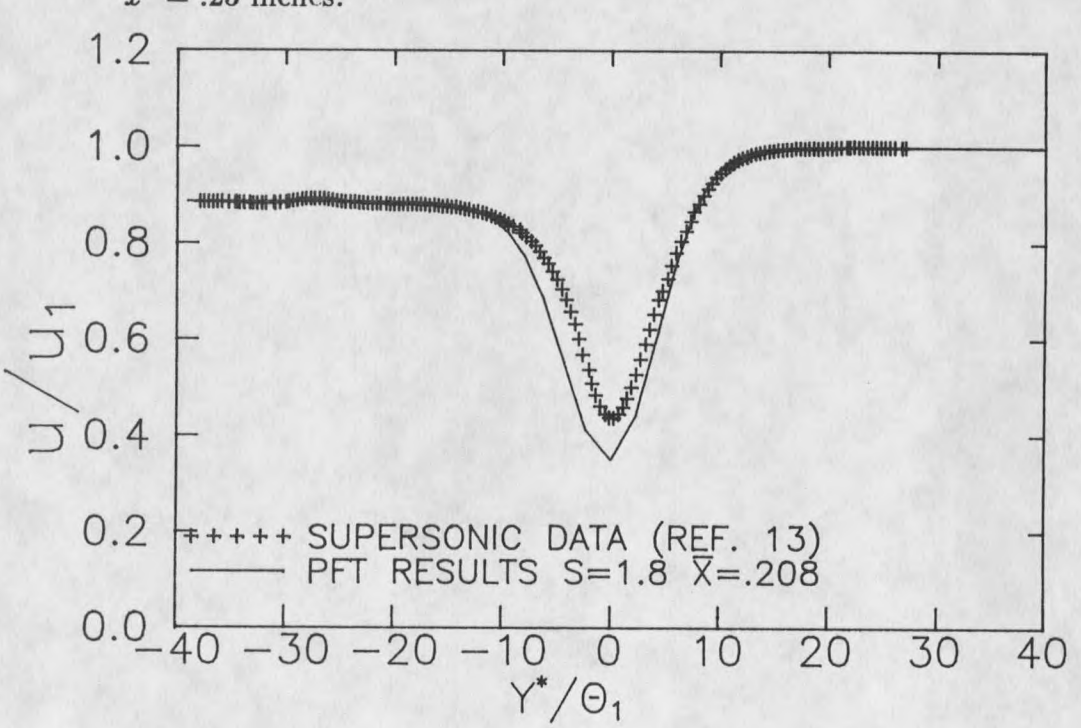


Figure 27. Comparison of PFT with Supersonic Data
$x^* = .5$ inches.

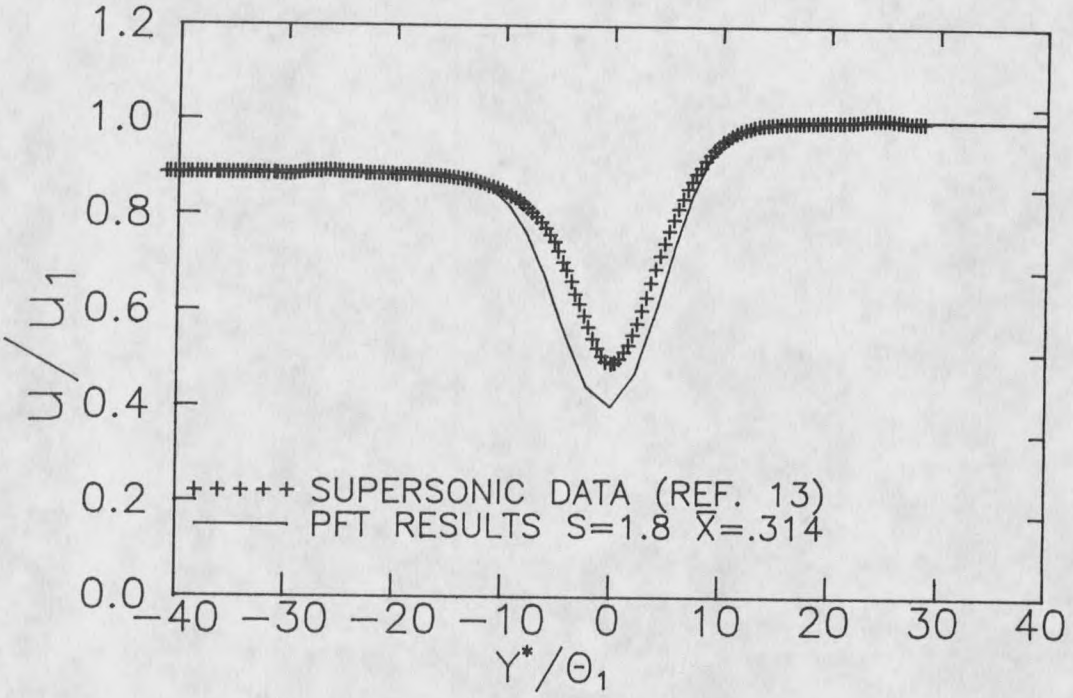


Figure 28. Comparison of PFT with Supersonic Data
$x^* = .75$ inches

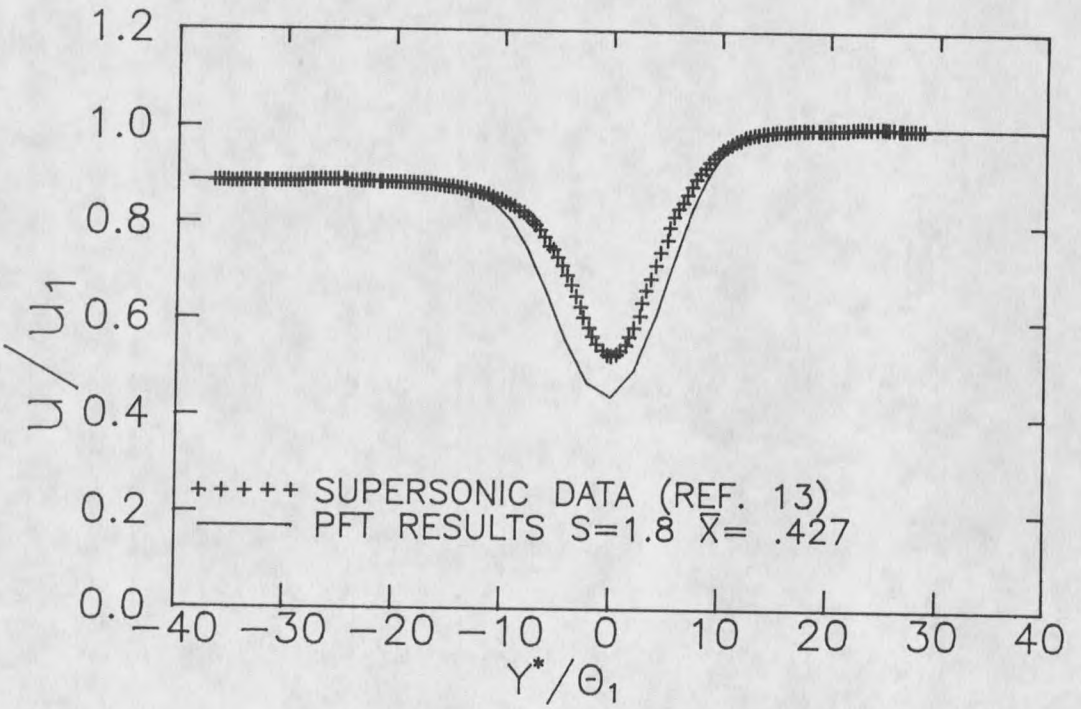


Figure 29. Comparison of PFT with Supersonic Data
$x^* = 1$ inch.

Resolution of Disparity between Supersonic Data and the PFT. Due to the differences observed in the previous four figures it was decided to determine by how much the two sets of data differed and if such a difference could be explained by an experimental error rather than a problem with the PFT. It was noticed that in Figure 25 the PFT and experimental data minimum velocities seemed to differ by a constant. This led to the decision to investigate the possibility that there was a measurement error in the momentum thickness. In earlier MSU wind tunnel tests, errors from 10 to 50 percent in momentum thickness measurements [22] have not been uncommon for measurements in very thin boundary layers. Such an error can be traced to the relative size of pitot probes to the thickness of the boundary layers being measured.

Therefore it was decided to match the minimum velocities of the experimental data with the minimum velocities of the PFT by assuming that the actual θ_1 differs from that reported by Brower [13]. The reason for using only the minimum velocities was that the stretching parameter (S) of the PFT has no effect on the theoretical minimum velocities.

This task was accomplished by iterating on the experimental minimum velocity positions by changing θ_1 which altered $\overline{x}$. The new $\overline{x}$ and the original minimum experimental velocities were then plotted against the PFT results as can be seen in Figure 30. A θ_1 of .00354 inches was observed to be the best fit. It is worth noting again that transition to turbulence was determined to occur at approximately 1.8 inches downstream of the splitter plate. Therefore in Figure 30 agreement with the PFT is not expected beyond the fifth minimum velocity point or at approximately $\overline{x} = .77$.

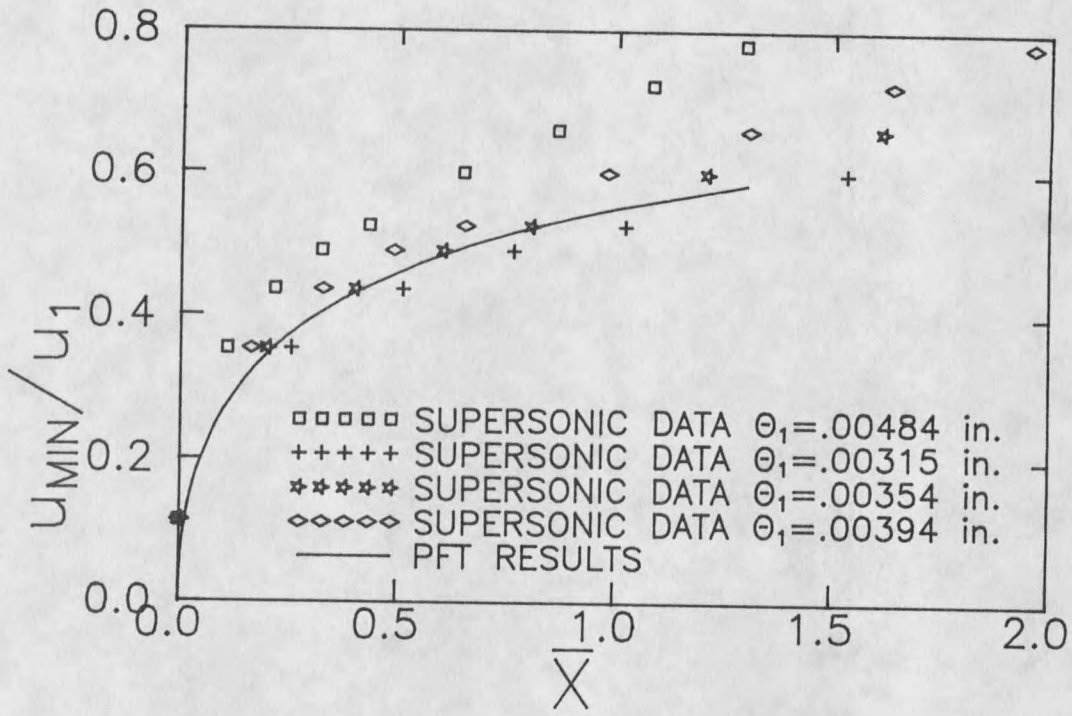


Figure 30. Iteration to Match Minimum Velocities via θ_1.

Then the trailing edge boundary layer was recalculated and a new S was determined. Figure 31 shows an S of 2.6 fits the altered boundary layer profile.

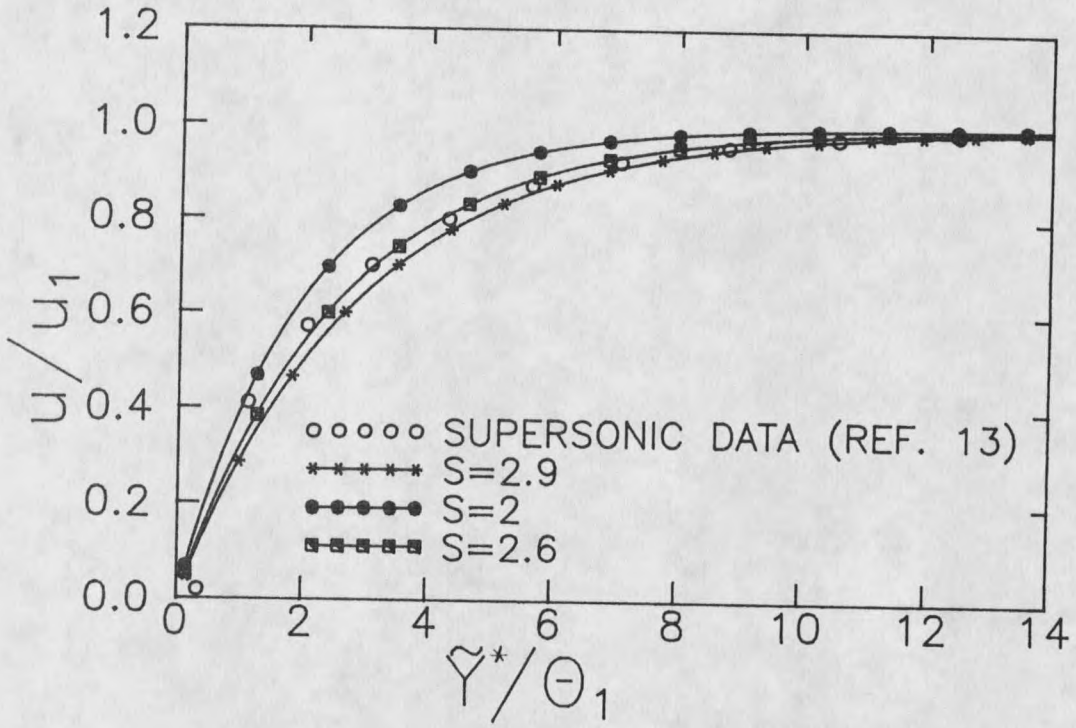


Figure 31. Determination of S for Revised Supersonic Data.

Comparison of Revised Supersonic Velocity Profiles and the PFT. With the new θ_1 of .00354 inches and a new S of 2.6 the complete profiles of the two data sets were re-evaluated. The minimum velocities were not replotted. This was due to the fact that the S uses the minimum velocity streamline as a reference to stretch the lateral coordinate. Therefore the S does not affect the minimum velocities. As can be seen in Figures 32 through 35 the minimum velocities match as they were forced to. As the velocity profiles develop downstream the PFT results start to diverge from the experimental data.

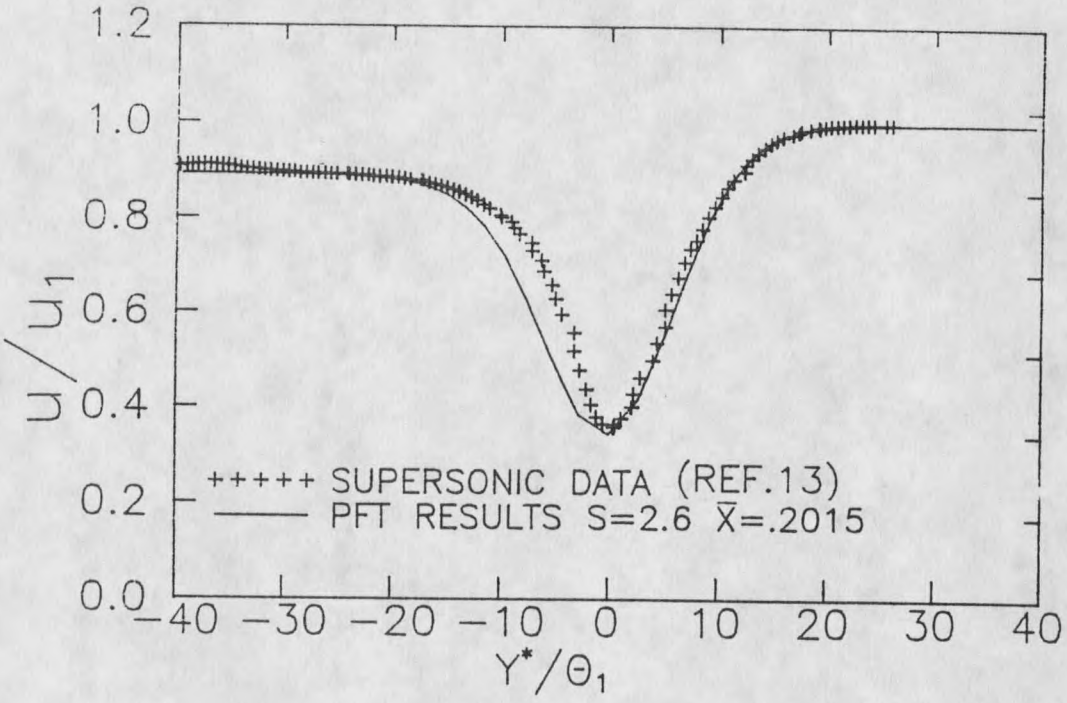


Figure 32. Comparison of PFT with Revised Supersonic Data
$x^* = .25$ inches.

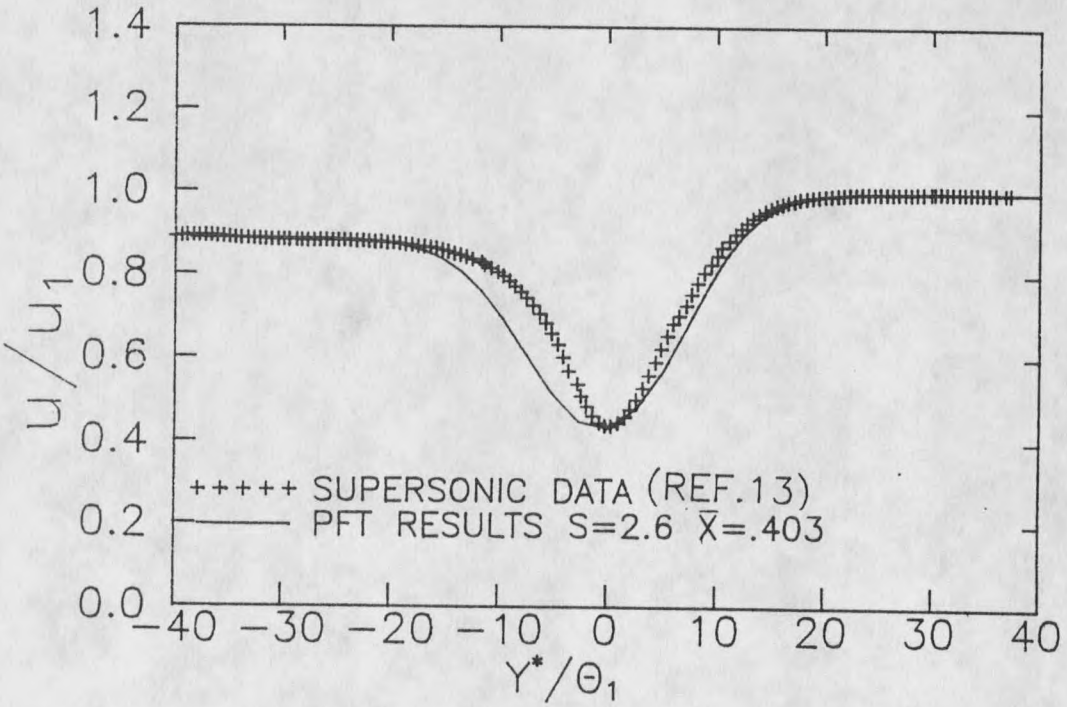


Figure 33. Comparison of PFT with Revised Supersonic Data
$x^* = .5$ inches.

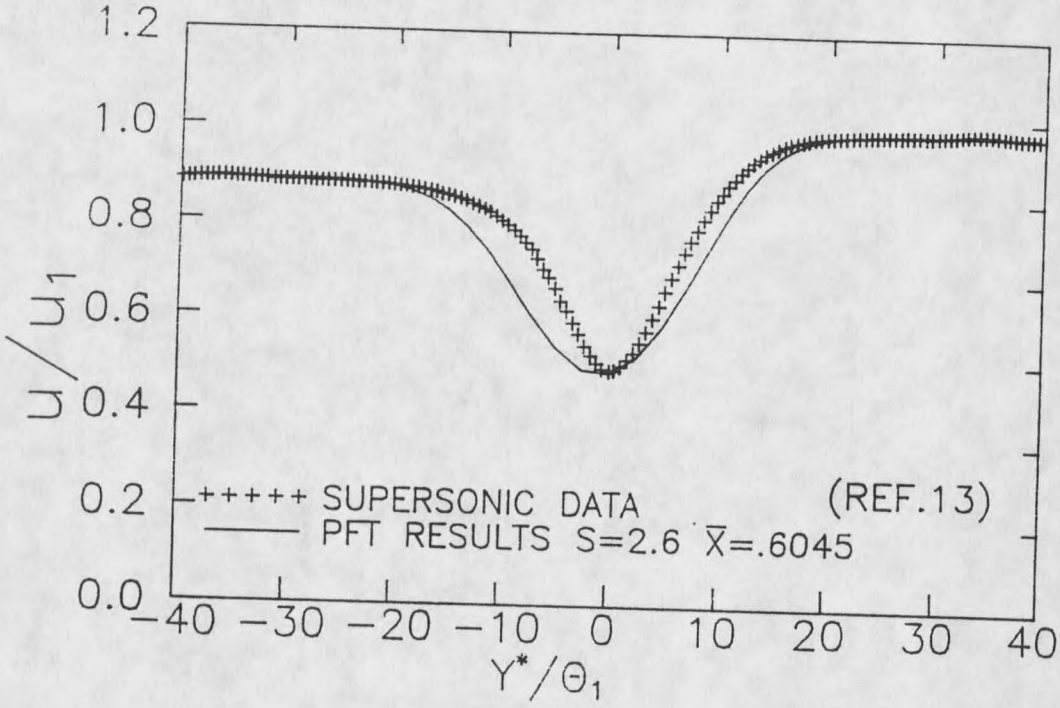


Figure 34. Comparison of PFT with Revised Supersonic Data
$x^* = .75$ inches.

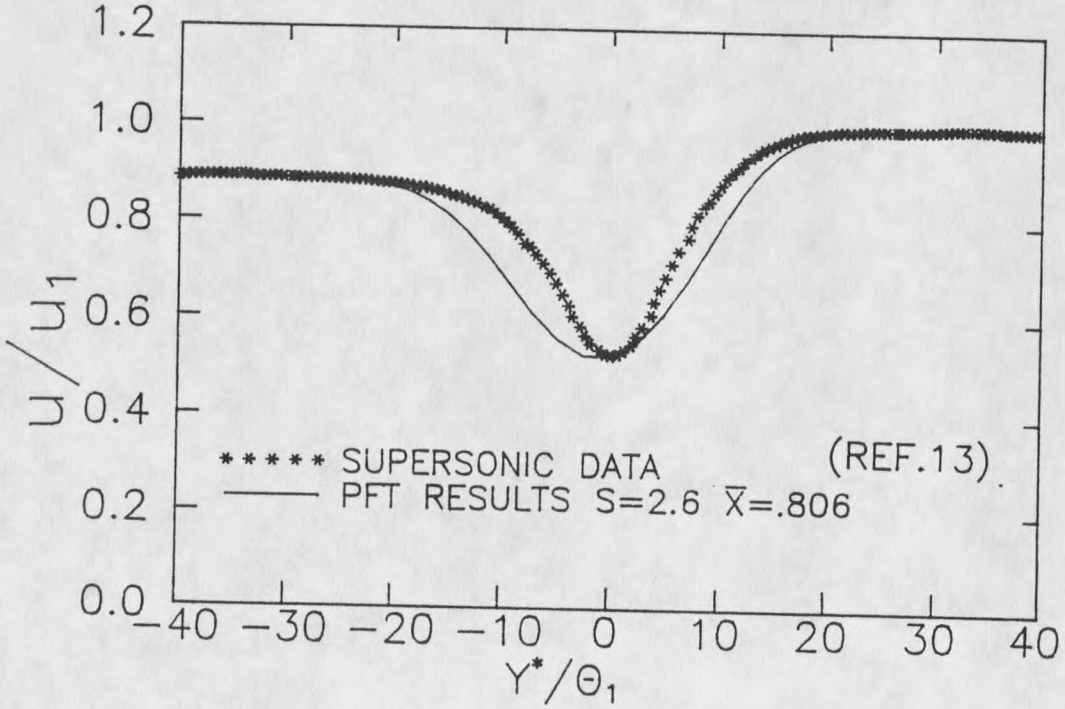


Figure 35. Comparison of PFT with Revised Supersonic Data
$x^* = 1$ inch.

The attempt to gain a better agreement between the entire experimental velocity profile and the PFT by correcting for a possible error in the measurement of the momentum thickness (θ_1) apparently was not successful. In light of this finding the comparison of the PFT against the supersonic data with a momentum thickness of .00484 inches should be considered the appropriate comparison for this work (see Figures 26–29).

The disparity evident in Figures 26 through 29 could be due to the restriction of a Prandtl number of unity and the use of the Oseen approximations near the trailing edge in the PFT. These conclusions will be discussed in more detail in Chapter 5.

Hypersonic Laminar Mixing

Experimental Setup. The second set of data to be compared with the PFT is given in [14]. A flat plate model shown in Figure 36 was immersed with its flat surfaces parallel to the flow, in a steady air flow at Mach number 8. As shown in the figure the plate formed a backward facing step at some distance beyond its trailing edge. A Mach 3 nozzle located inside the plate with its exit at the step discharged its airflow in the downstream direction parallel to the Mach 8 stream.

By controlling the stagnation pressures of the tunnel and jet independently it was possible to match the jet exit and steam static pressures so that the mixing layer stayed parallel to the plate surface. The laminar or turbulent state of the hypersonic boundary layer upstream of the jet could also be controlled by adding or removing boundary layer "trips" between the plate leading edge and the jet exit.

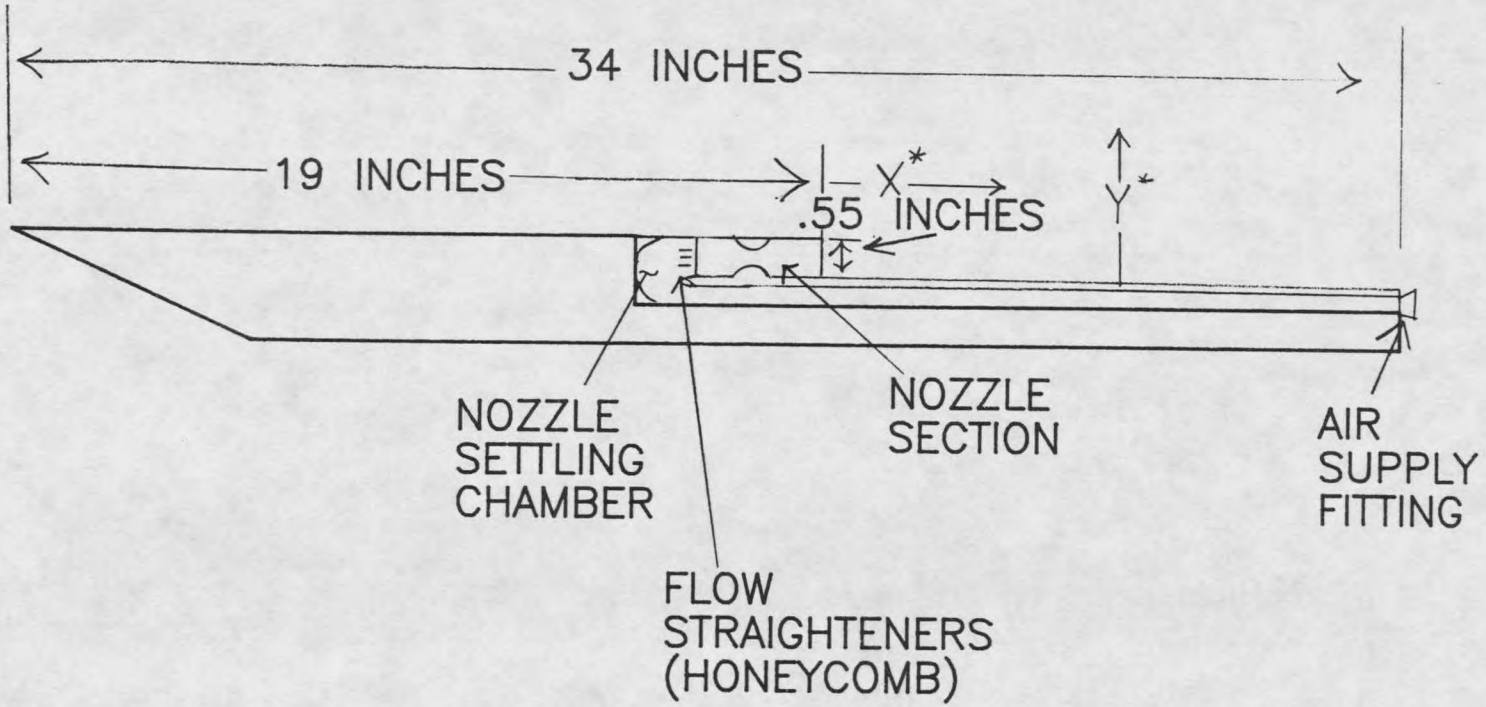


Figure 36. Schematic of Hypersonic Model.

With the trips in place the fast stream (Mach = 8) hypersonic layer was turbulent turning the entire shear layer turbulent. This case of a turbulent free shear layer is of no interest here since it cannot be compared with the PFT which deals with laminar flows only. Its discussion further below will be limited to an illustration of its drastic differences from the laminar case.

With the trips removed the boundary layer was laminar up to the jet. This was verified by the profile measurements to be discussed shortly and also by heat transfer and Schlieren measurements. For a tunnel stagnation pressure of 200 psia, the ensuing free shear layer was found to be laminar to a distance of eleven inches from the jet [23]. Henceforth this report will deal only with this untripped, laminar 200-psia free shear layer.

Table 2 outlines the parameters of the test. The origin for the longitudinal coordinate x^* was placed at the step. Laminar profiles were obtained at x^* (inches) = .1, .4, 1.5, 3.0, 4.5, 7.5, 9.0. The Y^* coordinate ran normal to the floor of the step. The profiles were measured from $Y^* = 0$ (the floor) to $Y^* = 1.7$ inches.

The data was taken by an overhead rake that included a pitot probe and total temperature probe. The rake was positioned such that the probes were on the same x^* and Y^* position.

The flow was considered two-dimensional for data reduction purposes. Data reduction [14] consisted of utilizing the total and static pressures in the Rayleigh pitot formula to solve for the local Mach number:

$$\frac{P}{P_0} = \frac{\left(\frac{2\gamma}{\gamma+1} M_1^2 - \frac{\gamma-1}{\gamma+1}\right)^{1/\gamma-1}}{\left(\frac{\gamma+1}{2} M_1^2\right)^{\gamma/(\gamma-1)}} .$$

In turn the Mach number and the total temperature used the appropriate isentropic formula to solve for the static temperature. The local velocity was solved for using the Mach number and static temperature.

Wind Tunnel Flow Conditions	
Mach number	(-.1,+.3) 8
Stagnation Pressure (psia)	(+.4,-0.0) 200
Stagnation Temperature (°R)	(+6.7,-4.4) 1302
Freestream Re′ (per foot)	(-.8E4,+.5E4) .902E6
Jet Flow Conditions	
Mach number	3
Stagnation Pressure (psia)	(-.002,+.003) .786
Stagnation Temperature (°R)	(-1.33,+.67) 647
Temperature of Partition (°R)	944

Static Pressure for each profile

location of	static pressure (psia)	
profile(inches)	fast side	slow side
0.1	.0237	.0300
0.4	.0223	.0318
1.5	.0240	.0240*
3.0	.0233	.0233*
4.5	.0243	.0243*
7.5	.0235	.0235*
9.0	.0236	.0237*

* varied in boundary layer

Table 2. Hypersonic Experimental Parameters.

In order to utilize the Rayleigh pitot formula the static pressure needed to be known. Because of the variation of the static pressure through the profiles it was determined to use an average of the static pressures recorded in Table 2, the static pressures measured for turbulent runs under the same conditions, and selected model surface pressures [24].

Because of the disparity between the static pressure in the first two profiles as shown in Table 2, the respective fast and slow side static pressures were used in the determination of the local Mach number at $x^* = .1$ and .4 inches. The rest of the downstream profiles utilized the wall pressure in the boundary layer and then the averaged static pressure for the rest of the profile.

Trailing Edge Boundary Layer. The experimental trailing edge velocity profile is necessary to have because the PFT utilizes it as an input. However the closest velocity profile to the trailing edge was at $x^* = .1$ inches. The decision was made to make the best estimate of the initial conditions at $x^* = 0$ by combining the data at $x^* = .1$ inches with expected boundary conditions.

The .1 inch velocity profile was extrapolated to $u/u_1 = 0.0$ at $Y^* = 0.0$ to meet the no-slip condition at the trailing edge as shown in Figure 37. By invoking the ideal gas law as the equation of state the density profile was extrapolated to meet the boundary condition of $T_W/T = 9.67$ (or actually $\rho/\rho_1 = .103$). The shape of the extrapolation from the .1 inch density data to the boundary condition just stated was based on Tritz's [25] numerical solution of the trailing edge density profile. The initial density profile is shown in Figure 38.

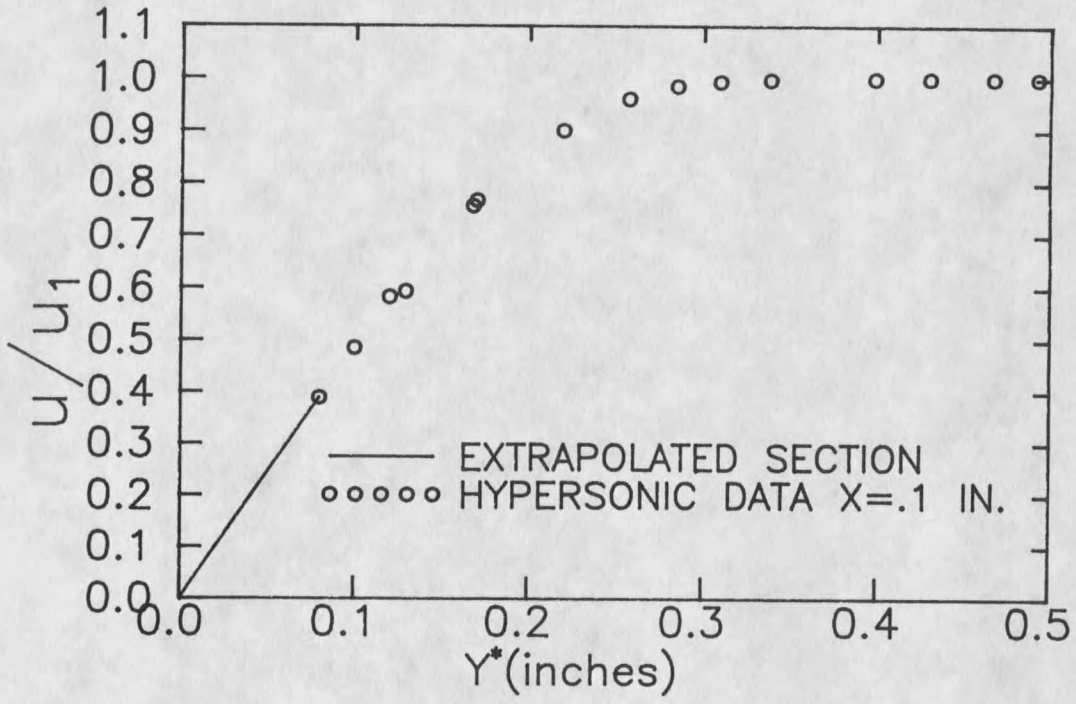


Figure 37. Velocity Profile used in Determining θ_1.

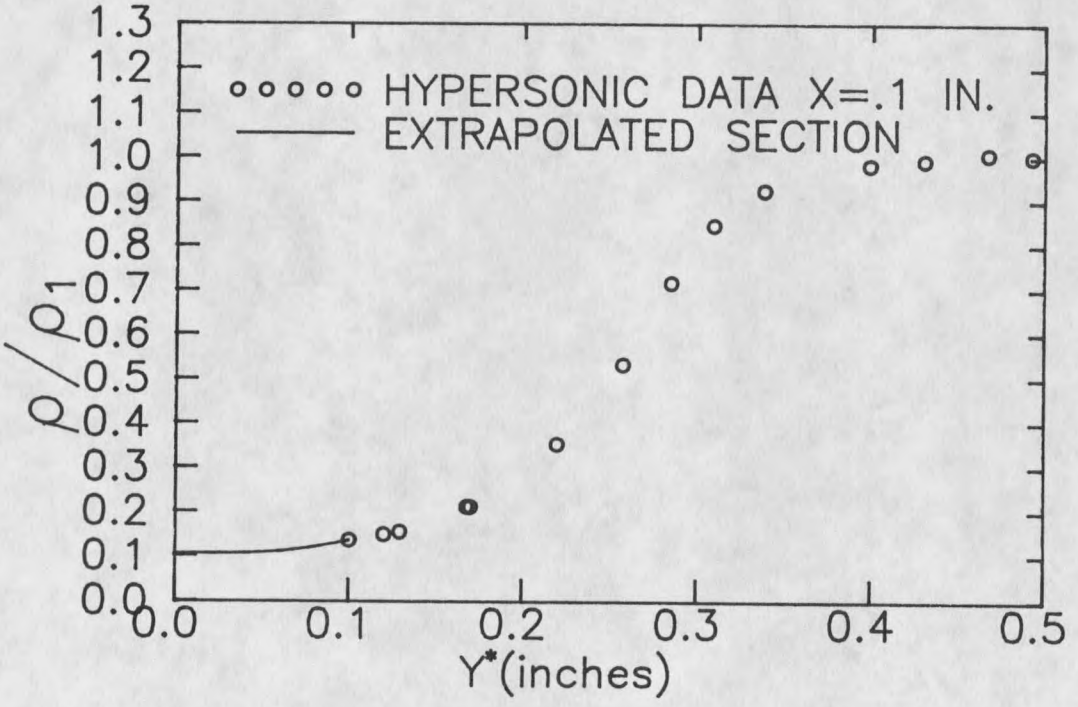


Figure 38. Density Profile used in Determining θ_1.

A second alteration to the .1 inch data was performed. A review of the minimum velocities showed the location of the minimum velocities to be located approximately at .65 inches from the model surface. The cause of an extra .1 inch above the trailing edge (located at $Y^* = .55$ inches) could be due to the complex shock interaction occurring at the lip as shown in the Schlieren photographs in Figure 39.

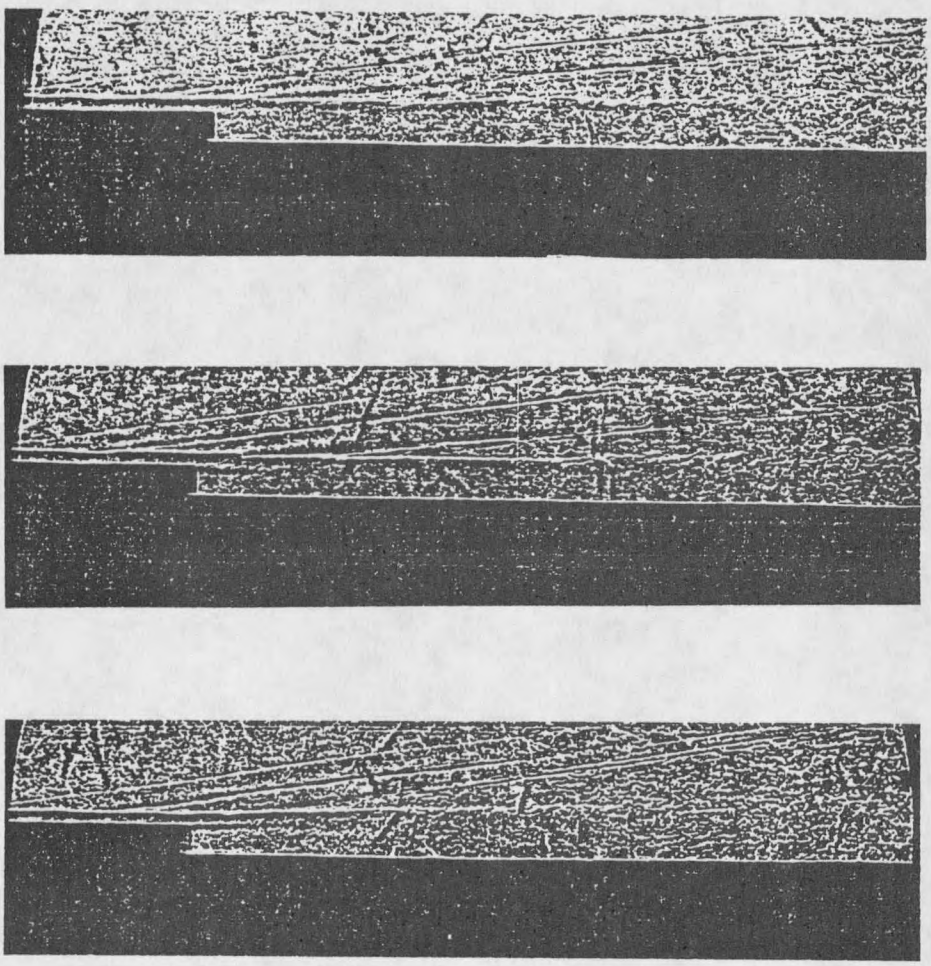


Figure 39. Spark-Schlieren Photographs of the Partition Flow for Air, Mach 8 fast stream, Mach 3 slow stream.

Therefore it was determined to shift the seven laminar velocity profiles by subtracting .1 inches from each of the lateral positions (Y^*/θ_1) that make up the velocity profiles. The momentum thickness was now determined utilizing the velocity and density profiles of Figures 37 and 38 in the following equation:

$$\theta_1 = \int_0^{Y^*} \frac{\rho}{\rho_e} \frac{u}{u_e} \left(1 - \frac{u}{u_e}\right) dY^* \quad . \tag{41}$$

The result was $\theta_1 = .008148$ inches.

Now a parameter unique to the PFT needed to be determined. The stretching factor S is used to allow for all types of Falkner-Skan type flows as described in Chapter 2. Figure 40 shows the curvefit of the newly determined initial velocity profile in the incompressible plane

$$\tilde{Y}^* = \int_0^{Y^*} \frac{\rho}{\rho_e} \, dY^* \quad . \tag{42}$$

An S of 2 was determined as shown in Figure 40. The basis for denoting $\tilde{Y}^*$ as the incompressible plane is the incorporation of the density profile into the lateral coordinate as a weighing factor as shown in (42).

Next, the PFT was compared against the experimental initial profile utilizing the dimensional lateral coordinate (Y^*). The purpose of this was to ensure the density profile had been correctly determined. In other words, the density profile was not utilized as a weighing factor in Figure 41. Therefore the effect of density is present in Figure 41 and not in Figure 42. If the density profile had been incorrectly determined there would have been disparity in these two figures.

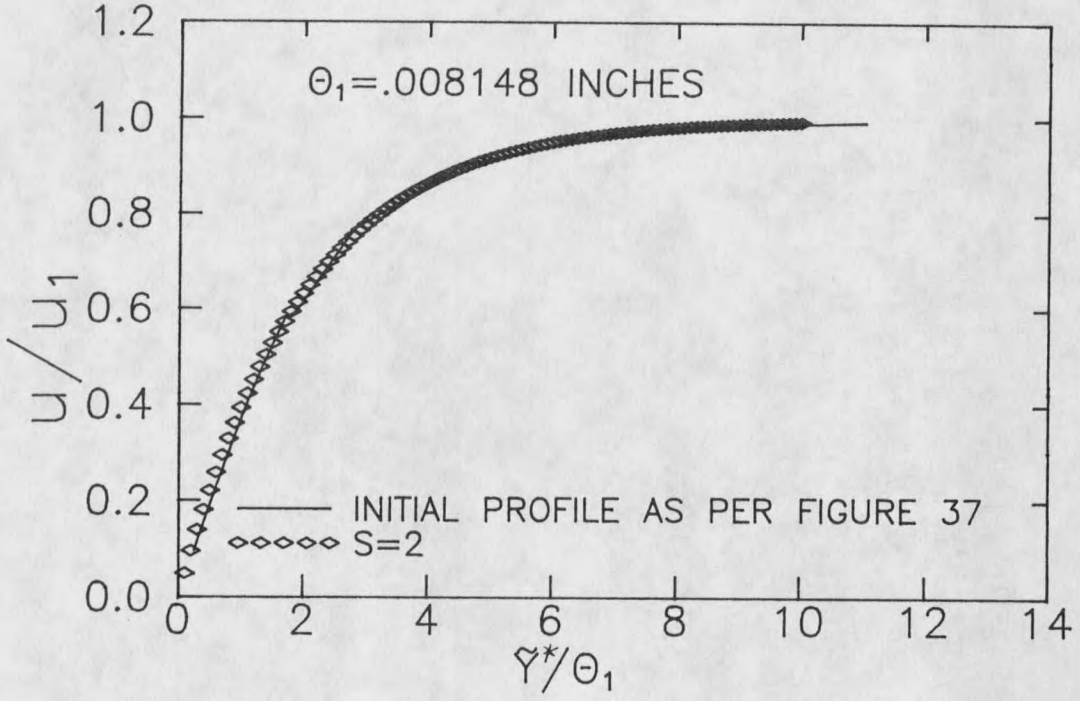


Figure 40. Determination of S for Hypersonic Initial Profile.

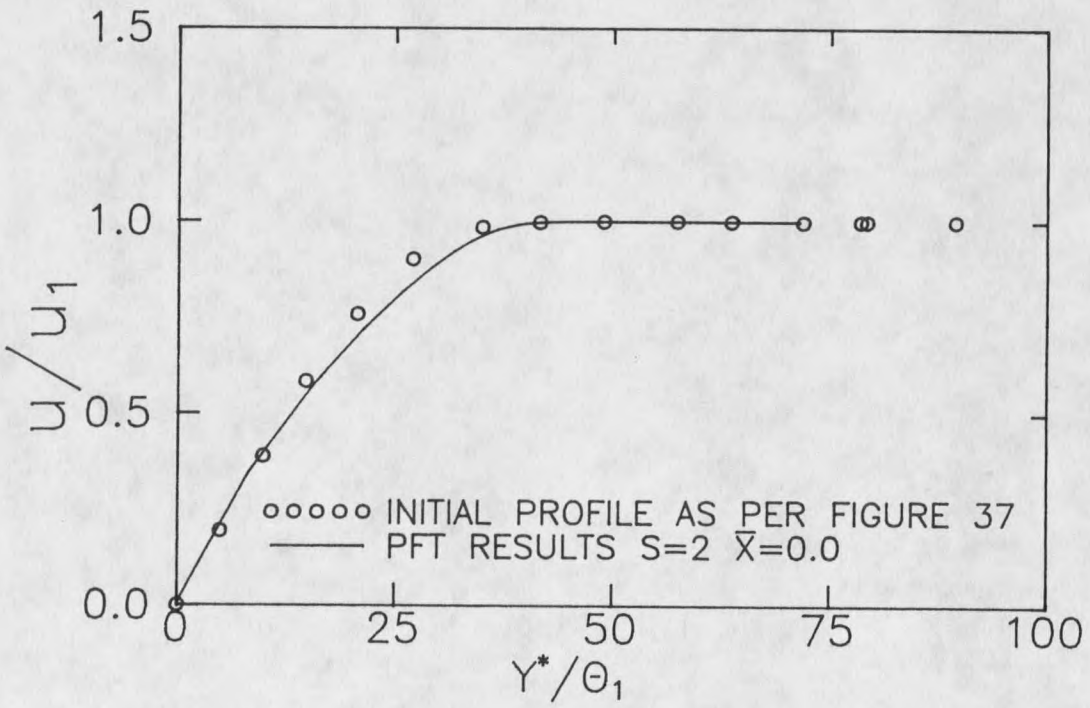


Figure 41. Comparison of PFT and Initial Profile.

Comparison of Hypersonic Laminar Velocity Profiles with the PFT. With $\theta_1 = .008148$ inches and $S = 2$ the hypersonic laminar velocity profiles were compared against the PFT. The initial comparison was performed on the minimum velocities as shown in Figure 42 below.

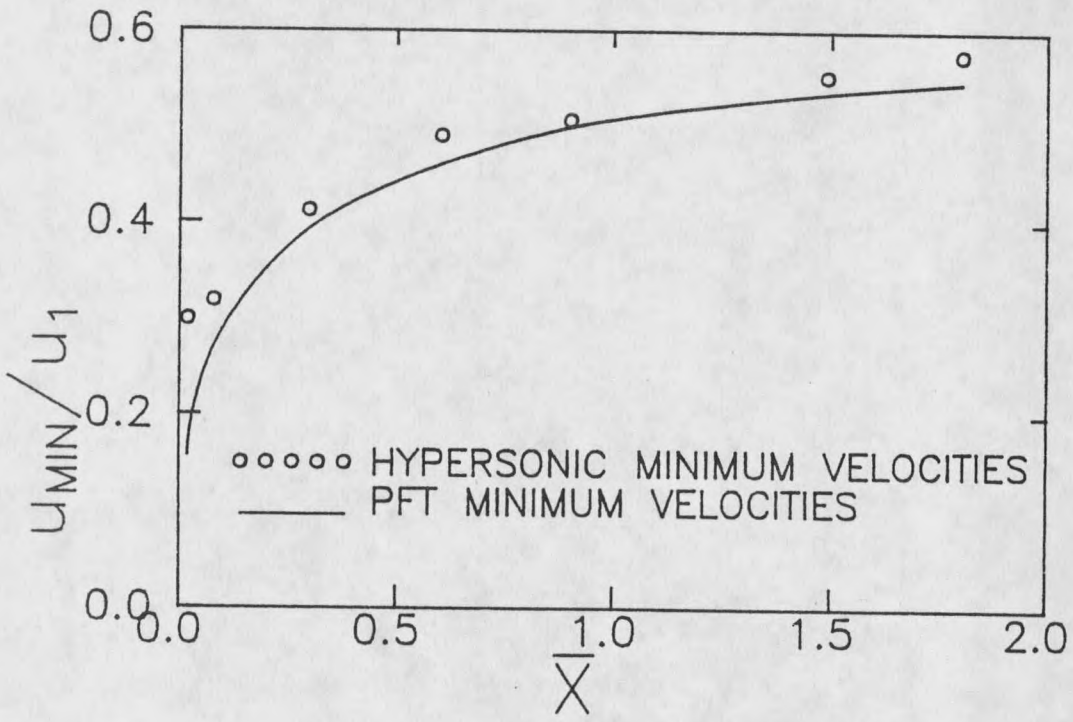


Figure 42. Comparison of PFT and Laminar Hypersonic Minimum Velocities.

This figure validates the postulate set forth in the PFT that the Chapman variable should have as its reference the wake component minimum. The disparity shown in the comparison of the PFT with the supersonic minimum velocities as seen in Figure 25 could be due to use of the Oseen aproximations in the near wake region. The $\overline{x}$ for the supersonic data extended only to .427 while the hypersonic data extended to $\overline{x} = 1.8$. This possibility will be discussed in Chapter 5.

The complete hypersonic laminar velocity profiles were then compared against the PFT solutions. Figure 43 is a duplication of Figure 41 in the vicinity of the shoulder of the profile. However Figure 43 does show the disparity between the minimum velocities at .1 inch which was not included in Figure 41. This disparity could be due to the variation of the static pressure that occurred during the experiment. Figure 44 shows good agreement between the PFT and the experiment.

After $x^* = .4$ inches a noticeable shift in the hypersonic laminar velocity profiles towards the fast stream occurred. This shift increased until the 4.5 inch position was reached at which point the shift remained constant.

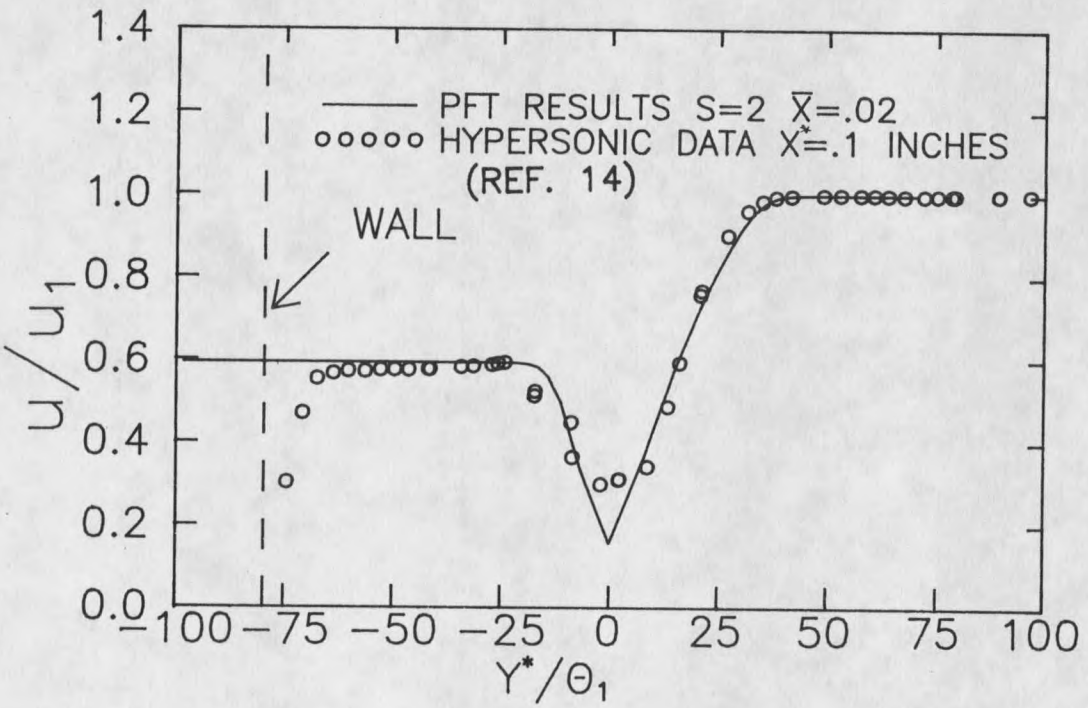


Figure 43. Comparison of PFT with Laminar Hypersonic Data
$x^* = .1$ inches.

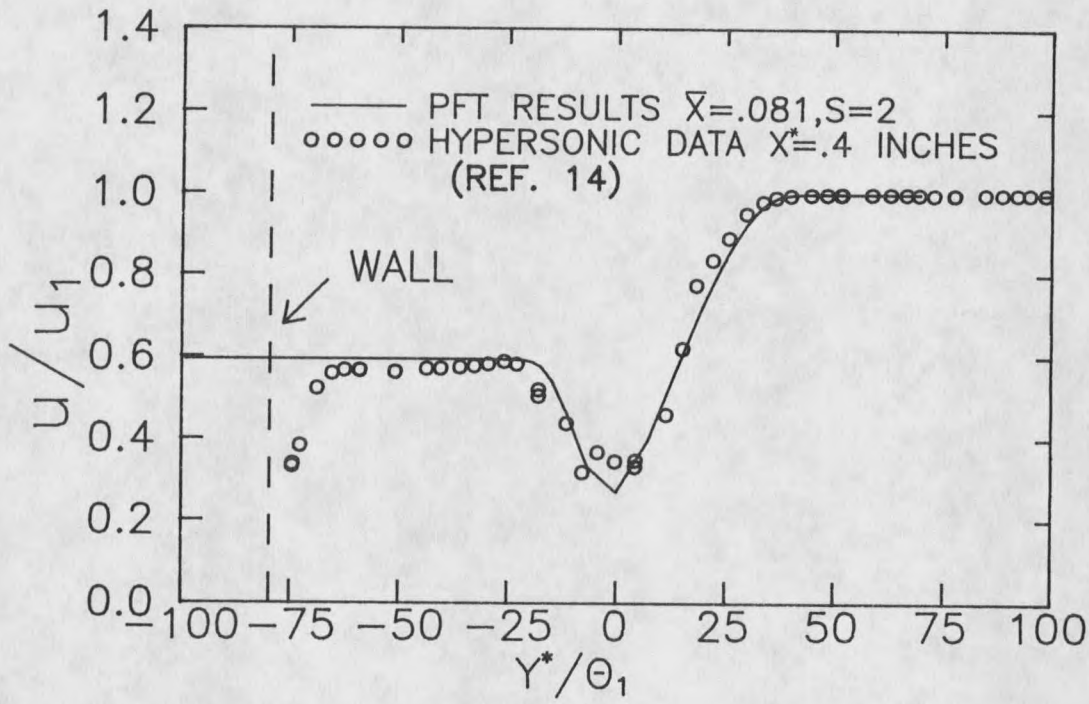


Figure 44. Comparison of PFT with Laminar Hypersonic Data
$x^* = .4$ inches.

The experimental profiles in Figures 45 through 49 were shifted laterally (i.e. in the Y^*/θ_1 direction) such that the minimum velocities of the PFT and the experimental data matched so a meaningful comparison could be done. The reason for this shift was that the slow stream of the hypersonic data was not infinite as assumed in the PFT. Therefore the mixing layer of the experimental data was being influenced by the boundary layer on the floor of the step.

Berger [26] came to this same conclusion when investigating the Chapman model. Berger assumed that the slow side would distort the mixing layer profile if the mixing layer was not small compared to the length of the slow side region as is the case for the hypersonic data.

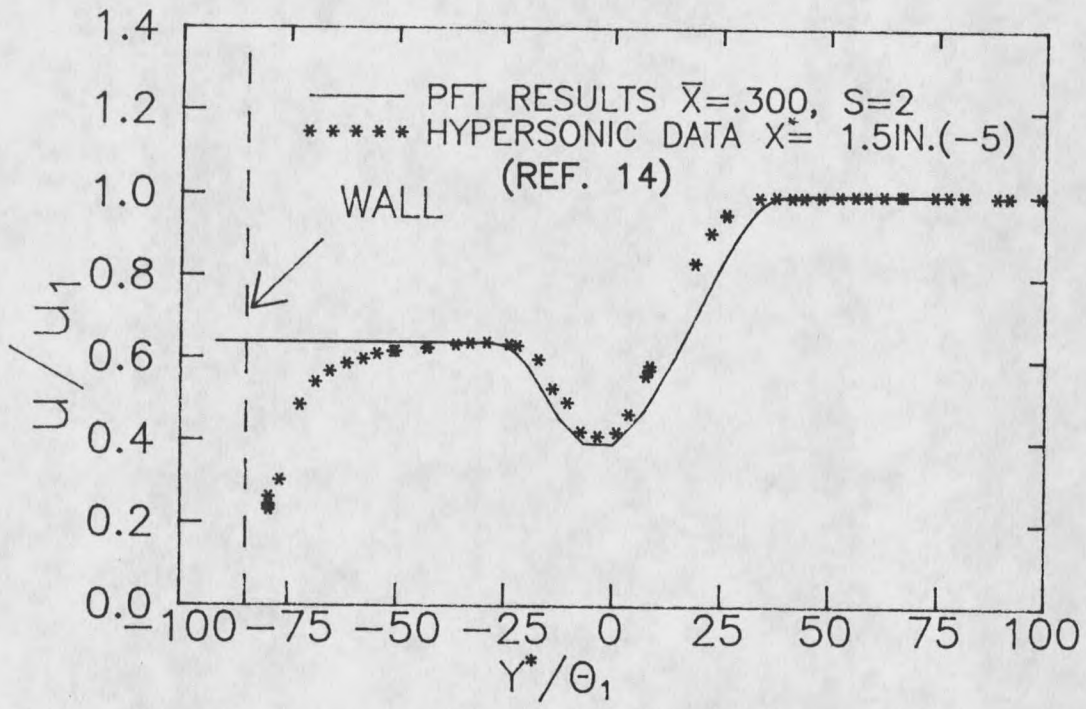


Figure 45. Comparison of PFT and Laminar Hypersonic Data
$x^* = 1.5$ inches.

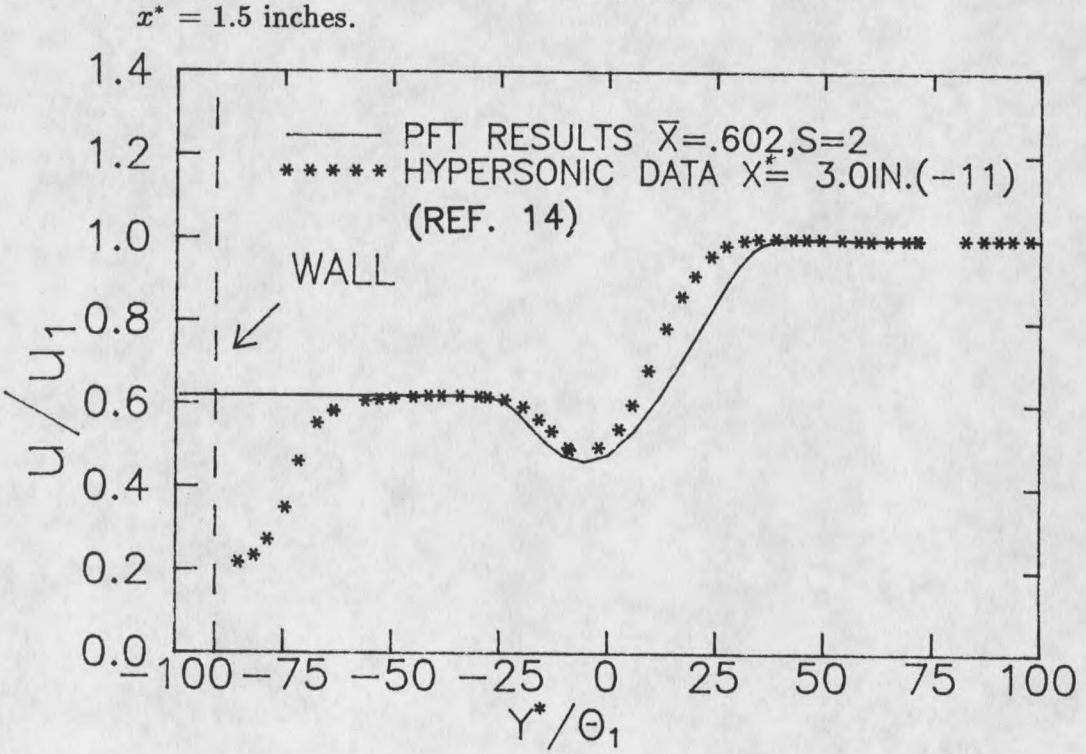


Figure 46. Comparison of PFT and Laminar Hypersonic Data
$x^* = 3$ inches.

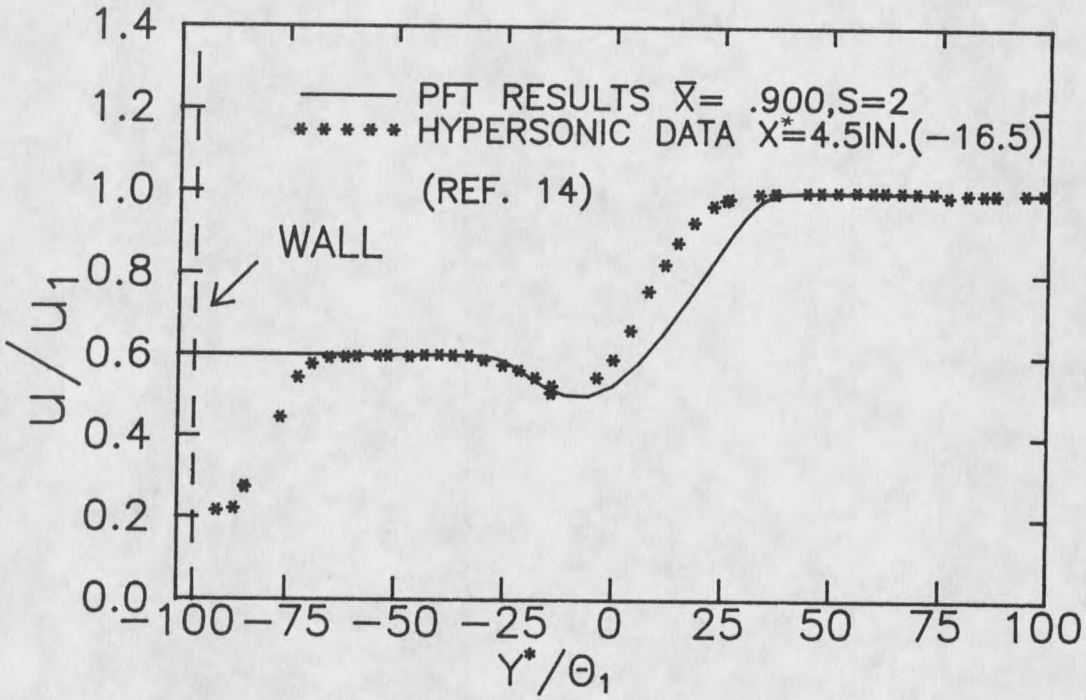


Figure 47. Comparison of PFT and Laminar Hypersonic Data
$x^* = 4.5$ inches.

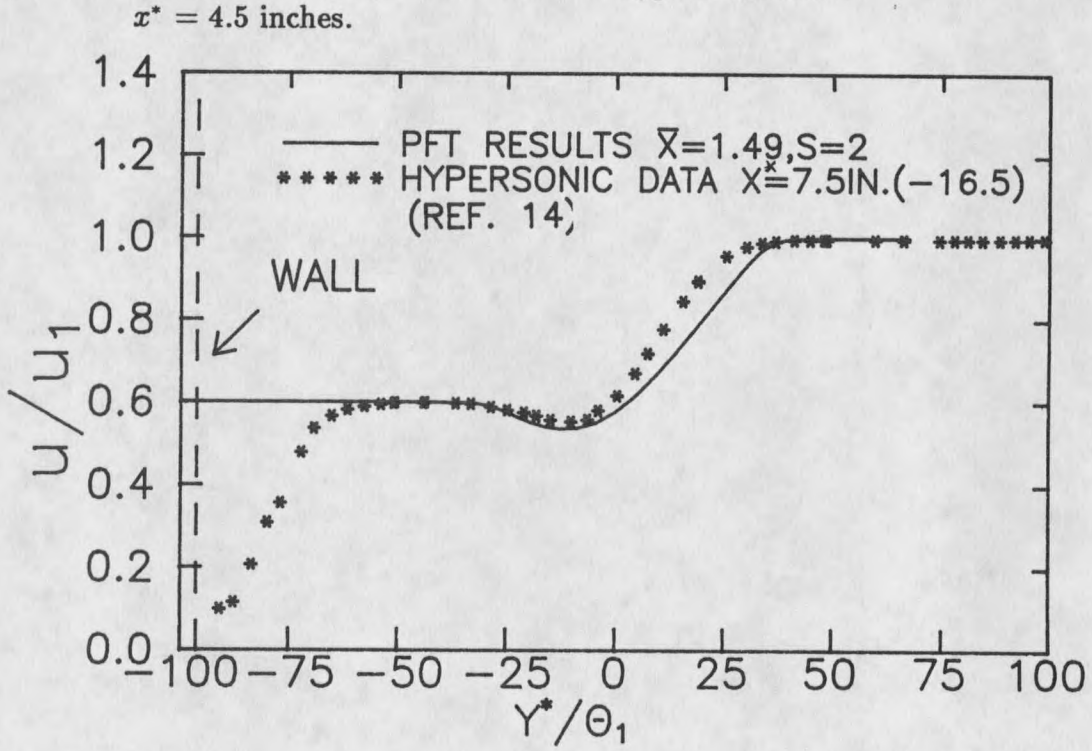


Figure 48. Comparison of PFT and Laminar Hypersonic Data
$x^* = 7.5$ inches.

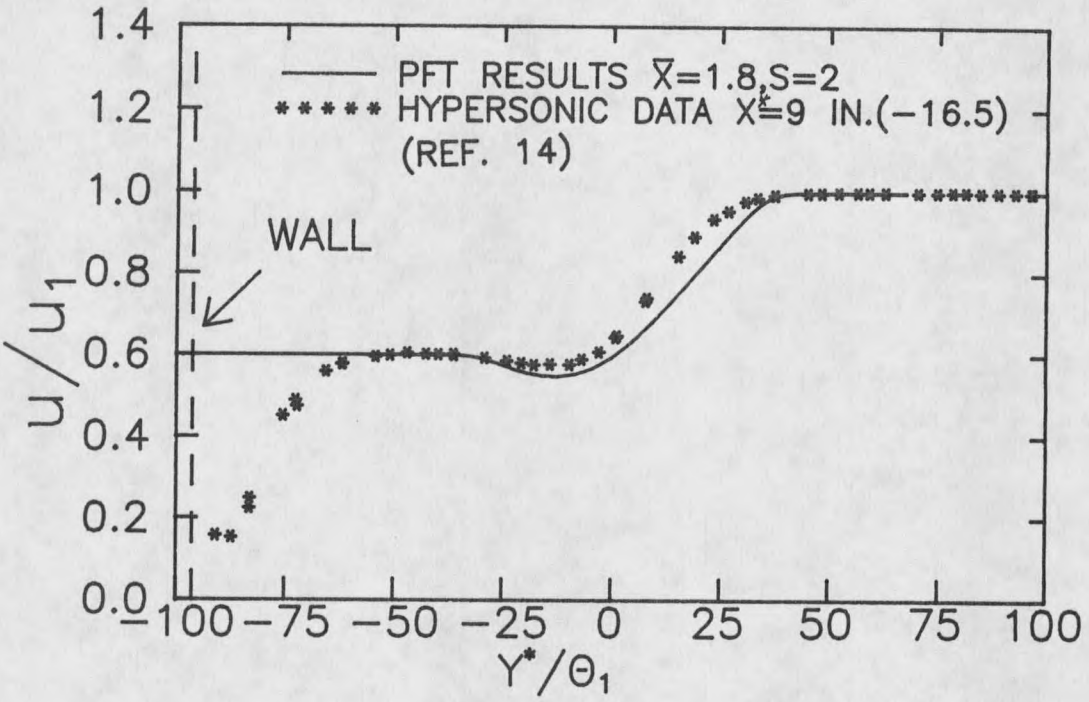


Figure 49. Comparison of PFT and Laminar Hypersonic Data
$x^* = 9$ inches.

Hypersonic Turbulent/Laminar Mixing

Velocity profiles under approximately the same conditions as stated in Table 2 but with the fast side turbulent were also obtained. The profiles were recorded at $x^* = .4$, 2, 4, 6 and 9 inches.

The basis for including these profiles in this assessment was twofold. First, it was determined that it would be interesting to observe the differences between the predicted laminar flow (the PFT) and the experimental turbulent flow. Second, the jet flow was still laminar and therefore could be modeled utilizing the PFT.

The momentum thickness was determined by reference [14] (.01788 inches) while the slow side momentum thickness used Demetriades' [27] laminar predicted

value (.00768 in). An S of .5 was based on the fast side of the profile at $x^* = .4$ inches. This determination of S was made with the realization that the PFT is based on laminar flow and therefore a comparison with turbulent flow cannot technically be made. However the comparison of the turbulent data with the theoretical laminar case gave insight to the differences in the two types of flow.

In Figures 50 through 54 the turbulent side expanded, as expected, more quickly than the laminar profiles. Also the rapidity of the distortion of the mixing layer by the turbulent fast stream was observed. By 4 inches the velocity trough is eradicated.

Also predicted by the PFT was the overshoot of the freestream velocities evident in all the laminar slow sides of Figures 50 to 54. This overshoot has been documented experimentally by McLeod and Serrin [28]. They determined that for a hot wall and an accelerated flow an overshoot of the freestream velocity will always exist.

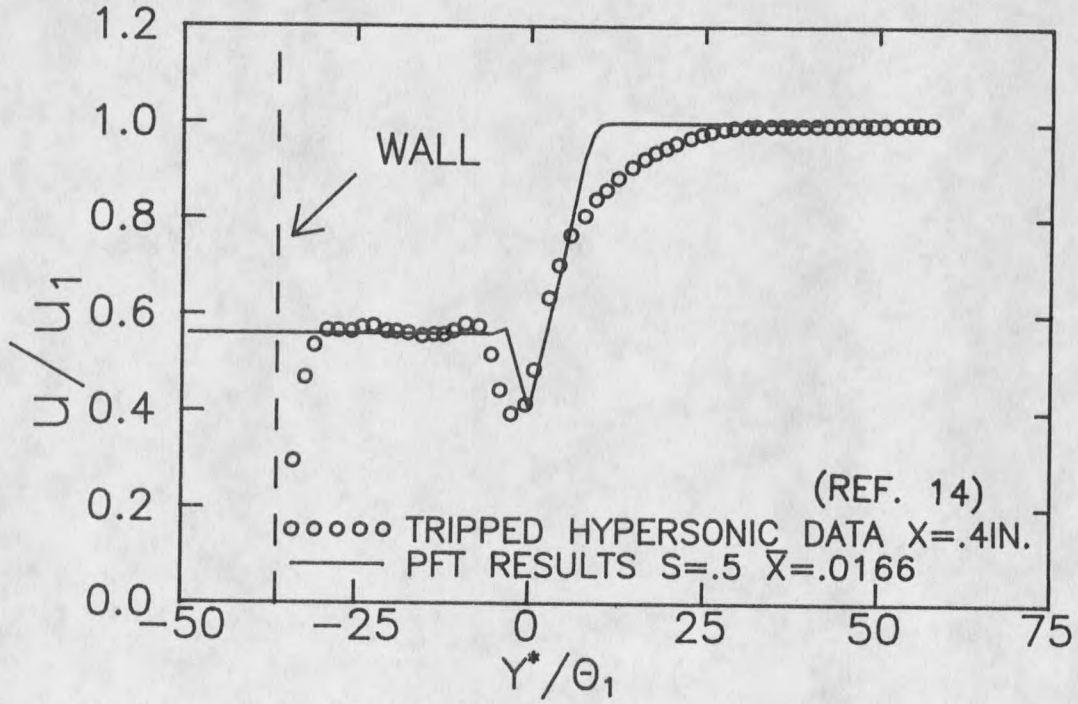


Figure 50. Comparison of PFT and Turbulent Hypersonic Data $x^* = .4$ inches.

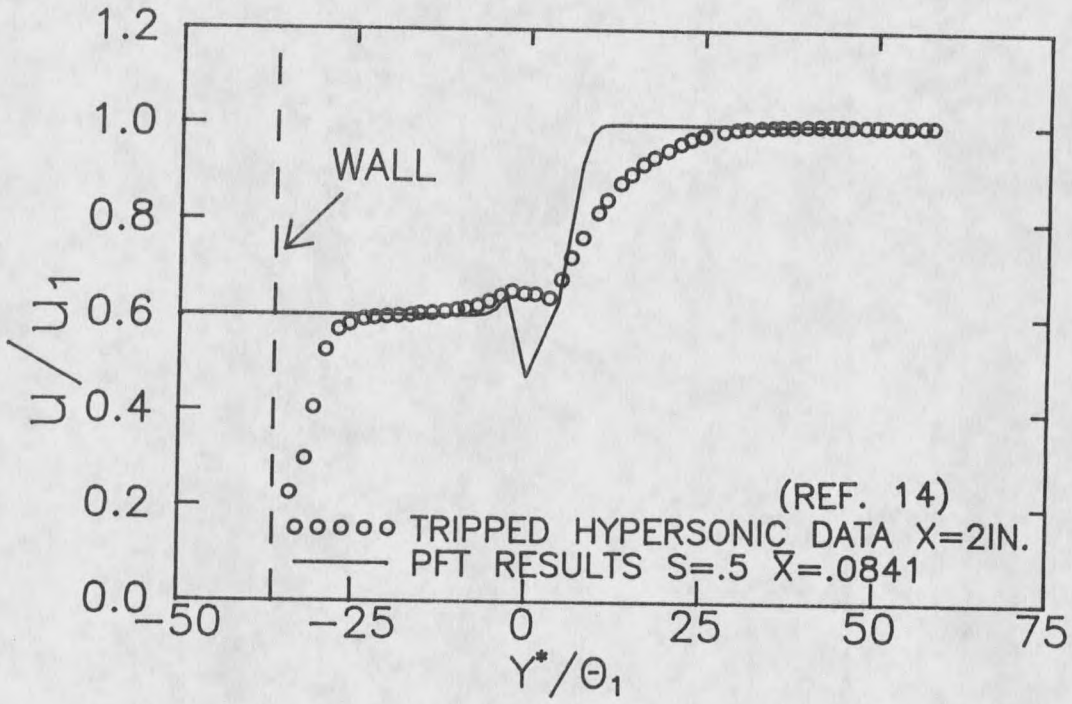


Figure 51. Comparison of PFT and Turbulent Hypersonic Data $x^* = 2$ inches.

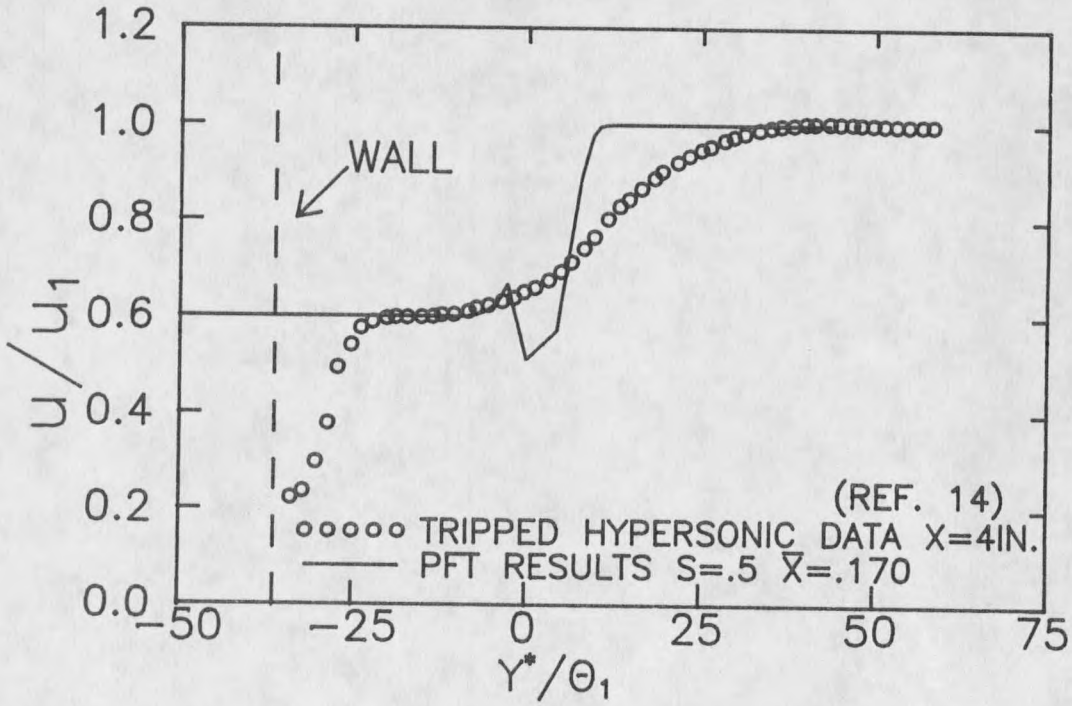


Figure 52. Comparison of PFT and Turbulent Hypersonic Data $x^* = 4$ inches.

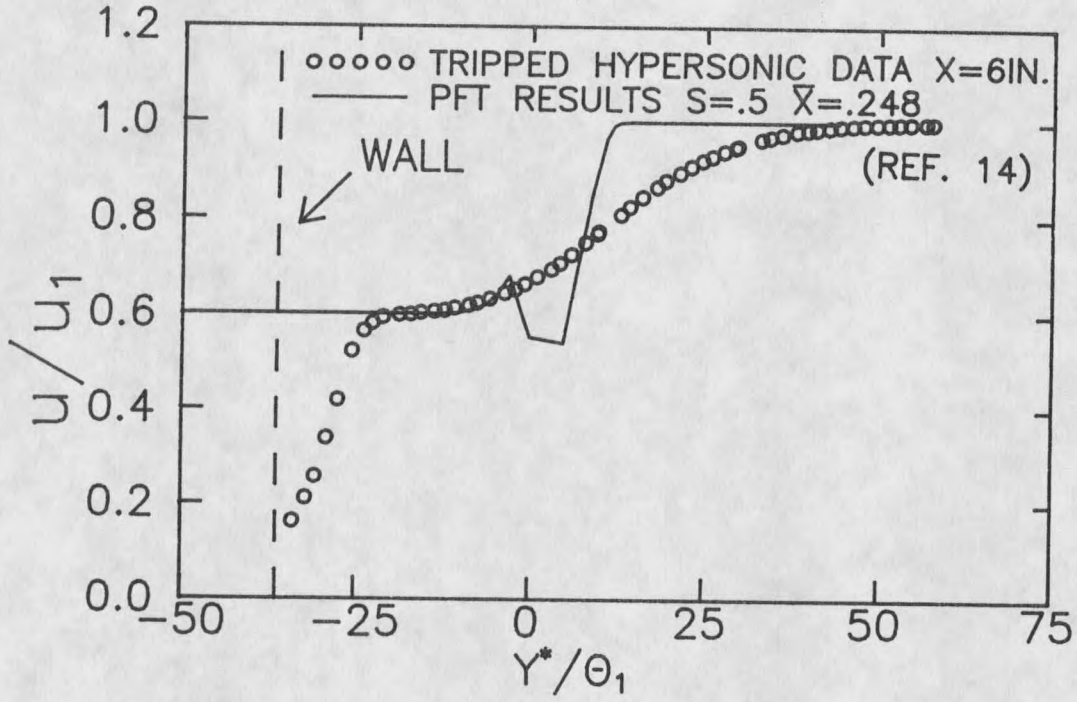


Figure 53. Comparison of PFT and Turbulent Hypersonic Data $x^* = 6$ inches.

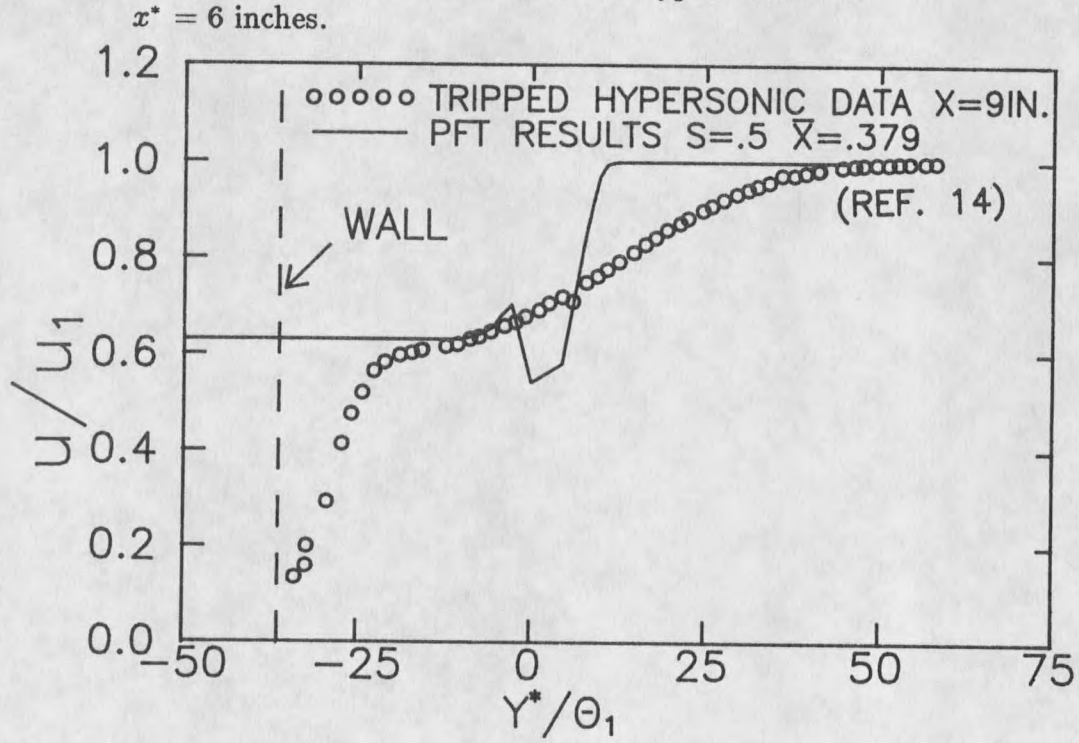


Figure 54. Comparison of PFT and Turbulent Hypersonic Data $x^* = 9$ inches.

Conclusions on the Comparison with Test Data

Wake experimental results had earlier validated the PFT and the use of the Oseen approximations near the trailing edge as did the numerical results [12]. However in both cases the data was either very scant or was only available for the zero streamline ($Y^* = 0$).

In this work the initial comparison of the supersonic laminar velocity profiles of Brower [13] shows the PFT predicting thicker profiles and an unsatisfactory matching of the minimum velocities.

Comparison was also made by assuming that the Brower measurement of θ_1 was in error. If a 27 percent error is assumed the minimum velocities match but the profiles predicted by the PFT were again found to be thicker than the experimental profiles. It is worth noting as the profiles progress downstream of the trailing edge the difference in the slow side stabilized while on the fast side the theoretical profile continued to separate from its experimental counterpart. This asymmetry could be due to the manner in which the algorithm for the PFT was developed.

The hypersonic laminar velocity profiles showed good agreement with the PFT with respect to the general shape. However, as the PFT solved for profiles further downstream the fast side comparison started to diverge while the slow side and minimum velocities show excellent agreement. Also, the minimum velocity comparison validated the PFT concept that the dividing stream line of both wake and free shear layer component must coincide and that they coincide at the wake minimum velocity.

The comparison of the turbulent/laminar profiles and the PFT laminar profiles delineated the differences between the two types of flows quite well. The PFT

predicted an overshoot due to the flow being accelerated and an existing hot plate condition with respect to the laminar slow stream. The width of the mixing layer was much greater in the turbulent flow. The effect of the turbulent flow was to erase the velocity trough very close to the trailing edge.

CHAPTER 5

EXTENSIONS OF THE PFT

Overview

In light of the discrepancies between the PFT and the partition flow as outlined in the previous chapter the PFT warranted further investigation. Use of the Oseen approximations, the choice of an exponential for the initial profile and the ramification of utilizing the Busseman-Crocco relation were the three areas scrutinized.

Oseen Approximations

The Oseen approximations are defined as small velocity and enthalpy defects as stated below:

$$u(x^*, y^*) = 1 - \tilde{\bar{u}}(x^*, y^*) \quad , \quad \tilde{\bar{u}}(x^*, y^*) << 1 \tag{43}$$

$$h(x^*, y^*) = 1 + \tilde{\bar{h}}(x^*, y^*) \quad , \quad \tilde{\bar{h}}(x^*, y^*) << 1 \quad . \tag{44}$$

When (43) and (44) are substituted into the momentum and energy equations via the correct transformations the momentum and energy equations become linear differential equations. This approach was used by Gold [8] to find the velocity and temperature solutions of (1) and (2).

The Oseen approximations are supposedly valid only in the far wake region where the velocity and temperature defects would be small. However the PFT utilizes Gold's findings for the entire flow. As shown with the Goldstein evaluation in Chapter 4 the PFT does show excellent agreement close to the trailing edge. However as shown in Figure 25 the minimum velocity comparison of the supersonic data which is fairly close to the trailing edge does not give good agreement. Also Figure 42 of the hypersonic data shows excellent agreement only after progressing downstream. The disparity in the first two points was originally thought to be due to variations in the static pressure but the use of the Oseen approximation could be entering the picture.

Initial Velocity Profile

The fit of the exponential to the Blasius [16] profile even with a stretching factor S is considered "fair" at best. Therefore several different initial profiles were investigated. Figure 55 shows that a third degree polynomial is an excellent fit to the Blasius profile especially when compared with the exponential fit. However the mathematics of integrating Gold's solutions become quite complicated. A hyperbolic tangent was recommended by Gasperas [29] and can be seen in Figure 56.

In summary, though there are better fits to the initial profile than an exponential, none seem to have the flexibility and ease of mathematics with respect to incorporating them into Gold's [8] velocity and temperature solutions as the exponential while at the same time delivering an acceptable fit. If the stretching factor is used correctly an excellent fit as demonstrated for the hypersonic initial profile can be achieved.

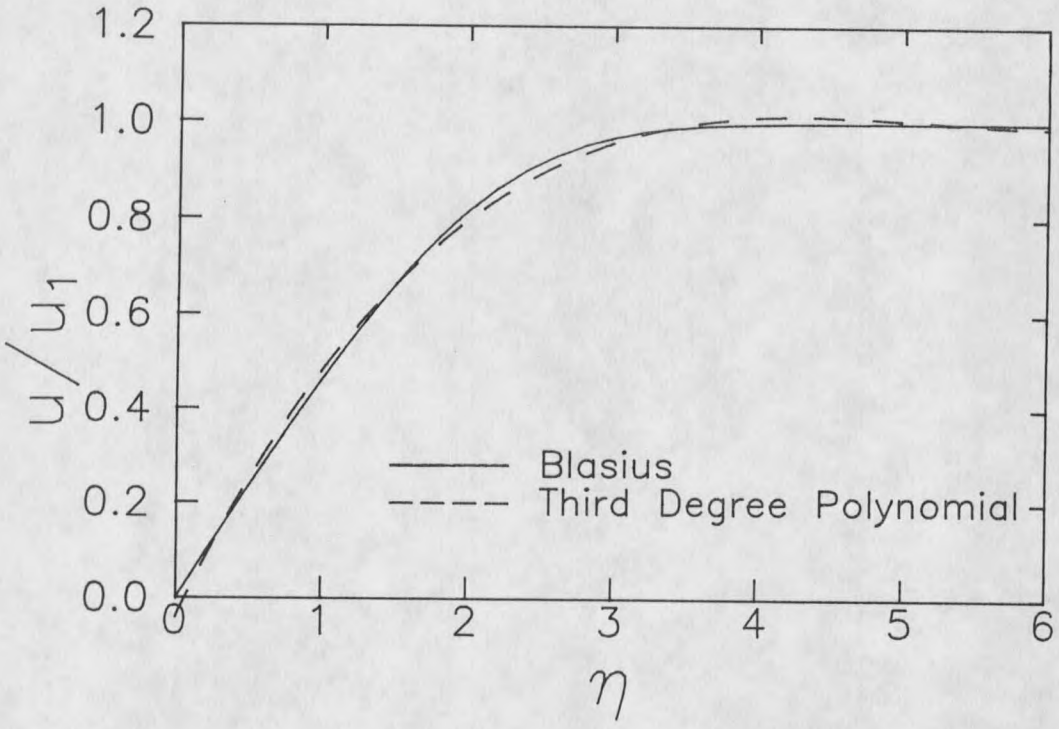


Figure 55. Polynomial Fit of Blasius Profile.

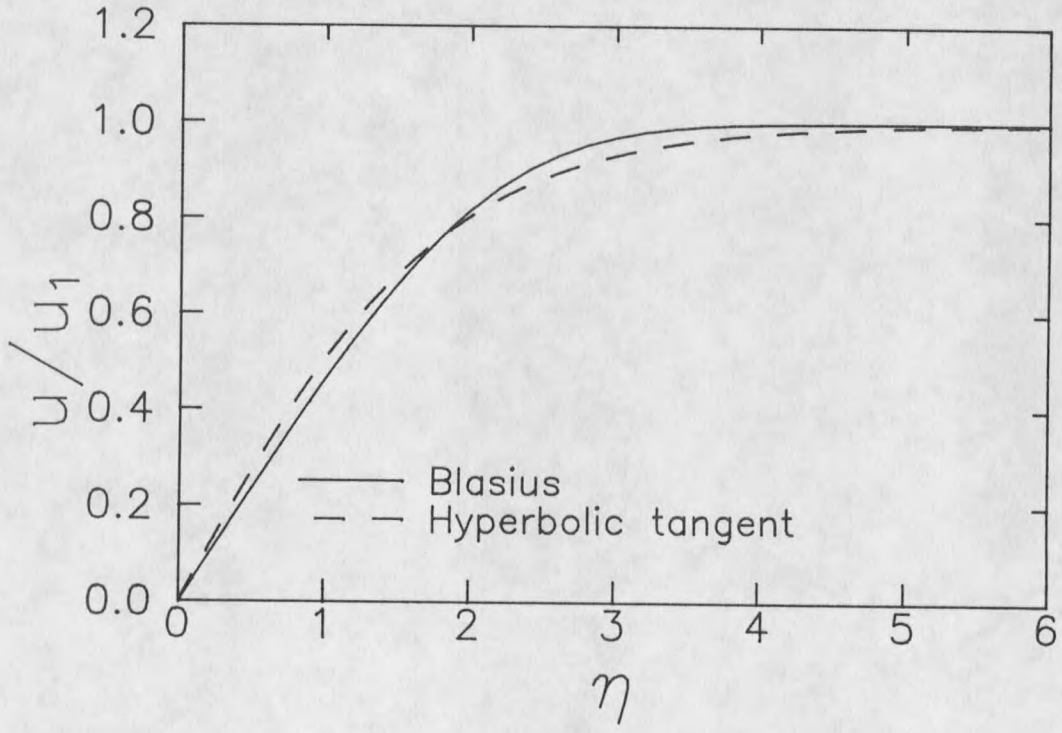


Figure 56. Hyperbolic Tangent Fit of Blasius Profile.

Variable Prandtl Number

To attempt to make the PFT more versatile it was decided to investigate the possibility of including a variable Prandtl number. The wake component without Chapman's free shear layer was investigated initially. As can be seen in Gold's velocity equation (1) is not affected by the Prandtl number.

Gold's temperature equation however is affected via the chosen initial temperature profile $\bar{h}_0$ which is the Busemann-Crocco relationship. The following Busemann-Crocco equation [30] has been modified to include a recovery factor r:

$$\frac{T}{T_e} = \frac{T_W}{T_e} + \frac{T_{aW} - T_W}{T_e} f' - \frac{r}{2}(\delta - 1) M_\infty^2 f'^2 \tag{45}$$

where

$$T_{aW} = T_\infty \left(1 + \sqrt{Pr}\, \frac{\delta - 1}{2} M_\infty^2\right)$$

$$r = \sqrt{Pr} \tag{46}$$

$$f' = u/u_e \quad \text{from Blasius Solution [28]} \quad .$$

Though this equation allows for various Prandtl numbers via the recovery factor, Figure 57 shows that (45) causes the thermal boundary layer to thicken for an increasing Prandtl number. This apparent contradiction to the actual phenomena is due to the assumption $T = T(u)$ in the Busseman-Crocco relationship. This assumption causes the temperature boundary thickness to follow the velocity boundary thickness. Figure 58 shows the results of Tritz's similarity solution [25] for the boundary layer temperature profile. These results show correctly the decreasing thermal boundary layer with an increasing Prandtl number as found by both Schlichting [31] and White [32].

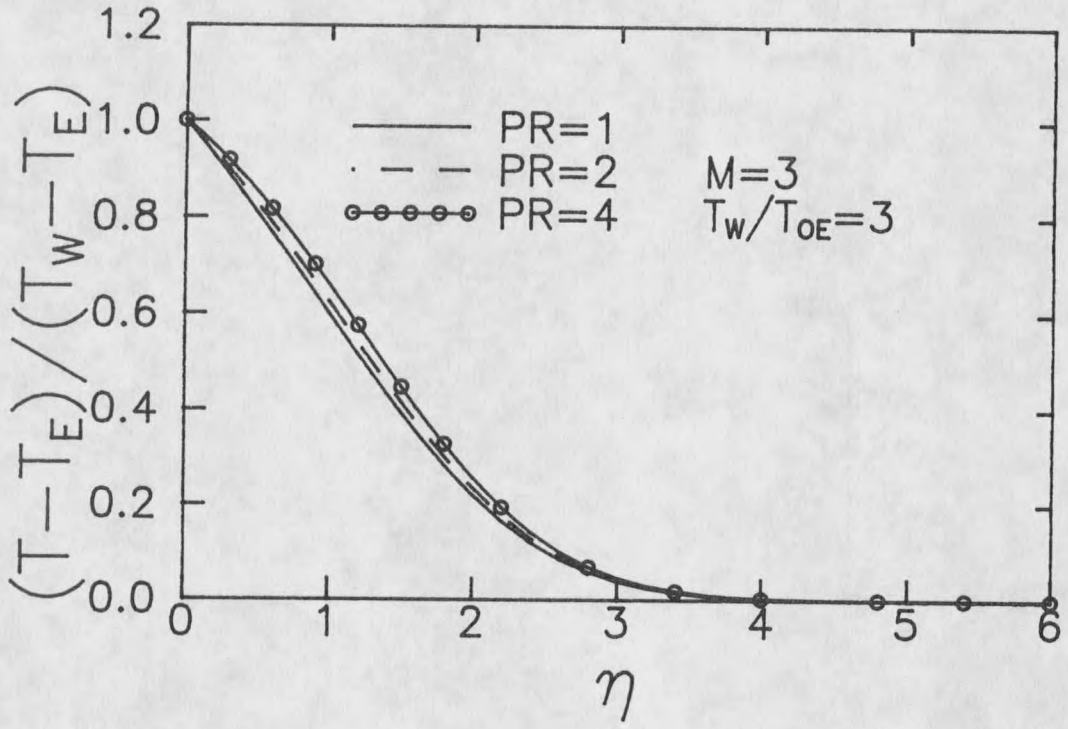


Figure 57. Busseman-Crocco Temperature Profile.

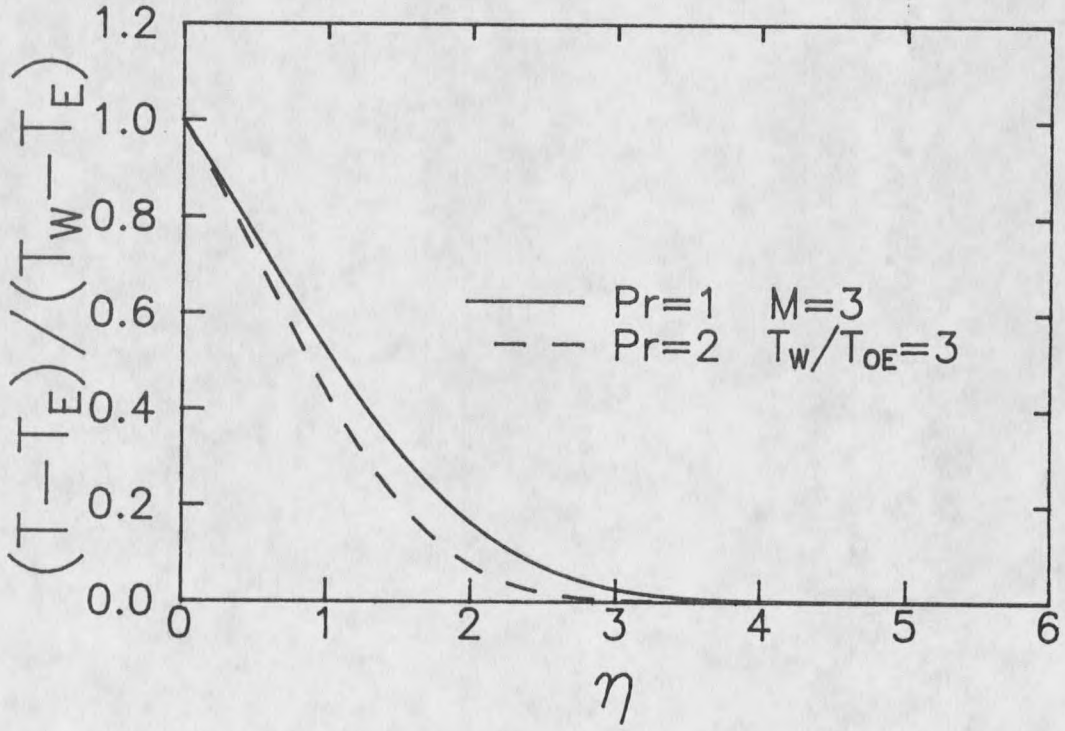


Figure 58. Similarity Temperature Profile.

Equation (47) below shows the Busseman-Crocco relationship rearranged to make the effect of the recovery factor more readily seen:

$$(47) \qquad \frac{T}{T_e} = \frac{u}{u_e} + \left(1 + \frac{u}{u_e}\right)\frac{T_w}{T_e} + \left(1 - \frac{u}{u_e}\right)\frac{u}{u_e}\left(\frac{\gamma - 1}{2}\right) M_\infty^2 r \quad .$$

Since PFT is founded on the Busemann-Crocco temperature relationship the restriction a Prandtl number of unity cannot be modified.

Secondly Chapman's [1] solution utilized in the PFT is based on a Prandtl number of unity. However, Berger [33] does provide a second solution to Chapman's work which does allow for a variable Prandtl number but no numerical solutions were available. For this second case to be used a numerical solution would have needed to be determined and then fit to a polynomial to be utilized in the PFT.

CHAPTER 6

CONCLUSIONS

The results of this investigation of solutions to laminar flow downstream of a splitter plate can be stated as follows:

1. The PFT was deemed to be the most complete theory dealing with laminar mixing behind a thin partition. The PFT encompasses the entire flow field allowing for viscous and inviscid factors. The uniqueness of the PFT is the combining of the wake and the free shear layer through superposition methods.
2. An independent assessment of the PFT was performed and no misinterpretation of the major works (i.e. Gold, Chapman, Crocco) were detected. Gold's velocity solution was integrated and compared with the PFT solution for correctness.
3. The PFT was utilized to solve for wake, base and partition flows under low speed, supersonic and hypersonic conditions. The results of these predications, qualitatively, agreed with the expected outcome. No discontinuities were observed in any of the flow fields determined by the PFT.
4. The PFT was tested against numerical results and wake experimental data. These comparisons validated the PFT's use of the Oseen approximations close to the trailing edge. However the test data was limited and only obtained for the minimum velocities and not the entire lateral profile.

5. The evaluation of the PFT with supersonic data was unsatisfactory. The profiles predicted by the PFT were thicker than the experimental data. Also, the minimum velocities of the two sets of data did not match. The attempt to improve the comparison by matching θ_1 did not provide any conclusive findings for the differences between the PFT and the supersonic data. The original comparison with $\theta_1 = .00484$ inches is considered the valid comparison for this work.

6. The comparison of the hypersonic data did strengthen one of the PFT's key postulates. The excellent agreement between the experimental minimum velocities and the PFT's minimum velocities for the laminar profiles verified the postulate that the dividing streamline of the free shear layer must coincide with that of the wake component. Also the PFT profiles showed excellent agreement on the slow side while the fast side profile was increasingly thicker than the experimental data. As in the supersonic data, this problem of a thicker velocity profile could be explained by the restriction of a Prandtl number of one.

7. The comparison of the turbulent/laminar hypersonic velocity profiles with the PFT illustrated the difference between the two types of flow. A major discovery was the PFT's ability to duplicate the known overshoot on the laminar slow side. As expected, the turbulent fast side spread much wider than the laminar theoretical results. This phenomenon is caused by the chaotic mixing of the turbulent flow causing the mean velocity of the flow to approach its asymptotic solution much slower than its laminar counterpart.

8. The use of the Oseen approximations in the near wake was supported by the numerical and wake comparisons. However the disparity in the supersonic data could be due to these approximations because the supersonic data was

close to the trailing edge. Further investigation of the use of these approximations close to the trailing edge is warranted.

9. The use of an exponential as a fit for the trailing edge profile even with a stretching factor does not fit the Blasius profile as accurately as a polynomial or a hyperbolic tangent fit.

10. The use of the Busseman-Crocco temperature relationship in the initial profile of the wake and Chapman's solution based on a Prandtl number of one for the free shear layer prevents the PFT from being expanded to incorporate to variable Prandtl numbers.

REFERENCES CITED

REFERENCES CITED

1. Chapman, D., "Laminar Mixing of a Compressible Fluid", National Advisory Committee for Aeronautics, Report 958 (1950).

2. Denison, M.R. and Baum, E., "Compressible Free Shear Layer With Finite Initial Thickness", *AIAA Journal*, Vol. 1, No. 2 (February 1963), 342.

3. Kubota, T. and Dewey, C.F. Jr., "Momentum Integral Methods for the Laminar Free Shear Layer", *AIAA Journal*, Vol. 2, No. 4 (April 1964), 625.

4. Berger, S.A., *Laminar Wakes*, Elsevier Publishing Company (1971), 63–64.

5. Schlichting, H., *Boundary-Layer Theory*, 7th Ed., McGraw-Hill Book Co. (1979), 177–179.

6. Goldstein, S., "Concerning Some Solutions of the Boundary Layer Equations in Hydrodynamics", *Proc. of the Cambridge Phil. Soc.*, Vol 26 (1930), 1–30.

7. Kubota, T., "Laminar Wake with Streamwise Pressure Gradient", GALCIT Hypersonic Research Project Memo No. 9, CIT, Pasadena, California (May 1962).

8. Gold, H., "Laminar Wake with Arbitrary Initial Profiles", *AIAA Journal*, Vol. 2, No. 5 (May 1964), 8.

9. Zeiberg, S.L and Kaplan, B., "Approximate Analysis of Free-Mixing Flows", *AIAA Journal*, Vol. 3 (March 1965).

10. Berger, S.A., *Laminar Wakes*, Elsevier Publishing Company (1971), 264–267.

11. Demetriades, A., "The Two-Dimensional Laminar Wake with Initial Asymmetry", *AIAA Journal*, Vol. 21, No. 9 (September 1983), 1347.

12. Demetriades, A., "Partition Flow Theory: A Novel Approach to the Mixing of Parallel Laminar Steady Flows", MSU/SWT Report TR89-03, Montana State University, Bozeman, Montana (September 1989).

13. Brower, T.L., "Experiments on the Free Shear Layer Between Two Supersonic Streams", AIAA 90-0710, 28th Aerospace Sciences Meeting, Reno, Nevada (January 8, 1990).

14. Grubb, J.P. and Donaldson, J.C., "Investigation of a Shear Layer Separating Mach 8 and Mach 3 Flow Fields", AEDC-TSR-89-V15 (July 1989).

15. Demetriades, A., "Partition Flow Theory: A Novel Approach to the Mixing of Parallel Laminar Steady Flows", MSU/SWT Report TR89-03, Montana State University, Bozeman, Montana (September 1989).

16. Schlichting, H., *Boundary-Layer Theory*, 7th Ed., McGraw-Hill Book Co. (1979), 135–139.

17. Schlichting, H., *Boundary-Layer Theory*, 7th Ed., McGraw-Hill Book Co. (1979), 332.

18. Sato, H. and Kuriki, K., "The Mechanism of Transition in the Wake of a Thin Flat Plate Placed Parallel to a Uniform Flow", *JFM*, Vol. II, Part 3 (November 1961), 321.

19. Demetriades, A., "Experimental Test of the Theory of GDL Nozzle-Cusp Wakes", Report U-6395, Aeronutronic Division, Newport Beach, California (1978).

20. Brower, T.L., "Experiments on the Free Shear Layer Between Adjacent Supersonic Streams", Master's Thesis, Montana State University, Bozeman, Montana (March 1983), Appendices D,E.

21. Schlichting, H., *Boundary-Layer Theory*, 7th Ed., McGraw-Hill Book Co. (1979), 335.

22. Demetriades, A., Personal Communications (October 1989).

23. Demetriades, A., "Transition to Turbulence in a Laminar Hypersonic Partition Flow", SWT Internal Memorandum 89-01 (March 1989).

24. Grubb, J., Personal Communications (May 1989).

25. Tritz, T., Personal Communications (December 1989).

26. Berger, S., *Laminar Wakes*, Elsevier Publishing Company (1971), 25.

27. Demetriades, A., Personal Communications (December 1988).

28. White, F., *Viscous Fluid Flow*, 1st Ed., McGraw-Hill Book Co. (1974), 265, 602.

29. Gasperas, G., Personal Communications (February 1990).

30. White, F., *Viscous Fluid Flow*, 1st Ed., McGraw-Hill Book Co. (1974), 587.

31. Schlichting, H., *Boundary-Layer Theory*, 7th Ed., McGraw-Hill Book Co. (1979), 295, Fig. 12.9.

32. White, F., *Viscous Fluid Flow*, 1st Ed., McGraw-Hill Book Co. (1974), 273.

33. Berger, S.A., *Laminar Wakes*, Elsevier Publishing Company (1971), 27–28.

34. Gradshteyn, I.S. and Ryzhik, I.M., *Tables of Integrals, Series, and Products*, Academic Press (1980), 339.

APPENDICES

APPENDIX A

INTEGRATION OF GOLD'S VELOCITY EQUATION

APPENDIX A

INTEGRATION OF GOLD'S VELOCITY EQUATION

Begin with equation (1)

$$\overline{u} = \frac{1}{2\sqrt{x}} \int_{-\infty}^{\infty} \overline{u}_0 \, \xi G(\xi; x^+, y^+) d\xi \tag{48}$$

where

$$x^+ = \frac{x^*}{\theta, \mathrm{Re}_\theta} \quad , \quad y^+ \frac{\tilde{Y}^*}{(\theta_1 + \theta_2)}$$

$$G(\xi, x^+, y^+) = \frac{1}{\sqrt{\pi}} \exp[-(y^+ - \xi)^2 / 4x^+]$$

$$\overline{u}_0(\xi) = \exp^{-\xi} \quad \text{for } y^+ > 0$$

$$\overline{u}_0(\xi) = \exp^{P'\xi} \quad \text{for } y^+ < 0 \quad .$$

Substitute the above into (48) and rearrange

$$\overline{u} = \frac{1}{2\sqrt{x^+ \pi}} \left[\int_{-\infty}^{0} \exp \left[\frac{4x^+ P' \xi - (y^+ - \xi)^2}{4x'} \right] d\xi \right. \tag{49}$$
$$\left. + \int_{0}^{\infty} \exp \left[\frac{-4x^+ \xi - (y^+ - \xi)^2}{4x^+} \right] d\xi \right] \quad .$$

Integrate the first half of (49)

$$\frac{1}{2\sqrt{x^+}} \int_{-\infty}^{0} \exp \left[\frac{4x^+ P' \xi - (y^+ - \xi)^2}{4x^+} \right] d\xi$$

$$\frac{\exp[-y^{+2}/4x^+]}{2\sqrt{x^+ \pi}} \int_{-\infty}^{0} \exp \left[P'\xi + \frac{2y^+ \xi - \xi^2}{4x^+} \right] d\xi$$

and let

$$-z^2 = \frac{4x^+ P' \xi + 2y^+ \xi - \xi^2}{4x^+} \quad . \tag{50}$$

Change limits

(51)
$$\begin{array}{cc} z=0 & z\to\infty \\ \xi\to 0 & \xi\to-\infty \end{array} ,$$

$$-z^2 4x^+ = 4x^+ P'\xi + 2y^+\xi - \xi^2$$

$$\xi^2 + (-4x^+ P' - 2y')\xi + (-4x^+)z^2 = 0$$

and let $B = -4x^+ P' - 2y^+$ and $C = -4x^+ z^2$. Apply quadratic

$$\xi = \frac{2y^+ + 4x^+ P' \pm \sqrt{(-4x^+ P' - 2y^+)^2 + 4\cdot 4x^+ z^2}}{2} ,$$

let sign be negative, and solve for $d\xi/dz$

(52)
$$\frac{d\xi}{dz} = -\left(\frac{1}{2}\right)\left(\frac{1}{2}\right)\left[(-4x^+ P' - 2y^+)^2 + 16x^+ z^2\right]^{-1/2} 32x^+ z$$

$$d\xi = -8\left[(-4x^+ P' - 2y^+)^2 + 16x^+ z^2\right]^{-1/2} x^+ z dz \quad .$$

Substitute (50), (51) and (52) into (49) and multiply by -1 to switch limits of integration

$$\frac{(-1) - 8x^+ \exp\left(-y^{+2}/4x^+\right)}{2\sqrt{x^+\pi}} \int_0^\infty \frac{z\exp[-z^2]\frac{1}{4\sqrt{x^+}}}{[(-4x^+ P' - 2y^+]^2 + 16x^+ z^2]^{1/2}\frac{1}{4\sqrt{x^+}}}\, dz \quad .$$

Rearrange

(53)
$$\frac{\exp\left(-y^{+2}/4x^+\right)}{\sqrt{\pi}} \int_0^\infty \frac{z\exp[-z^2]}{\left[\frac{(4x^+ P' - 2y')^2}{16x^+} + z^2\right]^{1/2}}\, dz$$

from [34]

(54)
$$\int_0^\infty \frac{ze^{-\mu z^2}}{\sqrt{a^2+z^2}}\, dz = \frac{1}{2}\sqrt{\frac{\pi}{\mu}}\, e^{a^2\mu}\left[1 - \phi\left(a\sqrt{\mu}\right)\right] \quad .$$

Letting

$$a^2 = \frac{(-4x^+ P' - 2y^+)^2}{16x^+} ,$$

and substituting a^2 in (53), (53) can be solved using (54) with $\mu = 1$, $\Phi = Erf$

$$(55) \qquad \exp[-y^{+2}/4x^{+2}] \int_0^\infty \frac{ze^{-z^2}}{(a^2+z^2)^{1/2}}\, dz = \frac{1}{2}\exp[P'x^+ + P'y^+]\left[1 - Erf\left(P\sqrt{x^+} + \frac{y^+}{2\sqrt{x}}\right)\right] \quad .$$

Integrate the second half of (48) in a similar fashion:

$$(56) \qquad \frac{1}{2\sqrt{x^+\pi}} \int_0^\infty \exp\left[\frac{-4x^+\xi - (y^+ - \xi)^2}{4x}\right] d\xi \quad ;$$

rearrange

$$(57) \qquad \frac{\exp\left(-y^{+2}/4x^+\right)}{2\sqrt{x^+\pi}} \int_0^\infty \exp\left[-\xi + \frac{2y^+\xi - \xi^2}{4x^+}\right] d\xi$$

and let

$$(58) \qquad -z^2 = \frac{-\xi 4x^+ + 2y^+\xi - \xi^2}{4x^+} \quad .$$

Change limits

$$(59) \qquad \begin{matrix} z \to 0 & , & z \to \infty \\ \xi \to 0 & , & \xi \to \infty \end{matrix}$$

and apply quadratic

$$-z^2 4x^+ + 4x^+\xi - 2y^+\xi + \xi^2 = 0$$

$$\xi = \frac{-4x^+ + 2y^+ \pm \sqrt{(4x^+ - 2y^+)^2 - 4(-4x^+z^2)}}{2} \quad .$$

Use + (positive) sign because there is no need to switch limits

$$(60) \qquad d\xi = \left(\frac{1}{4}\right)\left((4x^+ - 2y^+)^2 + 16x^+z^2\right)^{-1/2} 32zx^+\, d\xi \quad .$$

Substitute (58), (59) and (60) into (57) and $*/\div$ by $\frac{1}{4\sqrt{x}}$ to obtain proper form

$$(61) \qquad \frac{\exp\left[\frac{-y^{+2}}{4x^+}\right]}{\sqrt{\pi}} \int_0^\infty \frac{e^{-z^2}z}{\left(\frac{(4x^+ - 2y^+)^2}{16x^+} + z^2\right)^{1/2}}\, dz \quad .$$

Substituting the following variable into (61)

$$a^2 = \frac{(4x-2y)^2}{16x} \quad ,$$

(61) can be solved using [34] with $\mu = 1$, $\Phi = Erf$

$$\frac{\exp\left[\frac{-y^{+2}}{4x^+}\right]}{2\sqrt{x^+\pi}} \int_0^\infty \frac{ze^{-z^2}}{\sqrt{a^2+z^2}}\, dz = \tag{62}$$
$$\frac{1}{2}\exp[x^+ - y^+]\left[1 - Erf\left(\sqrt{x^+} - \frac{y}{2\sqrt{x^+}}\right)\right] \quad .$$

Using the identity

$$Erf(-x^+) = -Erf(x^+)$$

on (55) and (62), the complete solution to (48) becomes

$$\overline{u} = \frac{1}{2}\left[\exp[P'^2 x^+ + P'y^+]\left[1 - Erf\left(P'\sqrt{x^+} + \frac{y^+}{2\sqrt{x^+}}\right)\right]\right. \tag{63}$$
$$\left. + \exp[x^+ - y^+]\left[1 + Erf\left(\frac{y^+}{2\sqrt{x^+}} - \sqrt{x^+}\right)\right]\right] \quad .$$

Let

$$x' = \frac{P'^2}{(P'+1)^2}\, x^+ \quad , \quad y' = \frac{P'}{P'+1}\, y^+$$

or

$$(P'+1)^2 x' = P^2 x^+ \quad , \quad (P'+1)y' = P'y^+$$

and substitute into (63)

$$\overline{u} = \frac{1}{2}\left[\exp[(P'+1)^2 x' + (P'+1)y']*\right.$$
$$\left[1 - Erf\sqrt{x'}\left((P'+1)\sqrt{x'} + \frac{y'}{2\sqrt{x'}}\right)\right] \tag{64}$$
$$+ \exp\left[\frac{(P'+1)^2}{P'}\, x' - \left(\frac{P'+1}{P'}\right)y'\right]*$$
$$\left.\left[1 + Erf\left(\frac{y'}{2\sqrt{x'}} - \left(\frac{P'+1}{P'}\right)x'\right)\right]\right] \quad .$$

Equation (64) and equation (12) of [12], page 6 are the same.

APPENDIX B

THE PFT ALGORITHM "SHEAR 14"

APPENDIX B

THE PFT ALGORITHM "SHEAR 14"

```
REM SHEAR14 VERSION 6/30/89 ALTERED BY FLY FOR GRAPHING PURPOSES
REM Improves pre-1989 versions as follows: a) changes viscous asymmetry"
REM variable to theta1xrho1/theta2xrho2, b) adds inverse transformation to"
REM recover untransformed y, c) Corrects previous error of finding T by"
REM wrongly using Crocco relation for entire flow, d) shifts FSL center"
REM (0.587) to wake (min. vel.) center, e) Reminds us to use the fast-"
REM -side Re' in x, f) adds variable gamma and misc. graphics facilities"
REM g) stretches flow laterally by optionally stretching the initial
REM boundary layer profile (Note: during stretching wake center does
 REM not move.)
 DIM YA(50), UA(50), YB(50), UB(50)
 DIM Y(150), X1(50), Z(50), E1(50), F1(50), X2(50), D(50), E2(50)
 DIM Y1(150), T6(150)
 DIM F2(50), U(150), H(50), G(50), J(50), K(50), U1(150)
 DIM L(150)
 DIM T2(50), T3(50), T4(50), M(50)
 DIM U2(150), T5(150), RH(150), M3(150)
 DIM Y2(150), Y3(150)
 INPUT "ENTER RUN NUMBER:"; RUNI
 INPUT "ENTER FAST-SIDE MACH NO.: "; M
 INPUT "ENTER SLOW-TO-FAST TOTAL TEMP. RATIO T02/T01: "; T
 INPUT "ENTER SPECIFIC HEAT RATIO GAMMA: "; G1
 INPUT "ENTER PARTITION-TO-FAST-SIDE-TOTAL TEMP.RATIO TW/T01: "; TW
 INPUT "ENTER BOUNDARY-LAYER THICKNESS RATIO THETA1/THETA2: "; TH
 INPUT "ENTER SPEED RATIO U2/U1="; R
 PRINT "ENTER STRETCHING PARAMETER S (This is the factor needed to"
 PRINT "'stretch' to exponential profile laterally, so it can match"
 PRINT "the profile you want; for example S=3 will approximate a Blasius"
 INPUT "initial boundary layer profile="; S
 LPRINT "SUMMARY OF INPUTS "
 LPRINT
 LPRINT "RUN NUMBER ="; RUNI
 LPRINT "FAST-SIDE MACH NO.="; M
 LPRINT "SLOW-TO-FAST TOTAL TEMP. RATIO T02/T01="; T
 LPRINT "SPECIFIC HEAT RATIO GAMMA:"; G1
 LPRINT "PARTITION-TO-FAST-SIDE-TOTAL TEMP.RATIO TW/T01="; TW
 LPRINT "BOUNDARY-LAYER THICKNESS RATIO THETA1/THETA2="; TH
 LPRINT "SPEED RATIO U2/U1="; R
 LPRINT "INITIAL BOUNDARY LAYER PROFILE="; S
 FOR IL = 1 TO 9
```

Figure 59. The PFT Algorithm "Shear 14".

```
B$ = STR$(IL)
B$ = RIGHT$(B$, 1)
INPUT "DO YOU WANT TO CONTINUE (Y/N)"; DG$
IF DG$ = "N" GOTO 2420
INPUT "XBAR=X*/(RETHETA1)(THETA1)="; XBAR
LPRINT "XBAR="; XBAR
LET T1 = (1 + ((G1 - 1) / 2) * (M ^ 2)) * T - ((G1 - 1) / 2) * (R ^ 2) * (M ^ 2)
PRINT
PRINT
LET P1 = TH * T1
PRINT
PRINT
PRINT "PARTITION FLOW THEORY; SHEAR14 VERSION 4/10/89"
PRINT "Assumes initial exponential b.l.profile, Chapman FSL profile,"
PRINT "and coincident FSL and wake centers in the transformed Y' plane;"
PRINT "it also provides for stretching the initial boundary layer"
PRINT "profiles, which starts as an exponential, to accomodate Blasius"
PRINT "and other shapes."
PRINT "------------------------------------------------"
PRINT
PRINT "INPUT PARAMETERS:"
PRINT
LET X = XBAR / ((1 + (1 / P1)) ^ 2)
PRINT "XBAR=X*/(RETHETA1)(THETA1)="; XBAR
PRINT "X'="; X
PRINT "MOMENTUM THICKNESS RATIO THETA1/THETA2= "; TH
PRINT "SPEED RATIO U2/U1="; R
PRINT "FAST-SIDE MACH NO. M1="; M
PRINT "TOTAL TEMPERATURE RATIO T02/T01="; T
PRINT "GAMMA= "; G1
PRINT "PARTITION-TO-FAST-SIDE-TOTAL TEMPERATURE RATIO="; TW
PRINT "INITIAL PROFILE STRETCHING FACTOR S="; S
PRINT
PRINT "COMPUTED PROPERTIES IN SLOW STREAM:"
PRINT
PRINT "        T2/T1= "; T1
PRINT "        RHO2/RHO1= "; 1 / T1
PRINT "        M2= "; R * M * SQR(1 / T1)
PRINT
PRINT "ASYMMETRY PARAMETER P'=(THETA1/THETA2)X(RHO1/RHO2)= "; P1
```

Figure 59 (continued). The PFT Algorithm "Shear 14".

```
    PRINT
    LET P = .327591
    LET A1 = .254829592#
    LET A2 = -.284497
    LET A3 = 1.42141
    LET A4 = -1.45315
    LET A5 = 1.06141
    LET MIN = 1.2
    FOR I = 1 TO 20
    LET Y(I) = .15 * I - 1.5
    LET Y = Y(I)
    GOSUB 2430
    LET U(I) = 1 - U
    IF U(I) > MIN GOTO 950
    LET MIN = U(I)
    NEXT I
950 LET MIN = 1.2
    FOR J = 0 TO 20
    LET YA(J) = Y(I - 2) + (J / 20) * (Y(I) - Y(I - 2))
    LET Y = YA(J)
    GOSUB 2430
     LET UA(J) = 1 - U
     IF UA(J) > MIN GOTO 1040
     LET MIN = UA(J)
     NEXT J
1040 LET MIN = 1.2
     FOR K = 0 TO 20
     LET YB(K) = YA(J - 2) + (K / 20) * (YA(J) - YA(J - 2))
     LET Y = YB(K)
     GOSUB 2430
     LET UB(K) = 1 - U
     IF UB(K) > MIN GOTO 1130
     LET MIN = UB(K)
     NEXT K
1130 LPRINT "MINIMUM WAKE COMPONENT VELOCITY= "; UB(K - 1)
     LPRINT "OCCURS AT Y'= "; YB(K - 1)
     PRINT
     INPUT "INPUT RANGE -RA<y'<RA ENTER RA: "; RA
     LET L = 0
     FOR Y = -RA TO RA STEP RA / 50
```

Figure 59 (continued). The PFT Algorithm "Shear 14".

```
      LET Y = (Y + (S - 1) * YB(K - 1)) / S
      LET X1 = ((P1 + 1) * SQR(X)) + Y / (2 * SQR(X))
      IF X1 < 0 GOTO 1320
      LET Z = 1 / (1 + P * X1)
      LET F1 = (A1 * Z + A2 * (Z ^ 2) + A3 * (Z ^ 3)+
      A4 * (Z ^ 4) + A5 * (Z ^ 5)) * EXP(-(Y ^ 2) / (4 * X))
      GOTO 1360
1320  LET X1 = -((P1 + 1) * SQR(X)) - Y / (2 * SQR(X))
      LET Z = 1 / (1 + P * X1)
      LET E1 = 2 - (A1 * Z + A2 * (Z ^ 2) + A3 * (Z ^ 3) +
      A4 * (Z ^ 4) + A5 * (Z ^ 5)) * EXP(-(X1 ^ 2))
      LET F1 = EXP(((P1 + 1) ^ 2) * X + (P1 + 1) * Y) * E1
1360  LET X2 = (Y / (2 * SQR(X))) - ((P1 + 1) / P1) * SQR(X)
      IF X2 < 0 GOTO 1410
      LET D = 1 / (1 + P * X2)
      LET E2 = 2 - (A1 * D + A2 * (D ^ 2) +
      A3 * (D ^ 3) + A4 * (D ^ 4) + A5 * (D ^ 5)) * EXP(-(X2 ^ 2))
      GOTO 1450
1410  LET X2 = ((P1 + 1) / P1) * SQR(X) - (Y / (2 * SQR(X)))
      LET D = 1 / (1 + P * X2)
      LET F2 = (A1 * D + A2 * (D ^ 2) +
      A3 * (D ^ 3) + A4 * (D ^ 4) +
      A5 * (D ^ 5)) * EXP(-(Y ^ 2) / (4 * X))
      GOTO 1460
1450  LET F2 = EXP((((P1 + 1) / P1) ^ 2) * X - ((P1 + 1) / P1) * Y) * E2
1460  LET U = .5 * (F1 + F2)
      LET Y = S * Y - (S - 1) * YB(K - 1)
      LET H = (Y - YB(K - 1)) / SQR(X)
      IF H > 8 THEN GOTO 1700
      IF H < -10 THEN GOTO 1720
      IF H >= 0 THEN GOTO 1600
      LET C0 = .5874
      LET C1 = .202264
      LET C2 = 7.90697E-03
      LET C3 = -6.90281E-03
      LET C4 = -.0013746
      LET C5 = -1.02122E-04
      LET C6 = -2.72423E-06
      GOTO 1670
1600  LET C0 = .588094
```

Figure 59 (continued). The PFT Algorithm "Shear 14".

```
      LET C1 = .198703
      LET C2 = 5.08547E-03
      LET C3 = -.0206133
      LET C4 = 4.97013E-03
      LET C5 = -4.83879E-04
      LET C6 = 1.73527E-05
1670  LET V = C0 + C1 * H + C2 * (H ^ 2) + C3 * (H ^ 3) +
      C4 * (H ^ 4) + C5 * (H ^ 5) + C6 * (H ^ 6)
      LET U1 = (1 - R) * V + R
      GOTO 1730
1700  LET U1 = 1
      GOTO 1730
1720  LET U1 = R
1730  LET F = ((G1 - 1) / 2) * (M ^ 2)
      LET U2 = U1 * (1 - U)
      LET T2 = 1 + F * (1 - (U1 ^ 2))
      LET T3 = ((1 - T1) / (1 - R) + F * (1 + R)) * (U1 - 1)
      LET T4 = T2 + T3
      LET M2 = U1 * M * SQR(1 / T4)
      LET C = ((1 - G1) / 2) * (M2 ^ 2)
      LET B = (TW / T4) * (1 + ((G1 - 1) / 2) * (M ^ 2)) - 1 - C
      LET Y = (Y + (S - 1) * YB(K - 1)) / S
      LET X3 = (2 * (P1 + 1) / P1) * SQR(X) - Y / (2 * SQR(X))
      IF X3 < 0 GOTO 1870
      LET Z1 = 1 / (1 + P * X3)
      LET F3 = (A1 * Z1 + A2 * (Z1 ^ 2) +
      A3 * (Z1 ^ 3) + A4 * (Z1 ^ 4) +
      A5 * (Z1 ^ 5)) * EXP(-(Y ^ 2) / (4 * X))
      GOTO 1930
1870  LET X3 = (Y / (2 * SQR(X))) - (2 * (P1 + 1) / P1) * SQR(X)
      LET Z1 = 1 / (1 + P * X3)
      LET E3 = 2 - (A1 * Z1 + A2 * (Z1 ^ 2) +
      A3 * (Z1 ^ 3) + A4 * (Z1 ^ 4) + A5 * (Z1 ^ 5)) * EXP(-(X3 ^ 2))
      LET FA = EXP(4 * X * (((P1 + 1) / P1) ^ 2))
      LET FB = EXP(-2 * Y * ((P1 + 1) / P1))
      LET F3 = FA * FB * E3
1930  LET X4 = 2 * (P1 + 1) * SQR(X) + Y / (2 * SQR(X))
      IF X4 < 0 GOTO 1980
      LET Z2 = 1 / (1 + P * X4)
      LET F4 = (A1 * Z2 + A2 * (Z2 ^ 2) +
```

Figure 59 (continued). The PFT Algorithm "Shear 14".

```
    A3 * (Z2 ^ 3) + A4 * (Z2 ^ 4) +
    A5 * (Z2 ^ 5)) * EXP(-(Y ^ 2) / (4 * X))
    GOTO 2020
1980 LET X4 = -2 * (P1 + 1) * SQR(X) - Y / (2 * SQR(X))
    LET Z2 = 1 / (1 + P * X4)
    LET E4 = 2 - (A1 * Z2 + A2 * (Z2 ^ 2) +
    A3 * (Z2 ^ 3) + A4 * (Z2 ^ 4) + A5 * (Z2 ^ 5)) * EXP(-(X4 ^ 2))
    LET F4 = EXP(4 * ((P1 + 1) ^ 2) * X + 2 * (P1 + 1) * Y) * E4
2020 LET H1 = B * U + (C / 2) * (F3 + F4)
    LET Y = S * Y - (S - 1) * YB(K - 1)
    LET T5 = (1 + H1) * T4
    LET M3 = U2 * M * SQR(1 / T5)
    LET L = L + 1
    LET Y(L) = Y
    LET U2(L) = U2
    LET T5(L) = T5
    LET RH(L) = 1 / T5
    LET M3(L) = M3
    LET T6(L) = (T5(L) / (1 + ((G1 - 1) / 2) *
    (M ^ 2))) * (1 + ((G1 - 1) / 2) * (M3 ^ 2))
    NEXT Y
    LET LOW = 1000
    FOR I = 1 TO 100
    IF ABS(Y(I)) < LOW THEN GOTO 2190
    GOTO 2210
2190 LET LOW = ABS(Y(I))
    LET AA = I
2210 NEXT I
    FOR I = AA + 1 TO 101
    LET Y1(AA) = 0
    LET Y1(I) = Y1(I - 1) + (RA / 100) * (T5(I) + T5(I - 1))
    LET Y3(I) = Y1(I) * (1 + (1 / P1))
    NEXT I
    FOR I1 = 1 TO AA - 1
    LET I = AA - I1
    LET Y1(I) = Y1(I + 1) - (RA / 100) * (T5(I + 1) + T5(I))
    LET Y3(I) = Y1(I) * (1 + (1 / P1))
    NEXT I1
    OPEN "O", #1, "PLACE" + B$ + ".DAT"
XBAR$ = "'" + STR$(XBAR) + "'"
```

Figure 59 (continued). The PFT Algorithm "Shear 14".

```
     FOR I = 1 TO 100
     IF I = 100 THEN
PRINT #1, Y3(I), U2(I), M3(I), T5(I), 1 / T5(I), T6(I), XBAR$
ELSE
     PRINT #1, Y3(I), U2(I), M3(I), T5(I), 1 / T5(I), T6(I)
END IF
     NEXT I
     CLOSE
     NEXT IL
2420 END
2430 LET X1 = ((P1 + 1) * SQR(X)) + Y / (2 * SQR(X))
     IF X1 < 0 GOTO 2480
     LET Z = 1 / (1 + P * X1)
     LET F1 = (A1 * Z + A2 * (Z ^ 2) +
     A3 * (Z ^ 3) + A4 * (Z ^ 4) +
     A5 * (Z ^ 5)) * EXP(-(Y ^ 2) / (4 * X))
     GOTO 2520
2480 LET X1 = -((P1 + 1) * SQR(X)) - Y / (2 * SQR(X))
     LET Z = 1 / (1 + P * X1)
     LET E1 = 2 - (A1 * Z + A2 * (Z ^ 2) +
     A3 * (Z ^ 3) + A4 * (Z ^ 4) +
     A5 * (Z ^ 5)) * EXP(-(X1 ^ 2))
     LET F1 = EXP(((P1 + 1) ^ 2) * X +
     (P1 + 1) * Y) * E1
2520 LET X2 = (Y / (2 * SQR(X))) -
     ((P1 + 1) / P1) * SQR(X)
     IF X2 < 0 GOTO 2570
     LET D = 1 / (1 + P * X2)
     LET E2 = 2 - (A1 * D + A2 * (D ^ 2) + A3 * (D ^ 3) +
     A4 * (D ^ 4) + A5 * (D ^ 5)) * EXP(-(X2 ^ 2))
     GOTO 2610
2570 LET X2 = ((P1 + 1) / P1) * SQR(X) - (Y / (2 * SQR(X)))
     LET D = 1 / (1 + P * X2)
     LET F2 = (A1 * D + A2 * (D ^ 2) +
     A3 * (D ^ 3) + A4 * (D ^ 4) +
     A5 * (D ^ 5)) * EXP(-(Y ^ 2) / (4 * X))
     GOTO 2620
2610 LET F2 = EXP((((P1 + 1) / P1) ^ 2) * X -
     ((P1 + 1) / P1) * Y) * E2
2620 LET U = .5 * (F1 + F2)
     RETURN
```

Figure 59 (continued). The PFT Algorithm "Shear 14".

MONTANA STATE UNIVERSITY LIBRARIES
3 1762 10033647 6